SECURITY CLASSIFICATION OF THIS PAGE *(When Data Entered)*

REPORT DOCUMENTATION PAGE	READ INSTRUCTIONS BEFORE COMPLETING FORM

1. REPORT NUMBER NSWC/WOL/TR 75-39	2. GOVT ACCESSION NO.	3. RECIPIENT'S CATALOG NUMBER

4. TITLE *(and Subtitle)* "Scattering of Electromagnetic Radiation by Apertures" V. Surface Current, Tangential Aperture Electric Field,& Back Scattering Cross-Section For The Axially Slotted Cylinder at Normal,Symmetric Incidence	5. TYPE OF REPORT & PERIOD COVERED Topical Report
	6. PERFORMING ORG. REPORT NUMBER

7. AUTHOR(s) J. N. Bombardt, Jr. L. F. Libelo	8. CONTRACT OR GRANT NUMBER(s)

9. PERFORMING ORGANIZATION NAME AND ADDRESS Naval Surface Weapons Center,White Oak Lab. Silver Spring, Maryland 20910	10. PROGRAM ELEMENT, PROJECT, TASK AREA & WORK UNIT NUMBERS HDL:E052E6 Subtask EB-088 NMAT-03L-000/ZR011-01-01 DNA-EB088-52

11. CONTROLLING OFFICE NAME AND ADDRESS	12. REPORT DATE April 1975
	13. NUMBER OF PAGES 193

14. MONITORING AGENCY NAME & ADDRESS*(If different from Controlling Office)*	15. SECURITY CLASS. *(of this report)* Unclassified
	15a. DECLASSIFICATION/DOWNGRADING SCHEDULE

16. DISTRIBUTION STATEMENT *(of this Report)*

Approved for Public Release
Distribution Unlimited

17. DISTRIBUTION STATEMENT *(of the abstract entered in Block 20, if different from Report)*

18. SUPPLEMENTARY NOTES

The effort funded by Defense Nuclear Agency was performed jointly with Harry Diamond Laboratories, Washington, D. C.

19. KEY WORDS *(Continue on reverse side if necessary and identify by block number)*
Axially Slotted Cylinder
Electromagnetic Scattering
Surface Current
Aperture Field
Back-Scattering Cross-Section

20. ABSTRACT *(Continue on reverse side if necessary and identify by block number)*

In this report we consider the thin-walled perfectly conducting, axially slotted, infinite circular cylinder, and the infinite cylindrical strip. For the case of incidence simultaneously normal to the cylinder axis and parallel to the symmetry plane bisecting the infinite axial slot, we present the analytic formulation of the integral equations for the surface current on the conductor and also those for the tangential component of the

DD FORM 1473 EDITION OF 1 NOV 65 IS OBSOLETE
1 JAN 73
S/N 0102-014-6601

SECURITY CLASSIFICATION OF THIS PAGE *(When Data Entered)*

20. (Contd)

electric field over the slot. The incident radiation is assumed
merely for simplicity to be monochromatic, plane, and linearly
polarized parallel to the cylinder axis. Results obtained
numerically for the tangential field over the slot, the surface
current density on the conductor, and finally the back-scattering
cross-section are displayed in graphical form for intermediate to
large slot angles for the range of $\eta = 2\pi a/\lambda$ from 1 to 5. Some
newly observed relations for the slot field at wavelengths
corresponding to internal resonances are also considered.

SCATTERING OF ELECTROMAGNETIC RADIATION BY APERTURES V. SURFACE CURRENT, TANGENTIAL APERTURE ELECTRIC FIELD, AND BACK-SCATTERING CROSS-SECTION FOR THE AXIALLY SLOTTED CYLINDER AT NORMAL, SYMMETRIC INCIDENCE

JOHN B. WILCOX
By direction

TABLE OF CONTENTS

LIST OF ILLUSTRATIONS

LIST OF ILLUSTRATIONS (Contd)

LIST OF TABLES

I. INTRODUCTION

This report constitutes the fifth in a series[1-4] of theoretical

investigations of the scattering characteristics of apertures in

conducting surfaces. In particular, it is the third in a sequence

devoted especially to a study of the axially slotted, infinite, thin

walled, circular, conducting cylinder. The first two in the

series[1-2] may of course be considered the limiting case where the

radius of the cylinder increases to some very large magnitude while

all other parameters remain fixed and finite. In this paper, for

the geometry in a plane normal to the cylinder axis as illustrated

in Figure 1. we show in graphical form the results obtained by

1. L. F. Libelo and J. N. Bombardt (HDL) "Scattering of Electro-
   magnetic Radiation by Apertures: I. Normal Incidence on the
   Slotted Plane", ·NOLTR 70-58, Naval Surface Weapons Center,
   White Oak, Silver Spring, Md., April 1970

2. L. F. Libelo and J. N. Bombardt (HDL) "S.E.R.A.: II. Oblique
   Incidence on the Slotted Plane for Parallel Polarization",
   NOLTR 72-25, Naval Surface Weapons Center, White Oak, Silver
   Spring, Md., January 1972

3. J. N. Bombardt and L. F. Libelo (NAVSURFWPNCEN) "S.E.R.A.:
   III. An Alternative Integral Equation with Analytic Kernels
   for the Slotted Cylinder Problem", HDL-TR-1588, Harry Diamond
   Laboratories, Washington, D. C., August 1972

4. J. N. Bombardt and L. F. Libelo (NAVSURFWPNCEN) "S.E.R.A.:
   IV. Slotted Cylinders and Cylindrical Strips in the Rayleigh
   Limit", HDL-RT-1607, Harry Diamond Laboratories, Washington,
   D. C., August 1972
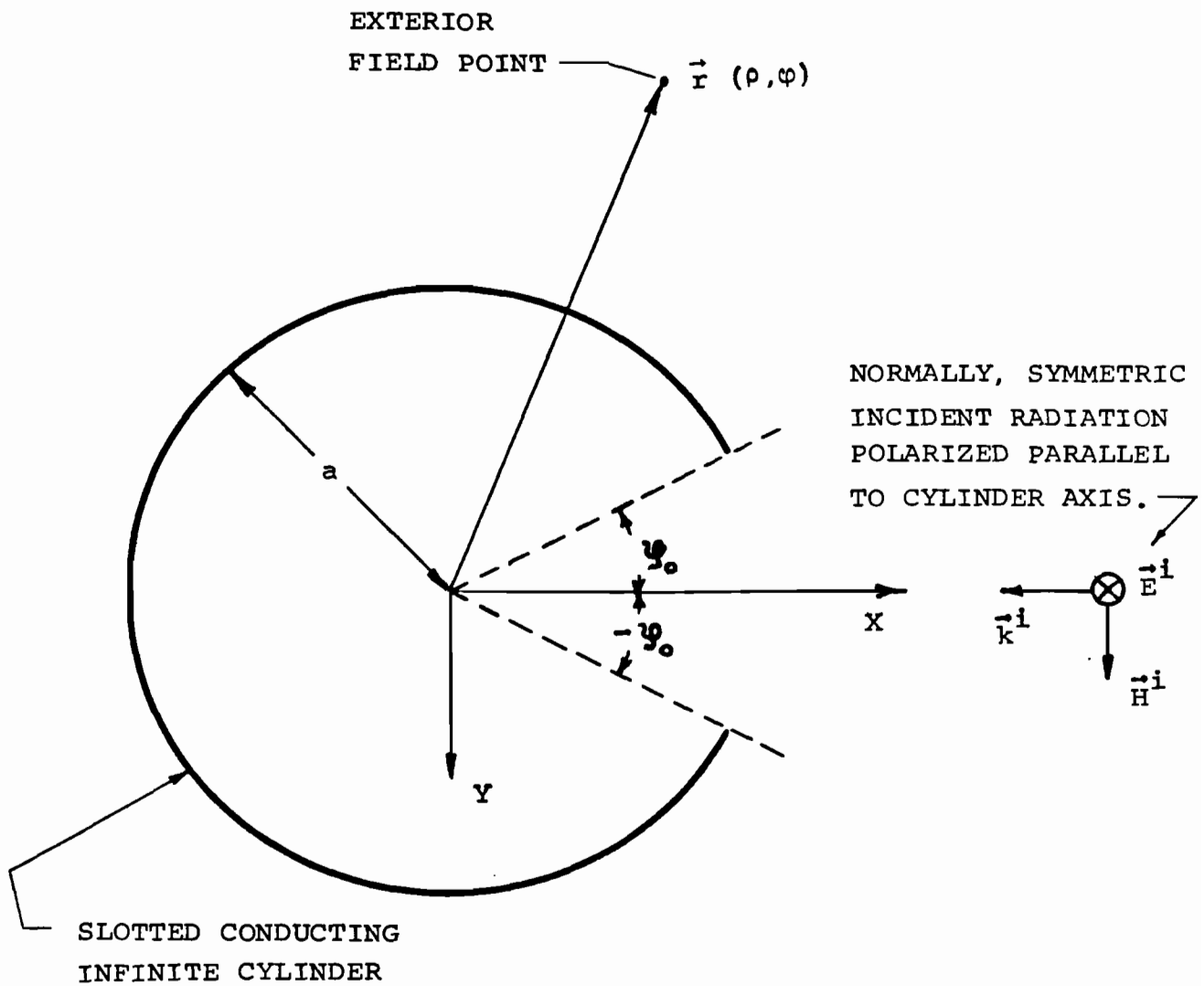
FIGURE 1.   GEOMETRY OF THE SCATTERING PROBLEM

numerically solving for the tangential component of the electric

field over the aperture, the surface current density on the curved

conductor and the back-scattering cross-section. Slots subtending

total angles of 60°, 90°, 120°, 180°, 240°, and 300° at the axis

are considered. Of course the latter three cases may be called

alternatively the half-cylindrical mirror and the 120° and 60°

circular cylindrical strips. In each case results have been

obtained for values of the parameter $\eta = 2\pi a/\lambda$ equal to 1, 2, 3, 4

and 5.

Before proceeding to the analysis itself, we first review the

earlier works by others on this scattering problem. Sommerfeld[5]

published what is probably the earliest work. In this attempt at

the problem he formulated the solution in terms of series expansions

for the fields internal as well as external to the slotted cylinder.

Since the application of the boundary conditions to these series

expansions did not result in explicit evaluation of the unknown

coefficients in these series, Sommerfeld attempted to obtain approx-

imate solutions. To achieve this, he restricted the problem to the

case where the slot arclength is small in comparison to the wave-

length. Using the method of least squares, he managed to derive

analytic expressions for the coefficients in this asymptotic limit.

5. A. Sommerfeld, "Partial Differential Equation", p 29-31
   Academic Press, New York, 1949

Unfortunately, however, he failed to publish any numerical results or any experimental measurements he may have had available. It is important to point out that in the results we report below of our investigations of the slotted cylinder we do not restrict ourselves to this asymptotic limit. Series expansions for the field were also assumed by Morse and Feshbach[6]. In the study they carried out the unknown series expansion coefficients are expressed in terms of an integral of the unknown electric field over the slot. They approximately solved this integral equation by assuming that the distribution of the field over the slot, for the slotted cylinder, is proportional to the electrostatic field distribution over the slot in an infinite plane. At the mid-point of the slot, they were able to derive an analytic result for the proportionality constant. Again we are unfortunate in that they also failed to furnish any numerical or experimental results. Somewhat about the same time Turner[7] investigated the half-cylindrical mirror, he derived an integral equation for the surface current density and by a variational approximation obtained an expression for the total scattering cross-section per unit length of the half cylindrical

6. P. M. Morse and H. Feshbach, "Methods of Theoretical Physics", Part II, 1387-1398, McGraw-Hill, New York, 1953

7. R. Turner, "Scattering of Electromagnetic Radiation by an Infinite Cylindrical Mirror", Tech. Rep. No. 161, Cruft Laboratory, Harvard University, Cambridge, MA, 1953

mirror. Once again no experimental or numerical results were reported even in this special case. Turner's formal equations were similar to the integral equation obtained earlier by Chambers[8] in his investigations of reflection by a cylindrical mirror. Again no scientific results for currents or fields were given. Barakat and Levin[9] reported in 1964 on their theoretical investigation of the slotted infinite cylinder using the least squares method of Sommerfeld. Their results covered the values of half-slot angle ϕ = 5°, 30°, 60°, 90°, 120°, 130°, 135°, 140°, 150° for the single value of the parameter $\eta = 2\pi/\lambda = 0.5$. They claim convergence of the numerical results in all cases for truncation of the infinite series representation of the scattered electric field at the fourth term. For the half cylindrical mirror (ϕ = 90°) they also present results for η = 0.25, 0.50, 0.75, 1.00 and 1.50. In Figure 24 below we superimpose their results for the slot electric field for $\eta = 1$ and ϕ = 90° on our results and shall discuss this further at that point in our report. We also include their slot field results for ϕ = 90° and η = 1.5 in Figure 25 displaying our results for ϕ = 90° and η = 2.0. This will be discussed at that point also. Barakat

---

8. L. Chambers, "Reflection of a Wave by a Cylindrical Mirror", Proc. Edinburgh Math. Soc. (2) 9, 1956

9. R. Barakat and E. Levin, "Diffraction of Plane Electromagnetic Waves by a Perfectly Conducting Cylindrical Lamina", Jour. Opt. Soc. of Amer. 54, 1089-1094, September 1964

and Levin also find numerically that the perturbation method of
Sommerfeld's is only applicable for small slot angles and long wave-
lengths, i.e. small η. Unfortunately, they appear to have an error
in their derivation of the perturbation solution. Consequently,
there is some question as to the validity of their conclusion con-
cerning narrow slots. Another attempt at the slotted cylinder
scattering problem was reported by Barth[10] in 1969. His approach was
fundamentally that of Morse and Feshbach. There was an essential
difference, however, in that Barth assumed a finite series for the
slot field. The corresponding finite number of series coefficients
were evaluated by satisfying the integral equation for the slot
field at an equal number of spatial points. This results in a
finite algebraic system of equations that is solvable at each wave-
length of interest. Barth calculated numerically the electric
field distribution in the slot at 500 MHz for a cylinder one meter
in radius. This corresponds to $\eta \approx 10$. The slot angle he con-
sidered was 60°. Specifically, Barth calculated the electric field
at the center of the slot in the Morse and Feshbach formulations
and further obtained an approximation to the slot electric field
distribution. His results are shown in Figure 50 juxtaposed on

---

10. M. J. Barth, "Interior Fields of a Slotted Cylinder Irradiated
with an Electromagnetic Pulse", Tech. Rep. No. AFSWC-TR-69-9,
Air Force Special Weapons Center, Kirtland Air Force Base,
New Mexico, August 1969

those of Morse and Feshbach and our own results. We reserve dis-

cussion of the comparison of these results until later. Koshparenok

and Shestopalov[11] published in 1971 a formal attempt at solving the

diffraction problem of the slotted cylinder for arbitrary η,

polarization, and direction of incidence of the linearly polarized

incoming plane wave. The approach used to derive the equations to

be solved is the Riemann-Hilbert method in the manner proposed

earlier by Agranovich et.al.[12] In this approach they explicitly

considered the long wavelength approximation for the case of

E-polarization for arbitrary incidence on a cylinder with a very

narrow longitudinal slot. The qualitative conclusions they

derived and their numerical calculations are very interesting. In

a later paper in our series of investigations we shall compare and

discuss these results with our results for the narrow slot problem.

This part of the slotted cylinder problem is of sufficient impor-

tance to merit a report devoted solely to it. The unfortunate

aspect of the Koshparenok and Shestopalov paper is the total

absence of numerical results for anything but the long wavelength-

narrow slot problem.

11. V. N. Koshparenok and V. P. Shestopalov, "Diffraction of a
     Plane Electromagnetic Wave by a Circular Cylinder with a Longi-
     tudinal Slot", Zh. Vychisl. i Mat. Fiz., 11, 719-737, 1971

12. Z. S. Agranovich, V. A. Marchenko and V. P. Shestopalov,
     "Diffraction of Electromagnetic Waves by Plane Metallic
     Gratings", Zh. tekhn. Fiz., 32, 4, 381, 1962

What constitutes, perhaps, the most extensive earlier treatment of scattering by axially slotted conducting cylinders is the work of Macrakis[13] His results are embodied in a Ph.D. dissertation to Harvard University in 1958. In this study the back-scattering cross-section was the quantity of primary interest. The approach was through the Green's function and resulted in the same integral equation for the slot electric field as obtained before by Morse and Feshbach[6]. Macrakis was fully cognizant of the difficulty involved in approximating the slot field if the aperture is a "wide" one. He further recognized the considerable difficulty one is faced with at an internal resonance and appropriately qualified his results at such frequencies. Keeping these constraints in mind, Macrakis assumed a static form with unknown constants for the slot field and obtained the back-scattering cross-section via a variational calculation. Although the results he obtained are somewhat limited in usefulness to narrow slots away from resonance, he did, nevertheless, provide analytical forms and numerical results. Probably the most important of his contributions are his published results of his measurements at many wavelengths. He reported on

6. P. M. Morse and H. Feshbach, "Methods of Theoretical Physics", Part II, 1387-1398, McGraw-Hill, New York, 1953

13. M. S. Macrakis, "Backscattering Cross-Section of Slotted Cylinders", Ph.D. Dissertation, Harvard University, Cambridge, MA, 1958

experimental data for back-scattering cross-sections for a narrow

slotted cylinder and a half cylindrical mirror. These measurements

were made using an adaption of Schmitt[14] from the parallel-plate

methods of Row[15] and Tang[16] called the "space separation method".

In the experimental set up the cylindrical tube when slotted results

in an effective change in ka. To bring the system back to the

desired ka value, a coaxial tuning probe along the axis of the

cylinder was utilized. The effect of this probe in the measurements

appears to be an open question. The data by Macrakis had not been

successfully interpreted and compared with theoretical results

(except at long wavelengths) prior to this time. In what follows

below we shall exhibit the results of comparing the work of Macrakis

with our theoretical predictions. At a later time we shall in a

subsequent report compare his results with more recent data.

We have now completed the review of the earlier attempts at the

problem of axially-polarized plane wave scattering by an axially

slotted cylinder. In the next two sections, to make this report

somewhat self-contained, we develop the theory and the numerical

14. H. J. Schmitt, "Backscattering Measurements with a Space Separation Method", Scientific Report No. 14, Cruft Laboratory, Harvard University, Cambridge, MA, 1957

15. R. V. Row, "Electromagnetic Diffraction in a Parallel Plate Region", Ph.D. Dissertation, Harvard U., Cambridge, MA, 1953

16. C. C. Tang, "Backscattering From Dielectric-Coated Infinite Cylindrical Obstacles", Ph.D. Dissertation, Harvard University, Cambridge, MA, 1956

method used to calculate our results. Following this we present

our results and then discuss our conclusions concerning them. Some

new observations on the behaviour of the electric field over the

aperture for incident radiation of wavelengths coinciding with

internal resonance are included in the discussion below.

II. INTEGRAL EQUATION FOR THE APERTURE TANGENTIAL ELECTRIC FIELD

The scattering problem being studied is essentially two-dimensional. Figure 1. illustrates all the necessary details of the geometry in a plane normal to the cylinder axis. The mono-chromatic, linearly polarized, plane wave is shown incident normal to the cylinder axis, symmetric with respect to the slot and with its electric field vector parallel to the z-axis. The latter coordinate axis is taken, for simplicity, coincident with the axis of the slotted cylinder. We assume harmonic time dependence of the form $e^{-i\omega t}$ and shall suppress the explicit time exponential from appearing throughout the following equations. The incident fields are then given by

$$(1) \qquad \vec{E}^i \ (\vec{r}) \ = \ E_z^i \ (\rho,\varphi) \ \vec{e}_z \ = \ E_0 \, e^{-ik\rho\cos\varphi} \ \vec{e}_z$$

and

$$(2) \qquad \vec{H}^i \ (\vec{r}) \ = \ H_y^i \ (\rho,\varphi) \ \vec{e}_y \ = \ H_0 \ e^{-ik\rho\cos\varphi} \ \vec{e}_y$$

where

$$(3) \qquad k \ = \ \frac{\omega}{c} \ = \ \frac{2\pi}{\lambda}$$

and $\vec{e}_z$ and $\vec{e}_y$ are respectively unit vectors along the positive z and y axes. In MKS units, with μ_0 and ϵ_0 as respectively the

magnetic permeability and electrical permitivity of free space, the

incident electric and magnetic field amplitudes are related as

follows:

(4) $\qquad E_0 = \sqrt{\mu_0/\epsilon_0} \ H_0$

Only a z-component of electric field exists in the problem.

This field at a source free point satisfies the homogeneous scalar

wave equation

(5) $\qquad \nabla^2 E_z(\vec{r}) + k^2 E_z(\vec{r}) = 0$

In polar cylindrical coordinates the magnetic field components can

be obtained from the axial electric field as follows

(6) $\qquad H_\rho(\rho,\varphi) = -(1/i\omega\mu_0\rho) \dfrac{\partial E_z(\rho,\varphi)}{\partial\varphi}$

(7) $\qquad H_\varphi(\rho,\varphi) = -(1/i\omega\mu_0) \dfrac{\partial E_z(\rho,\varphi)}{\partial\rho}$

One immediate important bit of information due to the symmetry is

that the electric field must be an even function of the angle φ.

For the interior region of the cylinder of radius a we assume

the form of the solution for the electric field to be

$$(8) \qquad E_z^{(1)} (\rho,\varphi) \;=\; \sum_{m=0}^{\infty} \frac{J_m (k\rho)}{J_m (\eta)} \, A_m \, \cos m\varphi$$

where we denote the region of space for $\rho < a$ by the superscript (1) and where A_m is an unknown expansion coefficient and finally

$$(9) \qquad \eta \equiv ka \equiv 2\pi a/\lambda$$

In the region exterior to the slotted cylinder we concoct a solution of the scalar wave equation (5) which is composed of two parts. One of these is the well-known field that would be present if there were no slot in the cylinder[17] This is the first sum in equation (10) immediately below. The remaining piece is a contribution to the field due solely to the presence of the slot. This is the second sum in eq. (10). Thus, in the exterior region which we denote by the superscript (2) we have

$$(10) \quad E_z^{(2)} (\rho,\varphi) \;=\; E_0 \sum_{m=0}^{\infty} \epsilon_m (-i)^m \left[J_m (k\rho) \;-\; \frac{J_m (\eta)}{H_m^{(1)} (\eta)} H_m^{(1)} (k\rho) \right] \cos m\varphi$$

$$+ \sum_{m=0}^{\infty} \frac{H_m^{(1)} (k\rho)}{H_m^{(1)} (\eta)} \, C_m \, \cos m\varphi \qquad \text{for } \rho < a$$

---

17. J. J. Bowman, T.B.A. Senior and P.L.E. Uslenghi, eds. "Electro-magnetic and Acoustic Scattering by Simple Shapes", p 92-93, North-Holland Publishing Co., Amsterdam, The Netherlands, 1969

where C_m is an unknown expansion coefficient and

$$(11) \qquad \epsilon_m = \begin{cases} 1 & m = 0 \\ 2 & m = 1, 2, 3, \ldots \end{cases}$$

We note at once that the interior and exterior E_z fields must be identical over the slot region and both vanish on the conductor. Then from eqs. (8) and (10) we find

$$(12) \qquad \sum_{m=0}^{\infty} A_m \cos m\varphi = \sum_{m=0}^{\infty} C_m \cos m\varphi$$

Since eq. (12) holds for all φ (at $\rho = a$) we must have

$$(13) \qquad C_m \equiv A_m \text{ for all } m$$

We can then replace the expansion coefficients in eq. (10) using the identity of eq. (13).

Now let us introduce some convenient notation. Let us denote the electric field in the slot by $\mathcal{E}(\varphi)$. Then we can write from eqs. (8) and (10)

$$(14) \qquad E_z(a,\varphi) = E_z^{(1)}(a,\varphi) = E_z^{(2)}(a,\varphi) = \begin{cases} \mathcal{E}(\varphi) & -\varphi_0 < \varphi < \varphi_0 \\ 0 & \varphi_0 < \varphi < -\varphi_0 \end{cases}$$

or equivalently we can write

21

(15) $\quad \displaystyle\sum_{m=0}^{\infty} A_m \cos m\varphi = \begin{cases} \mathcal{e}(\varphi) & -\varphi_0 < \varphi < \varphi_0 \\ 0 & \varphi_0 < \varphi < -\varphi_0 \end{cases}$

Consequently we can invert and express the unknown expansion coefficients in terms of the electric field over the slot as follows

(16) $\quad A_m = \dfrac{\epsilon_m}{2\pi} \displaystyle\int_{-\varphi_0}^{\varphi_0} d\varphi \; \mathcal{e}(\varphi) \; \cos m\varphi$

Clearly then determination of the electric field over the slot constitutes one way of solving the scattering problem.

Taking advantage of the requirement that the azimuthal component of the magnetic field must be continuous across the slot will lead us to an integral equation for the slot electrical field. We next show this. First we have necessarily

(17) $\quad H_{\varphi}^{(1)}(a,\varphi) = H_{\varphi}^{(2)}(a,\varphi) \qquad$ for $|\varphi| < \varphi_0$

Then from eqs. (7), (8), and (10) we obtain

(18) $\quad \displaystyle\sum_{m=0}^{\infty} \dfrac{J_m'(\eta)}{J_m(\eta)} A_m \cos m\varphi = \sum_{m=0}^{\infty} \dfrac{H_m^{(1)'}(\eta)}{H_m^{(1)}(\eta)} A_m \cos m\varphi \; +$

$\qquad E_0 \displaystyle\sum_{m=0}^{\infty} \epsilon_m (-i)^m \left[J_m'(\eta) - \dfrac{J_m(\eta)}{H_m^{(1)}(\eta)} H_m^{(1)'}(\eta) \right] \cos m\varphi$

$\qquad\qquad\qquad\qquad\qquad\qquad\qquad$ for $|\varphi| < \varphi_0$

after some simple rearrangement of terms in eq. (18) and use of the

Wronskian relation for J_m and $H_m^{(1)}$ namely

(19) $\qquad J_m'(\eta) H_m^{(1)}(\eta) - J_m(\eta) H_m^{(1)}{}'(\eta) = \dfrac{-2}{i\pi\eta}$

we get the simpler relation

(20) $\displaystyle\sum_{m=0}^{\infty} \left\{ A_m / J_m(\eta) H_m^{(1)}(\eta) \right\} \cos m\varphi = E_0 \sum_{m=0}^{\infty} \left\{ \epsilon_m (-i)^m / H_m^{(1)}(\eta) \right\} \cos m\varphi$

$\qquad\qquad\qquad\qquad\qquad\qquad\qquad\qquad$ for $|\varphi| < \varphi_0$

We shall need notation for the surface current for the conducting

cylinder without a slot. This quantity, which is well-known[17], we

denote by $K_z^o(\varphi)$:

(21) $\qquad K_z^o(\varphi) = \left(\dfrac{2}{\pi\eta}\right) \sqrt{\dfrac{\epsilon_0}{\mu_0}}\ E_0 \sum_{m=0}^{\infty} \left\{ \epsilon_m (-i)^m / H^{(1)}(\eta) \right\} \cos m\varphi$

Noting that the right hand sides of eqs. (20) and (21) differ merely

by a constant factor we find from eqs. (20), (21) and (16) the

integral equation for the aperture electric field:

(17)   J. J. Bowman, T.B.A. Senior and P. L. E. Uslenghi, eds.
        "Electromagnetic and Acoustic Scattering by Simple Shapes",
        p 92-93, North-Holland Publishing Co., Amsterdam, The
        Netherlands, 1969

$$(22) \quad \int_{-\varphi_0}^{\varphi_0} d\varphi' \mathcal{E}(\varphi') \left[\sum_{m=0}^{\infty} \frac{\epsilon_m}{2\pi} \frac{\cos m(\varphi-\varphi')}{J_m(\eta) H_m^{(1)}(\eta)} \right] = \frac{\pi\eta}{2} \sqrt{\frac{\mu_0}{\epsilon_0}} K_z^0(\varphi)$$

$$\text{for } |\varphi| < \varphi_0$$

Eq. (22) which is the relation we were seeking was obtained after some simple manipulation of trigonometric identities as follows

$$\int_{-\varphi_0}^{\varphi_0} d\varphi' \mathcal{E}(\varphi') \sin m\varphi \sin m\varphi' = \sin m\varphi \int_{-\varphi_0}^{\varphi_0} d\varphi' \mathcal{E}(\varphi') \sin m\varphi'$$

but $\mathcal{E}(-\varphi') = \mathcal{E}(\varphi')$. Then changing φ' into $-\varphi'$ gives

$$\int_{\varphi_0}^{-\varphi_0} d\varphi' \mathcal{E}(-\varphi') \sin m\varphi' = \int_{-\varphi_0}^{\varphi_0} d\varphi' \mathcal{E}(\varphi') \sin m\varphi' =$$

$$+ \int_{-\varphi_0}^{\varphi_0} d\varphi' \mathcal{E}(\varphi') \sin m\varphi' \equiv 0$$

Note that the sought after aperture field is given in Eq. (22) in terms of the surface current density that would be present over the corresponding angular portion of the cylinder in the absence of the aperture.

Before continuing to the next section on the surface current density for the slotted cylinder we shall briefly touch on some significant points regarding Eq. (22). First upon observation of

24

the kernel of the integral operator we find that it becomes singular at the zeros of the Bessel functions. Consequently, certain requirements must be placed on the electric field in the slot at the frequencies which give rise to the roots of the Bessel functions. The occurrence of these singularities is not unexpected since we have coupled the interior of the cylinder to its exterior via the existence of the slot. Thus we see that the singularities mentioned occur at the well-known interior modes[18] of the closed infinite circular conducting cylinder. A second characteristic of the kernel that we note is that it is rigorously a divergent infinite series. That this is the situation can be seen by using the large order approximations for $J_m(\eta)$[19]

$$(23a) \qquad J_m(\eta) \xrightarrow[m \to \infty]{} \frac{1}{\sqrt{2\pi m}} \left(\frac{e\eta}{2m}\right)^m$$

also

$$(23b) \qquad H_m^{(1)}(\eta) \xrightarrow[m \to \infty]{} (-i) \sqrt{2/\pi m}\left(\frac{e\eta}{2m}\right)^{-m}$$

---

18. G. Goubau, "Electromagnetic Waveguides and Cavities", p 185-191, Pergamon Press, New York, 1961

19. A. Erdélyi, Ed., "California Institute of Technology, Bateman Manuscript Project. Higher Transcendental Functions, Vol. II", eqs. 14 and 15, p 87, McGraw-Hill Book Co., Inc., N. Y., N. Y. 1953

Then it follows in this limit that

$$(23c) \qquad J_m(\eta) H_m^{(1)}(\eta) \xrightarrow[m \to \infty]{} -i/\pi m$$

and in turn the kernel diverges as can be easily seen.

Attempts to solve eq. (22) were reviewed in the previous section. All the earlier efforts focussed upon assuming a form for the electric field in the slot which permitted analytic integration. This appears to be the only readily tractable approach with the kernel of the integral operator in its present form. The very nature of this kernel precludes a direct numerical solution except for certain restricted ranges of the physical parameters. In particular we showed[4] that the kernel reduces to a manageable form in the Rayleigh limit and hence in the long wavelength approximation a solution can be found.

4. J. N. Bombardt and L. F. Libelo (NAVSURFWPNCEN) "S.E.R.A.: IV. Slotted Cylinders and Cylindrical Strips in the Rayleigh Limit, HDL-RT-1607, Harry Diamond Laboratories, Washington, D. C., August 1972

III. INTEGRAL EQUATION FOR THE SURFACE CONDUCTION CURRENT

On the boundary surface at $\rho=a$ the surface conduction current is defined by

(24) $\vec{K}(\varphi) = \vec{e}_\rho \times \left[\vec{H}^{(2)}(a,\varphi) - \vec{H}^{(1)}(a,\varphi) \right]$

Then, as is to be expected from the symmetry of the problem, the surface current has only a component in the Z-direction. This current is given by

(25) $K_z(\varphi) = H_\varphi^{(2)}(a,\varphi) - H_\varphi^{(1)}(a,\varphi)$

Using eqs. (7), (8), (10) and (13) we then obtain

(26) $K_z(\varphi) = \left(\dfrac{2}{\pi \eta} \right) \sqrt{\dfrac{\epsilon_\rho}{\mu_o}} \left\{ E_o \sum_{m=0}^{\infty} \dfrac{\epsilon_m (-i)^m}{H_m^{(1)}(\eta)} \cos m\varphi - \sum_{m=0}^{\infty} \dfrac{A_m \cos m\varphi}{J_m(\eta) H_m^{(1)}(\eta)} \right\}$

Each term in eq. (26) is readily identified. The first summation is the surface current on the infinite cylinder in the absence of the slot. The second summation containing the expansion coefficients, A_m, therefore represents the change in the total surface current due to the presence of the axial slot.

For convenience let us introduce a new form for the unknown expansion coefficients A_m, namely

(27) $\quad B_m \equiv E_0 \dfrac{\epsilon_m (-i)^m}{H_m^{(1)}(\eta)} - \dfrac{A_m}{J_m(\eta) H_m^{(1)}(\eta)} \qquad\qquad m = 0, 1, 2, \ldots$

This enables us to write the surface current more compactly as

(28) $\quad K_z(\varphi) = \left(\dfrac{2}{\pi\eta}\right) \sqrt{\dfrac{\epsilon_0}{\mu_0}} \displaystyle\sum_{m=0}^{\infty} B_m \cos m\varphi$

We next introduce some further useful notation. Since the current density vanishes over the slot region we write

(29) $\quad K_z(\varphi) = \begin{cases} 0 & 2\pi - \varphi < \varphi < \varphi_0 \\ \mathcal{K}(\varphi) & \varphi_0 < \varphi < 2\pi - \varphi_0 \end{cases}$

Thus $\mathcal{K}(\varphi)$ explicitly denotes the current density on the conducting surface itself. Inverting eq. (28) we obtain in the new notation of eq. (29)

(30) $\quad (2/\pi\eta) \sqrt{\epsilon_0/\mu_0}\, B_m = \dfrac{\epsilon_m}{2\pi} \displaystyle\int_{\varphi_0}^{2\pi - \varphi_0} d\varphi' \, \mathcal{K}(\varphi') \cos m\varphi'$

To derive the integral equation for the surface current consider eq. (28) for values of φ corresponding to the conducting surface, i.e. $\varphi_0 < \varphi < 2\pi - \varphi_0$. Start with eq. (27) multiplied thru by $J_m(\eta) H_m^{(1)}(\eta) \cos m\varphi$ and then summed on m, i.e.

$$(31) \quad \sum_{m=o}^{\infty} B_m J_m(\eta) H_m^{(1)}(\eta) \cos m\varphi = E_o \sum_{m=o}^{\infty} \epsilon_m (-i)^m J_m(\eta) \cos m\varphi$$

$$- \sum_{m=o}^{\infty} A_m \cos m\varphi$$

The first summation on the right hand side is merely the incident electric field, E_z^i, at the cylindrical surface $\rho = a$. According to eq. (15) the second sum vanishes identically on the metal. We then have the desired integral equation after manipulating the constants around and substituting in for B_m from eq. (30).

$$(32) \quad \frac{\eta}{4}\sqrt{\frac{\mu_o}{\epsilon_o}} \int_{\varphi_o}^{2\pi-\varphi_o} d\varphi' \, \varkappa(\varphi)\left[\sum_{m=o}^{\infty} \epsilon_m J_m(\eta) H_m^{(1)}(\eta) \cos m(\varphi-\varphi')\right]$$

$$= E_z^i(a,\varphi) \qquad \varphi_o < \varphi < 2\pi - \varphi_o$$

The kernel in eq. (32) can be simplified through the identity[20]

$$(33) \quad \sum_{m=o}^{\infty} \epsilon_m J_m(\eta) H_m^{(1)}(\eta) \cos m(\varphi-\varphi') = H_o^{(1)}\left(2\eta\left|\sin\left(\frac{\varphi-\varphi'}{2}\right)\right|\right)$$

20. J. A. Stratton, "Electromagnetic Theory" eq. (11) p 374, McGraw-Hill Book Co. Inc., N. Y., N. Y. 1941

Finally we have for the surface current integral equation

$$
(34) \quad \frac{\eta}{4} \sqrt{\frac{\mu_0}{\epsilon_0}} \int_{\varphi_0}^{2\pi-\varphi_0} d\varphi' \; \mathcal{K}(\varphi') \; H_0^{(1)} \left(2\eta \left| \sin\left(\frac{\varphi-\varphi'}{2} \right) \right| \right) = E_z^i (a,\varphi)
$$

$$
\text{for} \quad \varphi_0 < \varphi < 2\pi - \varphi_0
$$

Note that the surface current density on the conductor is given in terms of the incident electric field over the same azimuthal range (i.e. angles corresponding to that portion of the cylinder $\rho=a$ occupied by conductor).

Just as in the case of the aperture field integral equation no exact analytical solution has been reported for the surface current on the conductor. This time however the kernel of the integral operator in eq. (34) can be handled on the computer with confidence. Consequently a direct numerical approach for solving eq. (34) is feasible. The results of such calculation will in fact be shown below. It should also be pointed out that eq. (34) simplifies considerably in the Rayleigh region. We have already published[4] the analytical results obtained for narrow cylindrical strips.

4. J. N. Bombardt and L. F. Libelo (NAVSURFWPNCEN) "S.E.R.A.: IV. Slotted Cylinders and Cylindrical Strips in the Rayleigh Limit", HDL-RT-1607, Harry Diamond Laboratories, Washington, D. C., August 1972

At this stage in the development of the theory used in resolving the scattering problem we pause momentarily to make a brief comment on the surface current near the edges of the conductor. At an edge the current is defined in terms of a magnetic field component that is normal to the edge. For a perfect conductor of infinitesimal thickness the edge conditions require that field components parallel to the edge be bounded whereas those normal to the edge are singular at the edge. As a consequence of this the surface current is singular at the edges of the slot on our axially slotted perfectly conducting infinite cylinder. We shall return to discuss this subject in the following development below.

One further point will be discussed at this stage. In an earlier report[3] we presented a connective integral equation containing as simultaneous unknowns the aperture field and the surface conduction current. This alternative approach to the solution of the problem contained well-behaved kernels, i.e. they are functions with no singularities. However, direct numerical solution of that equation was not attempted as it was felt that such an approach would require an inordinate amount of computer time. This we believed to be the case since both $\mathcal{E}(\varphi)$ the aperture field and $K(\varphi)$ the surface conduction current had to be computed simultaneously.

---

3.   J. N. Bombardt and L. F. Libelo (NAVSURFWPNCEN) "S.E.R.A.: III. An Alternative Integral Equation with Analytic Kernels for the Slotted Cylinder Problem", HDL-TR-1588, Harry Diamond Laboratories, Washington, D. C., August 1972

IV.   SLOT ADMITTANCE AND CONDUCTOR IMPEDANCE

Eq. (22) is an integral equation relating the aperture electric field to the surface current on the conducting cylinder without a slot for the portion coincident with the slot, i.e. $|\varphi| < \varphi_0$. Let us rewrite the electric field in the slot as follows

$$(35) \qquad \mathcal{E}(\varphi) = \sum_{n=0}^{\infty} V_n \, \Psi_n^{(E)}(\varphi) / a \qquad\qquad |\varphi| < \varphi_0$$

where we have assumed $\mathcal{E}(\varphi)$ expandable over the slot region in the set of expansion functions $\Psi_n^{(E)}(\varphi)$ with the unknown expansion coefficients V_n. This expansion for the electric field in the aperture must, of course, satisfy edge conditions. Defining an inner product for the expansion functions as follows

$$(36) \qquad \Psi_{n\ell}^{(E)} \equiv \, <\Psi_n^{(E)}(\varphi), \cos\ell\varphi> \, \equiv \int_{-\varphi_0}^{\varphi_0} d\varphi \, \Psi_n^{(E)}(\varphi) \cos(\ell\varphi) \, d\varphi \quad n,\ell=0,1,2,\ldots$$

we can then rewrite the integral equation for the aperture field as

$$(37) \qquad \sum_{\ell,n=0}^{\infty} \left\{ \epsilon_\ell V_n \, \Big/ \, \left[\left(\frac{\pi\eta}{2}\right) \sqrt{\frac{\mu_0}{\epsilon_0}} \, J_\ell(\eta) H_\ell^{(1)}(\eta) \right] \right\} \Psi_{n\ell}^{(E)} \cos(\ell\varphi) = 2\pi a K_z^0(\varphi)$$

$$\text{for } |\varphi| < \varphi_0$$

Next let us introduce a second set of weighting (or testing functions); $\left\{ \Phi_j^{(E)}(\varphi) \right\}$ and then we can write some further inner products with this set of basis functions, namely

(38) $\Phi_{m\ell}^{(E)} \equiv <\Phi_m^{(E)}(\varphi), \cos\ell\varphi> \equiv \int_{-\varphi_0}^{\varphi_0} d\varphi \; \Phi_m^{(E)}(\varphi) \cos(\ell\varphi)$ $m, \ell = 0, 1, 2, \ldots$

and

(39) $<\Phi_m^{(E)}(\varphi), K_z^0(\varphi)> \equiv \int_{-\varphi_0}^{\varphi_0} d\varphi \; \Phi_m^{(E)}(\varphi) K_z^0(\varphi)$ $m = 0, 1, 2, \ldots$

Now we can utilize eqs. (38) and (39) to rewrite eq. (37) in the form

(40) $\displaystyle\sum_{n=0}^{\infty} V_n \left\{ \sum_{\ell=0}^{\infty} \frac{\epsilon_\ell \; \Phi_{m\ell}^{(E)} \Psi_{n\ell}^{(E)}}{\left[\left(\frac{\pi\eta}{2}\right)\sqrt{\frac{\mu_0}{\epsilon_0}} J_\ell(\eta) H_\ell^{(1)}(\eta)\right]} \right\} = 2\pi a <\Phi_m^{(E)}(\varphi), K_z^0(\varphi)>$

for $m = 0, 1, 2, \ldots$

Let us interject at this stage in the development a comment that is probably needed. We have treated the mathematical rigour concerning complete sets of basis function and projections onto their elements in a seemingly cavalier fashion. Although we shall make no attempt in this paper to establish the limitations on this approach let it suffice to merely point out that what we are doing here holds under

wide enough latitude to justify our derivations. With this in mind

let us then proceed.

For convenience we shall define the quantity

$$(41) \quad Y_{mn} \equiv \sum_{\ell=0}^{\infty} \frac{\epsilon_\ell}{\left[\left(\frac{\pi \eta}{2} \right) \sqrt{\frac{\mu_0}{\epsilon_0}} J_\ell(\eta) H_\ell^{(1)}(\eta) \right]} \Phi_{m\ell}^{(E)} \psi_{n\ell}^{(E)}$$

which upon simple inspection is found to possess the dimensions of an

admittance through the only parameter that is not dimensionless,

namely $\sqrt{\mu_0/\epsilon_0}$ in the denominator. Introducing the further notation

$$(42) \quad I_m^0 \equiv 2\pi a <\Phi_m^{(E)}(\varphi), K_z^0(\varphi)>$$

we find eq. (42) denotes a quantity with dimensions of just current

alone (recall that K_z^0 has dimensions of current per unit length).

In this new notation we can rewrite eq. (40) compactly as

$$(43) \quad \sum_{n=0}^{\infty} Y_{mn} V_n = I_m^0 \qquad m=0,1,2,\ldots$$

Formally then we define an "admittance matrix"

$$(44) \quad Y \equiv \begin{bmatrix} Y_{mn} \end{bmatrix} \qquad m,n=0,1,2,\ldots$$

where Y is the matrix whose elements are the Y_{mn}. Note that this matrix has an infinite number of columns and an infinite number of rows. Consequently this quantity should be handled with a degree of caution when manipulating with it. Similarly we define "voltage and current vectors"

$$(45) \qquad V \equiv \left[v_n \right] \qquad\qquad n = 0, 1, 2, \ldots$$

$$(46) \qquad I^\circ \equiv \left[I^\circ_m \right] \qquad\qquad m = 0, 1, 2, \ldots$$

where the voltage vector V has components V_n (note there are an infinite number of such components) and the current vector I° has components I°_m (again there are an infinite number of components). Now we can formally rewrite eq. (43) as

$$(47) \qquad Y \cdot V = I^\circ$$

If we formally introduce the inverse of the matrix defined in eq. (44) which we shall denote by Y^{-1} we obtain then

$$(48) \qquad V = Y^{-1} I^\circ$$

Eq. (48) formally states the solution of the aperture electric field integral equation, i.e. eq. (22).

We thus find that the integral equation for the electric field in the aperture leads to a statement of Ohm's law in matrix form. An admittance matrix for the aperture connects a known current vector to an unknown voltage vector. The integral equation for the surface current density on the conductor leads to a complementary statement of Ohm's law. This will be demonstrated next.

Eq. (32) is one form of the integral equation for the surface current density that relates this current to the incident electric field on the conductor. We expand the surface current density as follows

$$(49) \qquad \mathcal{K}(\varphi) \equiv \sum_{n=0}^{\infty} a^{-1} I_n \; \Psi_n^{(K)}(\varphi)$$

where the I_n are unknown expansion coefficients and the $\Psi_n^{(K)}(\varphi)$ are a basis of expansion functions for the surface current. Here also we must require that the expansion in eq. (49) satisfy the conditions at the slot edges. As above we define the inner products

$$(50) \quad \Psi_{n\ell}^{(K)} \equiv <\Psi_n^{(K)}(\varphi), \cos\ell\varphi> \equiv \int_{\varphi_0}^{2\pi-\varphi_0} d\varphi \; \Psi_n^{(K)}(\varphi) \cos\ell\varphi \; ; \; n,\ell = 0, 1, 2, ..$$

This then enables us to rewrite eq. (32) as follows

(51) $\displaystyle\sum_{n=o}^{\infty} I_n \sum_{\ell=o}^{\infty} \epsilon_\ell \left[\left(\frac{\pi\eta}{2}\right)\sqrt{\frac{\mu_o}{\epsilon_o}} J_\ell(\eta) H_\ell^{(1)}(\eta) \right] \Psi_{n\ell}^{(K)} \cos\ell\varphi = 2\pi a E_z^i(a,\varphi)$

$$\text{for } \varphi_o \leq \varphi \leq 2\pi - \varphi_o$$

Introducing another set of weighting functions; $\left\{ \Phi_m^{(K)}(\varphi) \right\}$ we again

define the inner products with this set of functions

(52) $\quad \Phi_{m\ell}^{(K)} \equiv <\Phi_m^{(K)}(\varphi), \cos\ell\varphi> \equiv \displaystyle\int_{\varphi_o}^{2\pi-\varphi_o} d\varphi\ \Phi_m^{(K)}(\varphi)\cos\ell\varphi \ ; \quad m,\ell = 0,1,2,..$

and analogous to eq. (39)

(53) $\quad <\Phi_n^{(K)}(\varphi), E_z^i(a,\varphi)> \equiv \displaystyle\int_{\varphi_o}^{2\pi-\varphi_o} d\varphi\ \Phi_m^{(K)}(\varphi) E_z^i(a,\varphi) \qquad m = 0,1,2,..$

With the help of eqs. (52) and (53) we can now rewrite eq. (51) in

the form

(54) $\displaystyle\sum_{n=o}^{\infty} I_n \left\{ \sum_{\ell=o}^{\infty} \left[\epsilon_\ell \left(\frac{\pi\eta}{2}\right) \sqrt{\frac{\mu_o}{\epsilon_o}} J_\ell(\eta) H_\ell^{(1)}(\eta) \right] \Phi_{m\ell}^{(K)} \Psi_{n\ell}^{(K)} \right\} =$

$$2\pi a <\Phi_m^{(K)}(\varphi), E_z^i(\varphi)> \qquad \text{for } m=0,1,2,..$$

Again we can simplify the appearance of this relation by

introducing the notation

(55) $\quad Z_{mn} \equiv \sum_{\ell=0}^{\infty} \left[\epsilon_\ell \left(\frac{\pi\eta}{2} \right) \sqrt{\frac{\mu_0}{\epsilon_0}} \, J_\ell(\eta) H_\ell^{(1)}(\eta) \right] \Phi_{m\ell}^{(K)} \, \Psi_{n\ell}^{(K)}$

$$\text{for} \quad m, n = 0, 1, 2, ..$$

This quantity upon inspection is easily found to possess the dimensions of an impedance. With the further definition of the quantity

(56) $\quad V_m^i \equiv 2\pi a < \Phi_m^{(K)}(\varphi), E_z^i(\varphi) >$

which obviously is a "voltage", we can cast eq. (54) into the more compact relation

(57) $\quad \sum_n I_n Z_{mn} = V_m^i \qquad\qquad m = 0, 1, 2, ..$

Formally then we can define an "impedance matrix"

(58) $\quad Z \equiv \left[Z_{mn} \right] \qquad\qquad m, n = 0, 1, 2, ..$

with matrix elements Z_{mn} , a "current vector"

(59) $\quad I \equiv \left[I_n \right] \qquad\qquad n = 0, 1, 2, ..$

with components I_n , and a "voltage vector"

(60) $V^i \equiv \left[V_m^i \right]$ $m = 0, 1, 2, ..$

with components V_m^i. Again it must be emphasized that Z has an infinite number of rows and an infinite number of columns, and I and V^i have an infinite number of components. Eq. (57) can be written formally as

(61) $Z \, I = V^i$

Then if we introduce formally the inverse of the impedance matrix we obtain the formal solution

(62) $I = Z^{-1} \, V^i$

We then observe that the integral equation for the surface current density on the conductor does indeed lead to a statement of Ohm's law in matrix form. Here, however, an impedance matrix for the conductor connects a known voltage vector to an unknown current vector.

The procedure followed in deriving eqs. (48) and (62) has become known and accepted by all but a handful of diehard dissidents

among electromagneticians as the "Method of Moments"[21-22]. We shall

return to further discuss this approach later in what follows.

Let us return to consider Macrakis'[13] earlier study. In his

work he discussed integral equations for the aperture electric field

and for the surface current density on the conductor in terms of

what he called "dual" quantities. That is, either of these integral

equations could be generated from the other one by introducing the

appropriate "dual" quantities. Macrakis then inferred that there

is a single unknown quantity, in this diffraction problem, which is

comprised of two parts: the electric field in the slot and the

surface current on the conductor.

We have presented an alternative view to that of Macrakis. In

our view of the problem the integral equation for the aperture

electric field and that for the surface current on the conductor can

be thought of as merely complementary statements of Ohm's law. The

solution of either integral equation can be used to generate all

quantities of interest in the scattering problem. It is interesting

21. R. F. Harrington, "Matrix Methods for Solving Field Problems",
    Technical Report No. RADC-TR-66-351 Rome Air Development Center,
    Griffiss Air Force Base, New York 1966

22. R. F. Harrington, "Field Computation by Moment Methods",
    The Macmillan Co., New York, N. Y. 1968

13. M. S. Macrakis, "Backscattering Cross-Section of Slotted
    Cylinders", Ph.D. Dissertation, Harvard University,
    Cambridge, MA, 1958

and significantly important to observe the generalization that, in principle, construction of such complementary formulations should be possible for any simply shaped enclosure with an aperture when illuminated by an electromagnetic field.

V.   THE BACK-SCATTERING CROSS-SECTION

Since Macrakis[13] reported on measured back-scattering cross-section per unit length for several slot angles we can compare some of our theoretical predictions with his results. For this reason we present in this section a short derivation of this quantity. The actual back-scattering cross-section expression[23] is a conventional one and we shall merely start our derivation with it.

$$(63) \quad \sigma_B = \lim_{\rho=\infty} 2\pi\rho |E_z^s (\rho,\varphi=0)|^2 / |E_0|^2$$

where E_z^s is the scattered field from the cylinder. The back-scattering cross-section, or b.s.c.s. for short, can be obtained from either the surface current on the conductor or the electric field in the aperture. We shall obtain first the b.s.c.s. from the current.

The scattered electric field can be readily obtained from the external electric field as given in eq. (10) by subtracting off the incident field. We have

13. M. S. Macrakis, "Backscattering Cross-Section of Slotted Cylinders", Ph.D. Dissertation, Harvard University, Cambridge, MA, 1958

23. R. W. P. King and T. T. Wu, The "Scattering and Diffraction of Waves", eq. 18.1, p 68, Harvard University Press, Cambridge, MA, 1959

(64) $\quad E_z^s \ (\rho, \varphi) = \sum_{m=o}^{\infty} \left[-E_0 \, \epsilon_m \, (-i)^m \, J_m(\eta) + A_{m_-} \right] \dfrac{H_m^{(1)}(k\rho)}{H_m^{(1)}(\eta)} \cos m\varphi$

Using eq. (27) which defines the coefficient B_m converts this to

(65) $\quad E_z^s \ (\rho, \varphi) = -\sum_{m=o}^{\infty} B_m \, J_m(\eta) H_m^{(1)}(k\rho) \cos m\varphi$

We also need the asymptotic form of the Hankel function for large argument;

(66) $\quad H_m^{(1)}(k\rho) \xrightarrow[\rho \to \infty]{} \sqrt{\dfrac{2}{\pi k\rho}} \ e^{i(k\rho - \pi/4) - im\pi/2}$

Using this in eq. (65) we get for the b.s.c.s.

(67) $\quad \sigma_B = \dfrac{4}{k} \left| \sum_{m=o}^{\infty} (-i)^m \, J_m(\eta) B_m \right|^2 \Big/ |E_0|^2$

Substituting for B_m from eq. (30) this becomes

(68) $\quad \sigma_B = \dfrac{\eta^2}{4k} \left| \int_{\varphi_0}^{2\pi - \varphi_0} d\varphi' \, \dfrac{\mathcal{K}(\varphi')}{H_0} \sum_{m=o}^{\infty} \epsilon_m (-i)^m \, J_m(\eta) \cos m\varphi' \right|^2$

or alternatively

$$(69) \qquad \sigma_B = \frac{\eta^2}{4k} \left| \int_{\varphi_0}^{2\pi - \varphi_0} d\varphi' \; \frac{E_z^i(a,\varphi')}{E_0} \; \frac{K(\varphi')}{H_0} \right|^2$$

A similar derivation yields for the b.s.c.s. in terms of the aperture electric field

$$(70) \qquad \sigma_B = \frac{\eta^2}{4k} \int_{-\pi}^{\pi} d\varphi' \; \frac{E_z^i(a,\varphi')}{E_0} \; \frac{K_z^0(\varphi')}{H_0} - \int_{-\varphi_0}^{\varphi_0} d\varphi' \; \frac{e(\varphi')}{E_0} \; \frac{K_z^0(\varphi')^2}{H_0}$$

We can also consider the b.s.c.s. in another form which yields some physical insight into the problem. Thus let us write the scattered field as the sum of two contributions, namely the scattered field in the absence of a slot which we shall call $E_z^0(\rho,\varphi=0)$ and that contribution of the scattered field which arises due to the presence of the slot which we shall denote by $E_z^{\varphi_0}(\rho,\varphi=0)$. We then have

$$(71) \qquad \sigma_B = \lim_{\rho \to \infty} 2\pi\rho \left| E_z^0(\rho,\varphi=0) + E_z^{\varphi_0}(\rho,\varphi=0) \right|^2 \Big/ \left| E_0 \right|^2$$

It is clear from the explicit form of eq. (71) then that the b.s.c.s. should exhibit maxima and minima at wavelengths where the component scattered fields constructively and destructively interfere with one another. Since the scattered fields are separately bounded the resonances they give rise to must in turn be finite in amplitude. We shall discuss these resonances below when we present the results.

44

VI. THE FORMULATION OF THE NUMERICAL METHOD OF CALCULATION

In part IV of this report we developed "admittance" and "impedance" matrices of infinite order. The approach used to obtain these was the so-called method-of-moments which Harrington[21] developed and applied to electromagnetic field problems[22]. Now it should be realized that matrices of infinite order are as a rule not the ordinary garden variety matrix that one usually has to deal with in classical electromagnetic phenomena and consequently a considerable amount of caution must be exercised in manipulating them. For example our impedance and admittance matrices can be inverted only in special situations. Of course a diagonal matrix of infinite order can be inverted (provided its trace is not null). In the case where the set of expansion functions, $\Psi_n^{(\ )}(\varphi)$ and the set of weight-int functions $\Phi_m^{(\ )}(\varphi)$ are "orthogonal" sets over the range of the independent variable the "impedance" and "admittance" matrices are diagonal. Classical eigenfunction methodology for solving integral equations relies on the availability of such complete sets of orthogonal functions. On the other hand, numerical implementation of the "method-of-moments" restricts the matrix of inner products to

21. R. F. Harrington, "Matrix Methods for Solving Field Problems", Technical Report No. RADC-TR-66-351 Rome Air Development Center, Griffiss Air Force Base, New York 1966

22. R. F. Harrington, "Field Computation by Moment Methods", The Macmillan Co., New York, N. Y. 1968

be of finite order. This recasts the calculation back into more familiar territory. The matrices that are actually to be dealt with can then be inverted by the more familiar conventional numerical techniques. To accomplish this contraction to finite matrices for a particular problem in essence then merely requires solving a numerical approximation to the problem. These "method-of-moment" numerical approximations, as Reilly[24] pointed out, were observed by Harrington[22] to be essentially equivalent to those employed by others in point-matching techniques[25-27] where the boundary conditions are enforced at a finite number of discrete points using truncated series representations for the electromagnetic fields.

22. R. F. Harrington, "Field Computation by Moment Methods", The Macmillan Co., New York, N. Y. 1968

24. E. D. Reilly, Jr., "Resonant Scattering From Inhomogeneous Nonspherical Targets", Journal of Computational Physics, Vol. 11, No. 4, p 463-492, April 1973

25. E. M. Kennaugh, "Multipole Field Expansions and Their Use in Approximate Solutions of Electromagnetic Scattering Problems". Ph.D. Dissertation, Dept. of Electrical Engineering, Ohio State University 1959, Columbus, Ohio

26. L. F. Libelo, Jr., "Scattering by Axisymmetric Particles Whose Size is of the Order of the Wavelength", Ph.D. Dissertation, Dept. of Physics, Rensselaer Polytechnic Institute, Troy, N. Y. 1964

27. C. R. Mullin, R. Sandburg and C. O. Velline, "A Numerical Technique for the Determination of Scattering Cross-Sections of Infinite Cylinders of Arbitrary Geometrical Cross-Section", IEEE. Transactions on Antennas and Propagation, AP 13, 141, 1965

A simple illustration of the point matching method was published earlier by the present authors[1].

One well-known classical variational technique for solving linear integral equations is that of Galerkin and is described at length by Kantorovich and Krylov[28]. This method is fundamentally a special case of the method-of-moments in that the set of expansion functions coincides with the set of weighting functions. Harrington[22] has observed further that Galerkin's method and the rigorous method-of-moments itself are in essence equivalent to the older Rayleigh-Ritz[29-30] variational method which is a much more widely known numerical technique.

Having, we hope, set the philosophic background properly for the method to be used in the computations let us continue the development of the approach to solving the problem. We have, we

1. L. F. Libelo and J. N. Bombardt (HDL) "S.E.R.A.: I. Normal Incidence on the Slotted Plane", NOLTR 70-58, Naval Surface Weapons Center, White Oak, Silver Spring, Md., April 1970

22. R. F. Harrington, "Field Computation by Moment Methods", The Macmillan Co., New York, N. Y. 1968

28. L. V. Kantorovich and V. I. Krylov, p 304,"Approximate Methods of Higher Analysis", Interscience Publishers, Inc., NY 1958

29. Lord Rayleigh "Theory of Sound", sections 88 and 89, Vol. I, Dover Publications, New York 1945

30. W. Ritz, "Über eine neue Methode zur Losung gewisser Variations probleme der mathematischen Physik", Journal fur die Reine und Angewandte Mathematik Vol. CXXXV, p 1-61, 1909

recall, three integral equations which have been derived for the problem at hand. These are the slot electric field equation, i.e. eq. (22), the surface current density integral equation, i.e. eq. (34) and the connective integral equation of an earlier report[3]. We felt that the integral equation for the surface current was, all things considered, best suited for numerical solution and devoted all our efforts to it.

We shall now proceed to consider in more detail the approximate numerical treatment we applied to the slotted cylinder problem. First it should be noted that a stable and accurate solution of the surface current integral equation by the method-of-moments depends on a number of factors; the choice of the set of expansion functions, the choice of the weighting functions, the accuracy of the computed elements in the matrix of inner products, the generation of a "well-conditioned" matrix of inner products and the size of this matrix of inner products. Judgement should be given to selecting the set of expansion functions so that one does not require an inordinately large number of them to adequately represent the unknown quantity in the integral equation. At the same time they should be chosen so as to be relatively independent functions. Similar care should be

3.   J. N. Bombardt and L. F. Libelo (NAVSURFWPNCEN) "S.E.R.A.: III. An Alternative Integral Equation with Analytic Kernels for the Slotted Cylinder Problem", HDL-TR-1588, Harry Diamond Laboratories, Washington, D. C., August 1972

devoted to selecting the set of weighting functions so that they are
a set of relatively independent functions. They should be chosen so
that the inner products formed with them test independent properties
of the integral equation. The accuracy with which elements in the
inner product matrix can be computed depends critically upon the
sets of expansion and weighting functions chosen for the computation.
Of course analytic closed form expressions for each element in the
inner product matrix is highly desirable. K. Mei[31] discussed the
conditioning of a matrix in terms of the orientations of the hyper-
planes represented by the rows of the matrix in an n-dimensional
vector space. His results indicate essentially that a "well-
conditioned" matrix results if the hyperplanes are nearly perpen-
dicular to one another whereas an "ill-conditioned" matrix results
if two or more hyperplanes are nearly parallel. Furthermore, after
a certain number of arithmetic operations are performed during
numerical inversion óf a matrix a round-off error check is necessary
to determine if the matrix is well-conditioned. We shall postpone
detailed discussion of other numerical considerations until later
when we discuss the computer program itself.

The method-of-moments shall be applied to the slotted-cylinder
scattering problem in the same manner that Harrington treated the

31. K. K. Mei, "On the Integral Equations of Thin Wire Antennas",
      IEEE Transactions on Antenna and Propagation AP 13, 374 (196⁵

scattering problem of an infinite cylinder of arbitrary cross-section without a slot. On the conducting portion of the scatterer the surface current will be approximately represented as an ensemble of constant current elements with unknown amplitudes. Only at the midpoint of each such current element will the surface current density integral equation be assumed to hold. This procedure yields a finite system of algebraic equations where the unknowns of the system are the constant current amplitudes in the approximation. Clearly, in principle, if the sizes of these constant current elements are sufficiently small when compared to the size of the wavelength we should obtain a fairly decent approximation to the actual exact solution provided we treat any singularities in a proper manner. The surface current integral equation, namely eq. (34) will be repeated for convenience

$$(34) \quad \int_{\varphi_0}^{2\pi-\varphi_0} d\varphi' \; \frac{K(\varphi')}{H_0} \; H_0^{(1)} \left(2\eta \left| \sin \frac{(\varphi-\varphi')}{2} \right| \right) = \left(\frac{4}{\eta} \right) e^{-i\eta \cos\varphi}$$

$$\text{for } \varphi_0 \leq \varphi \leq 2\pi-\varphi_0$$

For purposes of calculating by the method-of-moments we approximately represent the surface current density as

$$(72) \quad K(\varphi)/H_0 = \sum_{\ell=1}^{L} B_\ell P_\ell (\varphi)$$

where L is an even integer for reasons which shortly shall become evident, $P_\ell(\varphi)$ is a unit step-function which shall be defined in more detail in a moment, and B_ℓ is the amplitude of this step-function. The step-function is defined as follows

(73) $\qquad P_\ell(\varphi) \equiv u(\varphi-\varphi_{\ell-1}) - u(\varphi-\varphi_\ell)$

where we have

$$u(\alpha) = \begin{cases} 1 & \alpha > 0 \\ 0 & \alpha < 0 \end{cases}$$

In eq. (73) for the definition of the unit step-function the angle φ_ℓ is given by

(74) $\qquad \varphi_\ell = \varphi_0 + \ell\Delta\varphi$

where we take

(75) $\qquad \Delta\varphi = 2(\pi-\varphi_0)/L$

and we recall φ_0 the semi-slot angle was illustrated in Figure 1. Eq. (75) tells us merely that we have divided the angular range of the conducting portion of the cylinder of radius a into L equal intervals. Now if we substitute eq. (72) into eq. (34) for the

51

surface current density we generate the approximately correct

relation

$$(76) \qquad \sum_{\ell=1}^{L} B_{\ell} f_{\ell}(\eta,\varphi) = \frac{4}{\eta} e^{-i\eta \cos\varphi}$$

where we have introduced the notation

$$(77) \qquad f_{\ell}(\eta,\varphi) = \int_{\varphi_{\ell-1}}^{\varphi_{\ell}} d\varphi' \, H_o^{(1)} \left(2\eta | \sin \left(\frac{\varphi'-\varphi}{2} \right) | \right)$$

We choose the set of weighting functions as the following set

of Dirac delta functions

$$(78) \qquad \delta(\varphi - \bar{\varphi}_m) \qquad\qquad \text{for } m = 1,2,\ldots L$$

where

$$(79) \qquad \bar{\varphi}_m \equiv \tfrac{1}{2}(\varphi_{m-1} + \varphi_m)$$

Thus we see that the method-of-moments yields for eq. (34) the

set of L simultaneous equations

$$(80) \qquad \sum_{\ell=1}^{L} B_{\ell} f_{\ell}(\eta,\bar{\varphi}_m) = \left(\frac{4}{\eta} \right) e^{-i\eta \cos\bar{\varphi}_m}$$

$$\text{for } m = 1,2,\ldots,L$$

This set can be solved for a given η and φ_0 i.e. a cylinder radius to wavelength ratio and a slot angle. Symmetry considerations reduce the size of the system of simultaneous equations to be solved numerically. Thus, for the incident plane wave as shown in Figure 1, the surface current is symmetrical about $\varphi = \pi$. Consequently the number of unknown step current amplitudes to be found is reduced since

$$(81) \qquad B_{L+1-\ell} = B_\ell \qquad\qquad \text{for } \ell = 1,2,\ldots,L/2$$

Therefore we can write

$$(82) \qquad \sum_{\ell=1}^{L/2} B_\ell \left[f_\ell(\eta,\bar\varphi_m) + f_{L+1-\ell}(\eta,\bar\varphi_m) \right] = \left(\frac{4}{\eta}\right) e^{-i\eta\,\cos\bar\varphi_m}$$

$$\text{for } m = 1,2,\ldots,L/2$$

Now eq. (82) can be cast into the same matrix form as eq. (61). It should be noted, however, that the approximate "impedance" matrix associated with eq. (82) is of finite order and can in principle be inverted (if it is not singular) by conventional numerical techniques. We have written a computer program for solving the system of eqs. (82) and shall discuss it later.

At this point we have approximated the slotted cylinder by zoning it into elements of uniform currents. An immediate question

thrusts itself forward concerning the validity of this approximation

to the current density near the edges of the slotted scatterer where

in the ideal mathematical model the surface current must become

unbounded in amplitude. This difficulty we feel is not too serious

to have to deal with. To begin with the surface current amplitude

for each zone can be interpreted as an approximation for the surface

current at the midpoint of the element. Consequently the current

precisely at an edge is never computed! Instead an approximate

value is calculated for the surface current at the mid-point of a

zone that has an edge as one of its boundaries. At the mid-point of

such a zone the surface current density may be very large but can't

become infinite. Then numerical approximation at mid-points of such

a zone is a meaningful quantity. Secondly, physical quantities such

as the electric field in the aperture and the back-scattering cross-

section are obtained from integrals of the surface current which are

relatively insensitive to small changes in surface current near the

ideal edges of the scatterer. Finally, it should be borne in mind

that any experimental approach to the scattering problem of a

perfectly conducting slotted cylinder or an infinite cylindrical

strip must, of necessity, employ scatterers constructed of a metal

which is finitely conducting with finite thickness. Of course all

probes and detectors are also finite in size and possess limited

ability to accurately define an edge. Consequently the ideal

mathematical model of a slotted perfectly conducting cylinder displaying singular behaviour at an edge is impossible to achieve experimentally. Thus, eq. (72) should, if properly handled, adequately represent the surface current for most practical purposes.

Next we shall enter into detailed discussion of the elements for the matrix of inner products. The expansion and weighting functions introduced above have led to inner products for the surface current integral equations which were denoted by $f_\ell(\eta,\bar{\varphi}_m)$. A numerical solution of eq. (82) requires the analytical evaluation of these inner products which are explicitly displayed in eq. (77). Note that it may occur that $\bar{\varphi}_m$ does not lie within the range of integration in eq. (77). Should this be the situation a Taylor series expansion of the integrand can be integrated in order to provide an analytical result for $f_\ell(\eta,\bar{\varphi}_m)$. If $\bar{\varphi}_m$ does lie within the range of integration we can get an analytical result for $f_\ell(\eta,\bar{\varphi}_\ell)$ by integrating the small argument expansion of the Hankel function in the integrand. We shall demonstrate both situations next.

The inner products in eq. (82) are defined by

$$f_\ell(\eta,\bar{\varphi}_m) = \int_{\varphi\ell}^{\varphi_{\ell-1}} d\varphi' \; H_o^{(1)}\left(2\eta\left|\sin\left(\frac{\varphi'-\bar{\varphi}_m}{2}\right)\right|\right)$$

where $\ell = 1,2,\ldots,L$ and $m = 1,2,\ldots,L/2$. The first case to be considered is that where $\bar{\varphi}_m$ does not lie within the range of integration. More specifically we shall take $\bar{\varphi}_\ell > \bar{\varphi}_m$ such that

55

$$f_{\ell>m}(\eta,\bar{\varphi}_m) = \int_{\varphi_{\ell-1}}^{\varphi_\ell} d\varphi' \ H_o^{(1)}\left(2\eta\left|\sin\left(\frac{\varphi'-\bar{\varphi}_m}{2}\right)\right|\right)$$

Then a Taylor series expansion of the integrand about $\bar{\varphi}_\ell$ becomes

$$H_o^{(1)}\left(2\eta\left|\sin\left(\frac{\varphi'-\bar{\varphi}_m}{2}\right)\right|\right) = H_o^{(1)}\left(2\eta\ \sin\left(\frac{\bar{\varphi}_\ell-\bar{\varphi}_m}{2}\right)\right) + (\varphi'-\bar{\varphi}_\ell)\ .$$

$$\left|\frac{d}{d\varphi'}\ H_o^{(1)}\left(2\eta\ \sin\left(\frac{\varphi'-\bar{\varphi}_m}{2}\right)\right)\right|_{\varphi'=\bar{\varphi}_\ell}$$

$+ \ldots$

where $\varphi',\varphi_\ell > \varphi_m$. Term by term integration of this Taylor series

leads to

$$f_{\ell>m}(\eta,\bar{\varphi}_m) = H_o^{(1)}\left(2\eta\ \sin\left(\frac{\bar{\varphi}_\ell-\bar{\varphi}_m}{2}\right)\right)\Delta\varphi + \left[\left(\frac{\varphi_\ell^2-\varphi_{\ell-1}^2}{2}\right) - \bar{\varphi}_\ell\ \Delta\varphi\right]\ .$$

$$\left|\frac{d}{d\varphi'}\ H_o^{(1)}\left(2\eta\ \sin\left(\frac{\varphi'-\bar{\varphi}_m}{2}\right)\right)\right|_{\varphi'=\bar{\varphi}_\ell}$$

$+ \ldots$

where

$$\bar{\varphi}_\ell\Delta\varphi = \left(\frac{\varphi_\ell+\varphi_{\ell-1}}{2}\right)\ (\varphi_\ell-\varphi_{\ell-1}) = \frac{(\varphi_\ell^2-\varphi_{\ell-1}^2)}{2}$$

Then to first order in $\Delta\varphi$ the inner product is

$$f_{\ell > m}(\eta, \bar{\varphi}_m) \approx H_o^{(1)}\left[2\eta \, \sin\left(\frac{\bar{\varphi}_\ell - \bar{\varphi}_m}{2}\right) \right] \Delta\varphi$$

A similar development for the case $\bar{\varphi}_\ell < \bar{\varphi}_m$ leads to

$$f_{\ell < m}(\eta, \bar{\varphi}_m) \approx H_o^{(1)}\left[2\eta \, \sin \frac{\bar{\varphi}_m - \bar{\varphi}_\ell}{2} \right] \Delta\varphi$$

Therefore to first order in $\Delta\varphi$ we have

$$(83) \qquad f_{\ell \neq m}(\eta, \bar{\varphi}_m) \approx H_o^{(1)}\left[2\eta \, \sin \left| \frac{\bar{\varphi}_m - \bar{\varphi}_\ell}{2} \right| \right] \Delta\varphi$$

for $\ell = 1, 2, \ldots, L$ and $m = 1, 2, \ldots, L/2$

For the second situation i.e. when $m = \ell$ the Hankel function integrand simplifies since

$$\left| \sin (\varphi' - \bar{\varphi}_\ell)/2 \right| \approx \left| (\varphi' - \bar{\varphi}_\ell)/2 \right| \qquad \text{for } \varphi_{\ell-1} \leq \varphi_\ell$$

It then follows that

$$(84) \quad f_\ell(\eta, \bar{\varphi}_\ell) \approx \int_{\varphi_{\ell-1}}^{\bar{\varphi}_\ell} d\varphi' \; H_o^{(1)}[\eta(\bar{\varphi}_\ell - \varphi')] d\varphi' + \int_{\bar{\varphi}_\ell}^{\varphi_\ell} d\varphi' \; H_o^{(1)}[\eta(\varphi' - \bar{\varphi}_\ell)]$$

These integrals can be evaluated by requiring

$$\tfrac{1}{2}\eta\Delta\varphi \ll 1$$

so that a small argument asymptotic form of expansion for the Hankel function can be employed i.e.

$$H_0^{(1)}(x) \underset{x \ll 1}{\longrightarrow} 1 - \left(\frac{x}{2}\right)^2 + i\frac{2}{\pi}\left\{\left[1 - \left(\frac{x}{2}\right)^2\right]\left[\ell n\left(\frac{x}{2}\right) + \gamma_e\right] + \left(\frac{x}{2}\right)^2\right\}$$

where $\gamma_e \equiv 0.5772\ldots$ is the Euler constant. Then, in terms of the small argument expansion the first integral in $f_\ell(\eta,\bar{\varphi}_\ell)$ becomes

$$\int_{\varphi_{\ell-1}}^{\bar{\varphi}_\ell} d\varphi' \, H_0^{(1)}\left[\eta(\bar{\varphi}_\ell - \varphi')\right] \approx \left\{1 + i\frac{2}{\pi}\left[\gamma_e + \ell n\left(\frac{\eta}{2}\right)\right]\right\}\int_{\varphi_{\ell-1}}^{\bar{\varphi}_\ell} d\varphi'$$

$$-(\tfrac{1}{2}\eta)^2\left\{1 - i\frac{2}{\pi}\left[1 - \gamma_e - \ell n(\eta/2)\right]\right\}\int_{\varphi_{\ell-1}}^{\bar{\varphi}_\ell} d\varphi' \, (\bar{\varphi}_\ell - \varphi')^2 +$$

$$+ i\frac{2}{\pi}\int_{\varphi_{\ell-1}}^{\bar{\varphi}_\ell} d\varphi' \, \ell n(\bar{\varphi}_\ell - \varphi') - i\frac{2}{\pi}\left(\frac{\eta}{2}\right)^2\int_{\varphi_{\ell-1}}^{\bar{\varphi}_\ell} d\varphi' \, (\bar{\varphi}_\ell - \varphi')^2 \, \ell_n(\bar{\varphi}_\ell - \varphi')$$

where we have

$$\int_{\varphi_{\ell-1}}^{\bar{\varphi}_\ell} d\varphi' = \tfrac{1}{2}\Delta\varphi$$

$$\int_{\varphi_{\ell-1}}^{\bar{\varphi}_{\ell}} d\varphi' \, (\bar{\varphi}_{\ell} - \varphi')^2 = \frac{1}{3} \, (\Delta\varphi/2)^3$$

$$\int_{\varphi_{\ell-1}}^{\bar{\varphi}_{\ell}} d\varphi' \, \ln(\bar{\varphi}_{\ell} - \varphi') = \frac{1}{2} \, (\Delta\varphi) \, \ln\left(\frac{1}{2} \, \Delta\varphi\right) - \frac{1}{2} \, \Delta\varphi$$

and

$$\int_{\varphi_{\ell-1}}^{\bar{\varphi}_{\ell}} d\varphi' \, (\bar{\varphi}_{\ell} - \varphi')^2 \, \ln(\bar{\varphi}_{\ell} - \varphi') = \frac{1}{3} \left(\frac{1}{2}\Delta\varphi\right)^3 \, \ln\left(\frac{1}{2} \, \Delta\varphi\right) - \frac{1}{9} \left(\frac{1}{2} \, \Delta\varphi\right)^3$$

which in turn gives us then

$$\int_{\varphi_{\ell-1}}^{\bar{\varphi}_{\ell}} d\varphi' \, H_0^{(1)}[\eta(\bar{\varphi}_{\ell} - \varphi')] = \left\{1 + i \, \frac{2}{\pi}[\gamma_e + \ln(\eta/2)]\right\} \left(\frac{\Delta\varphi}{2}\right)$$

$$- \frac{1}{3} \, (\eta/2)^2 \left\{1 - i \, \frac{2}{\pi} \left[1 - \gamma_e - \ln(\eta/2)\right]\right\} \left(\frac{\Delta\varphi}{2}\right)^3 + i \, \frac{2}{\pi} \left[\left(\frac{\Delta\varphi}{2}\right) \ln\left(\frac{\Delta\varphi}{2}\right) - \left(\frac{\Delta\varphi}{2}\right)\right]$$

$$- i \, \frac{2}{\pi} \left(\frac{\eta}{2}\right)^2 \left[\frac{1}{3} \left(\frac{\Delta\varphi}{2}\right)^3 \ln\left(\frac{\Delta\varphi}{2}\right) - \frac{1}{9} \left(\frac{\Delta\varphi}{2}\right)^3\right].$$

The second integral in eq. (84) for $f_{\ell}(\eta, \bar{\varphi}_{\ell})$ can be evaluated as follows. We define new variables

(85) $u \equiv \eta \, (\bar{\varphi}_{\ell} - \varphi')$

(86) $\qquad v \equiv \eta \ (\varphi' - \bar{\varphi}_\ell)$

Then we have

$$\int_{\varphi_{\ell-1}}^{\bar{\varphi}_\ell} d\varphi' \ H_o^{(1)} [\eta (\bar{\varphi}_\ell - \varphi')] = \frac{1}{\eta} \int_0^{\eta \Delta\varphi/2} du \ H_o^{(1)} (u)$$

and

$$\int_{\bar{\varphi}_\ell}^{\varphi_\ell} d\varphi' \ H_o^{(1)} [\eta (\varphi' - \bar{\varphi}_\ell)] = \frac{1}{\eta} \int_0^{\eta \Delta\varphi/2} dv \ H_o^{(1)} (v)$$

From these two relations we conclude that the second integral in eq. (84) is given simply as

$$\int_{\bar{\varphi}_\ell}^{\varphi_\ell} d\varphi' \ H_o^{(1)} [\eta (\varphi' - \bar{\varphi}_\ell)] = \int_{\varphi_{\ell-1}}^{\bar{\varphi}_\ell} d\varphi' \ H_o^{(1)} [\eta (\bar{\varphi}_\ell - \varphi')]$$

Consequently the value of $f_\ell (\eta, \bar{\varphi}_\ell)$ is

$$(87) \qquad f_\ell (\eta, \bar{\varphi}_\ell) \approx \left\{ 1 + i \frac{2}{\pi} [\gamma_e + \ell n (\eta/2)] \right\} \Delta\varphi -$$

$$- \frac{2}{3} \left(\frac{\eta}{2}\right)^2 \left\{ 1 - i \frac{2}{\pi} \left[1 - \gamma_e - \ell n \left(\frac{\eta}{2}\right) \right] \right\} \left(\frac{\Delta\varphi}{2}\right)^3 +$$

$$+ i \frac{4}{\pi} \left[\left(\frac{\Delta\varphi}{2}\right) \ell n \left(\frac{\Delta\varphi}{2}\right) - \left(\frac{\Delta\varphi}{2}\right) \right] - i \frac{4}{\pi} \left(\frac{\eta}{2}\right)^2 \left[\frac{1}{3} \left(\frac{\Delta\varphi}{2}\right)^3 \ell n \left(\frac{\Delta\varphi}{2}\right) - \frac{1}{9} \left(\frac{\Delta\varphi}{2}\right)^3 \right]$$

$$\text{for } \ell = 1, 2, \ldots, L/2$$

Equations (83) and (87) provide analytical expressions that can be used to numerically evaluate the known coefficients in the systems of algebraic equations in eq. (82). These analytical expressions have been derived on the condition that $\Delta\varphi$ is very small and where $\frac{1}{2}\eta\Delta\varphi$ is also a small number. What this implies is that the wavelength of the incident radiation must be long compared to the zone, or element, of constant current dimension. This is of course necessary from a physical point of view if the approximating ensemble of discrete current elements is to accurately represent a continuous surface current distribution at wavelengths of interest.

Next we turn to the evaluation of the slot electric field. Once the surface current density has been determined in the manner described just above the electric field in the opening or slot can be found in a direct straightforward manner. Using eqs. (31), (33) and (15) we can obtain the connective integral equation which we showed in earlier paper[3] between the slot electric field and the surface current density.

$$(88) \quad \mathcal{E}(\varphi) = E_z^i(a,\varphi) - \left(\frac{\eta}{4}\right)\sqrt{\frac{\mu_o}{\epsilon_o}} \int_{\varphi_o}^{2\pi-\varphi_o} d\varphi' \; \varkappa(\varphi') H_o^{(1)}\left(2\eta\left|\sin\left(\frac{\varphi-\varphi'}{2}\right)\right|\right),$$

$$\text{for } 2\pi-\varphi_o < \varphi < +\varphi_o$$

3. J. N. Bombardt and L. F. Libelo (NAVSURFWPNCEN) "S.E.R.A.: III. An Alternative Integral Equation with Analytic Kernels for the Slotted Cylinder Problem", HDL-TR-1588, Harry Diamond Laboratories, Washington, D. C., August 1972

Using eq. (72) this becomes

$$\mathscr{E}(\varphi)/E_0 = e^{-i\eta\cos\varphi} - \left(\frac{\eta}{4}\right) \sum_{\ell=1}^{L} B_\ell f_\ell(\eta,\varphi)$$

and taking symmetry into account we obtain for the slot electric field

$$(89) \quad \mathscr{E}(\varphi)/E_0 = e^{-i\eta\cos\varphi} - \left(\frac{\eta}{4}\right) \sum_{\ell=1}^{L/2} B_\ell\left[f_\ell(\eta,\varphi) + f_{L+1-\ell}(\eta,\varphi)\right]$$

$$\text{for} \quad 2\pi-\varphi_0 < \varphi < \varphi_0$$

Calculation of the slot electric field is one property of the problem which proves useful as a vehicle for comparison with the results of other workers. The computer program constructed for the slotted cylinder problem evaluates eq. (89) for the slot electric field for a given set of parameters λ, η and φ_0.

The surface current density can also be used to compute the back-scattering cross-section. This is done using eq. (69) which we repeat here.

$$(69) \quad k\sigma_B = (\eta/2)^2 \left| \int_{\varphi_0}^{2\pi-\varphi_0} d\varphi' \; \frac{E_z^i(a,\varphi')}{E_0} \; \frac{\mathscr{K}(\varphi')}{H_0} \right|^2$$

Thus we have also

$$k\sigma_B = (\eta/2)^2 \left| \sum_{m=0}^{\infty} \epsilon_m (-i)^m J_m(\eta) \sum_{\ell=1}^{L} B_\ell \int_{\varphi_0}^{2\pi-\varphi_0} d\varphi' \; P_\ell(\varphi')\cos m\varphi' \right|^2$$

or in turn

$$(90) \quad k\sigma_B = (\eta/2)^2 \left| \sum_{\ell=1}^{L} B_\ell \left[J_0(\eta)\Delta\varphi + 2\sum_{m=1}^{\infty} (-i)^m J_m(\eta) \right. \right.$$

$$\left. \left. \left(\frac{\sin m\varphi_\ell - \sin m\varphi_{\ell-1}}{m} \right) \right] \right|^2$$

Now if we define a new function by

$$(91) \quad g_\ell(\eta) \equiv J_0(\eta)\Delta\varphi + 2\sum_{m=1}^{\infty} (-i)^m J_m(\eta) \left[\frac{\sin(m\varphi_\ell) - \sin(m\varphi_{\ell-1})}{m} \right]$$

we can write the back-scattering cross-section in the simpler form

$$(92) \quad k\sigma_B = (\eta/2)^2 \left| \sum_{\ell=1}^{L/2} B_\ell [g_\ell(\eta) + g_{L+1-\ell}(\eta)] \right|^2$$

These b.s.c.s. were also incorporated into the computer program for the problem. The calculated values obtained for eq. (92) will be compared with available experimental data below.

Having completed our general discussion of the formulation of the method used for the numerical calculations in our diffraction problem we next proceed to present the results obtained. We shall compare these to the results obtained by others whenever they are available for this purpose.

VII. NUMERICAL RESULTS FOR INFINITE CYLINDER WITH NO SLOT

The exact series solution of the surface current density on an infinite perfectly conducting circular cylinder with no slot was given earlier in eq. (26), i.e.

$$(93) \qquad K_z^0(\varphi) = H_0 \left(\frac{2}{\pi\eta}\right) \sum_{m=0}^{\infty} \frac{\epsilon_m(-i)^m}{H_m^{(1)}(\eta)} \cos m\varphi$$

Using eqs. (64) and (63) with the A_m all identically set to zero gives the b.s.c.s. for the cylinder with no slot as

$$(94) \qquad \sigma_B^0 = \frac{4}{k} \left| \sum_{n=0}^{\infty} (-1)^n \epsilon_n J_n(\eta) / H^{(1)} \right|^2$$

We have computed the surface current density at 40 values of azimuth in the range $0 \le \varphi \le \pi$, i.e. for $L = 80$. Figures 2 and 3 display the numerical results for the surface current at wavelengths corresponding to values of $\eta = 1,2,3,4,5$ respectively. Numerical evaluation of the exact series of eq. (93) for the surface current when there is no slot in the cylinder yields numerical results that are in extremely close agreement with those of Figures 2 and 3. In fact the exact results cannot be distinguished from the approximate results when plotted on the same graphs.

The accuracy obtained for the numerical results using the method of moments for the cylinder without a slot improves with increasing L. This is indicated in Table 1. where we have listed
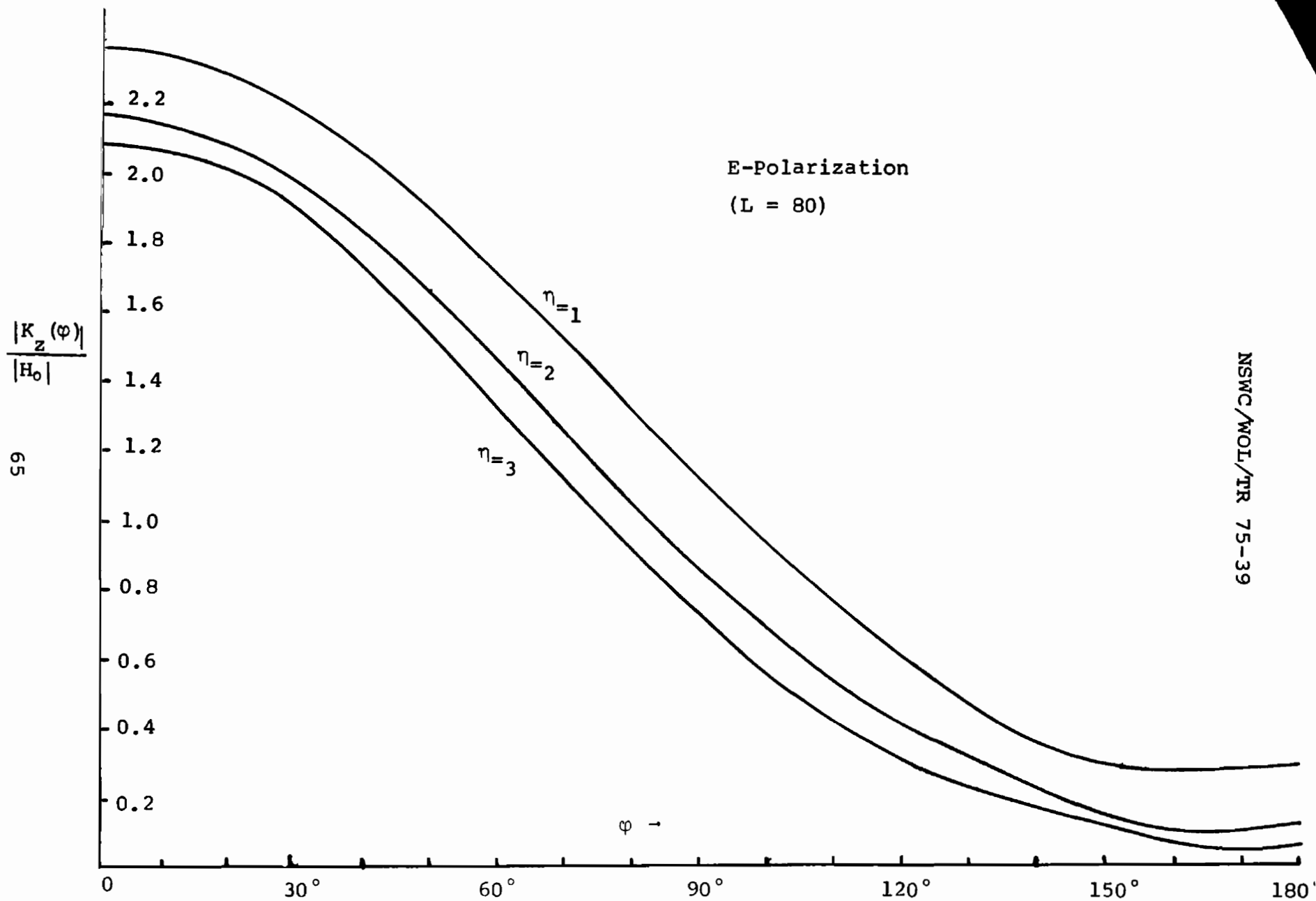
Figure 2. SURFACE CURRENT DENSITY ON A CYLINDER WITH NO SLOT: $\eta = 1, 2, 3$.
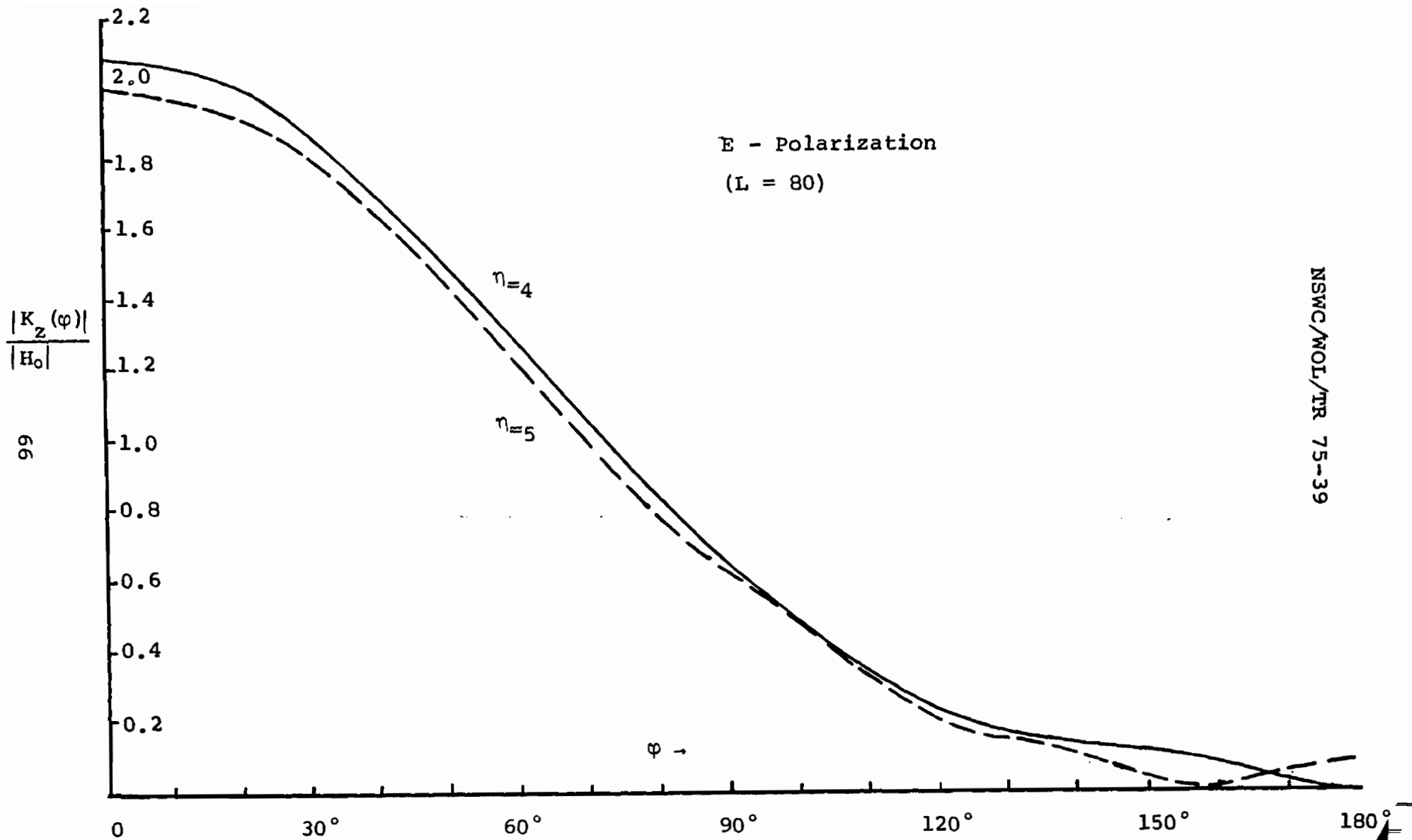
Figure 3. SURFACE CURRENT DENSITY ON A CYLINDER WITH NO SLOT: $\eta = 4,5$

Plot of $\dfrac{|K_z(\varphi)|}{|H_0|}$ versus φ with curves labeled $\eta=4$ and $\eta=5$.

E - Polarization

(L = 80)

Table 1. Numerical Values of Back-Scattering Cross-Section, $k\sigma_B$, from the Method of Moments and from Exact Theory With No Slot

	L = 40	L = 60	L = 80	EXACT
$\eta = 0.5$	2.3636	2.3619	2.3611	2.3590
1.0	3.8747	3.8706	3.8686	3.8627
1.5	5.3493	5.3429	5.3401	5.3325
2.0	6.8589	6.8482	6.8438	6.8321
2.5	8.4039	8.3806	8.3724	8.3559
3.0	9.9184	9.8889	9.8789	9.8589
3.5	11.4882	11.4470	11.4339	11.4106
4.0	13.0785	12.9890	12.9629	12.9256
4.5	14.6640	14.5573	14.5267	14.4849
5.0	16.2379	16.1047	16.0664	16.0166
5.5	17.7468	17.6214	17.5957	17.5738

values of $k\sigma_B$ for η varying from 0.5 to 5.5. For each value of η we show the exact result and the numerical approximation for L = 40, 60 and 80. The improvement with increasing L is readily evident in this table. For the range of η considered we note that for L = 80 the departure from the exact b.s.c.s. is less than one part in three hundred.

Clearly the numerical approximation used leads to excellent prediction of the surface current density and b.s.c.s. for the infinite cylinder with no slot.

VIII. TANGENTIAL APERTURE ELECTRIC FIELD AND CONDUCTOR SURFACE CURRENT DENSITIES FOR THE SLOTTED CYLINDER

1. General Comments

In Part VI of this report we presented a discussion of the method utilized to calculate the quantities of interest. This was followed by an illustration of the method applied to a problem that has a known solution and is familiar certainly to nearly all workers in the field of electromagnetic scattering and probably all first year graduate students in Electrical Engineering and in Physics. The results displayed for the method are undoubtedly extremely accurate for that problem. In this part of the report we present the results obtained using the same technique for the slotted infinite circular cylinder. More specifically we show graphically the tangential electric field in the slot and simultaneously in the same graph the surface current density over the conductor for the same cylinder. This is done for $\eta = 1,2,3,4,5$ to obtain the behaviour as a function of the ratio of the cylinder radius to the incident wavelength. Along with the graphically represented results we show for each slot angle considered the corresponding results for the backscattering cross-section as a function of the parameter η. These b.s.c.s. results were obtained by the same numerical technique.

2. The $\varphi_0 = 30°$ Slot Characteristics

The first case considered is that for which $\varphi_0 = 30°$ or equivalently a slot subtending a total angle of $60°$ at the cylinder axis.

In this case the surface current density was evaluated at 50 points in the range $\varphi_0 < \varphi < \pi$. This means of course that L = 100 or the conducting portion of the circular cylinder of radius a was approximated by assuming that it consisted of 100 zones each carrying a surface current of constant amplitude. The increment for the 50 equally spaced points over half the conductor implies

$$\frac{\Delta\varphi}{\varphi_0} = \frac{(\pi-\pi/6)/50}{\pi/60} = \frac{\pi/60}{\pi/6} = \frac{1}{10}$$

Furthermore for the largest η considered we find for the arclength of each of these zones

$$\frac{a\Delta\varphi}{\lambda} = \frac{2\pi a}{\lambda}\frac{\Delta\varphi}{2\pi} = \eta\frac{\Delta\varphi}{2\pi} = 5 \times \frac{1}{120} = \frac{1}{24} \approx .04$$

This is the maximum ratio of arclength per zone to incident wavelength. We conclude from this that we should be able to numerically generate in the manner described good results for the quantities we are evaluating. In Figures 4 through 8 respectively we show the results obtained for the aperture electric field and the surface current density for η = 1,2,3,4 and 5. It must be emphasized that the results being presented in this paper are the first published results for this particular case of a slotted cylinder. As a result of this we cannot compare our data to those obtained by others. Nevertheless we can establish some points which would tend to lend support to the accuracy of our theoretical results. First, calculations we performed for L = 80 for this case gave results which

indicate strongly that the results presented here for L = 100 have

already converged rather closely to the exact results. From this

aspect we believe the results depicted in Figures 4 through 8 are not

in error by more than a few per-cent. The second point to be made is

that the current densities displayed in Figures 4, 5 and 6 are quali-

tatively similar at the larger angles of φ to the current densities

of the slot-less cylinder shown in Figure 2. For angles closer to

the slot edges much stronger distortion must necessarily be present

and this accounts for the marked deviations in current density of the

$\varphi_0 = 30°$ case from the $\varphi_0 = 0$ case for $\eta = 1,2,3$. For the current

densities shown in Figures 7 and 8 for $\varphi_0 = 30°$ and $\eta = 4$ and 5 we

note the occurrence of three maxima which are quite sharply defined

in the $\eta = 5$ case. This is in qualitative agreement with the $\eta = 5$

situation shown in Figure 3 for the $\varphi_0 = 0$ case which has two clearly

evident maxima at the larger angles and two inflexion points at about

$\varphi = 90°$ and 105°. The $\eta = 4$, $\varphi_0 = 0$ curve in Figure 3 possesses two

inflexion points at the larger angles which the corresponding slotted

cylinder for $\varphi_0 = 30°$ seems to have resolved into the three peaks as

a result of the presence of the slot edges. Recall now that the cal-

culated surface current densities were utilized to calculate the slot

electric field distributions. In all cases we find for $\varphi_0 = 30°$ the

distribution of the electric field over the aperture region is quali-

tatively in agreement with the long-wavelength or electrostatic

approximation for narrow slots. Although $\varphi_0 = 30°$ is not strictly

Figure 4. Electric Field In The Slot, Surface Current On The Conductor; $\eta=1, \varphi_0=30°$

Figure 5. Electric Field In The Slot, Surface Current On The Conductor; $\eta=2, \varphi_0=30°$

Figure 6. Electric Field In The Slot, Surface Current On The Conductor; $\eta=3$, $\varphi_0=30°$
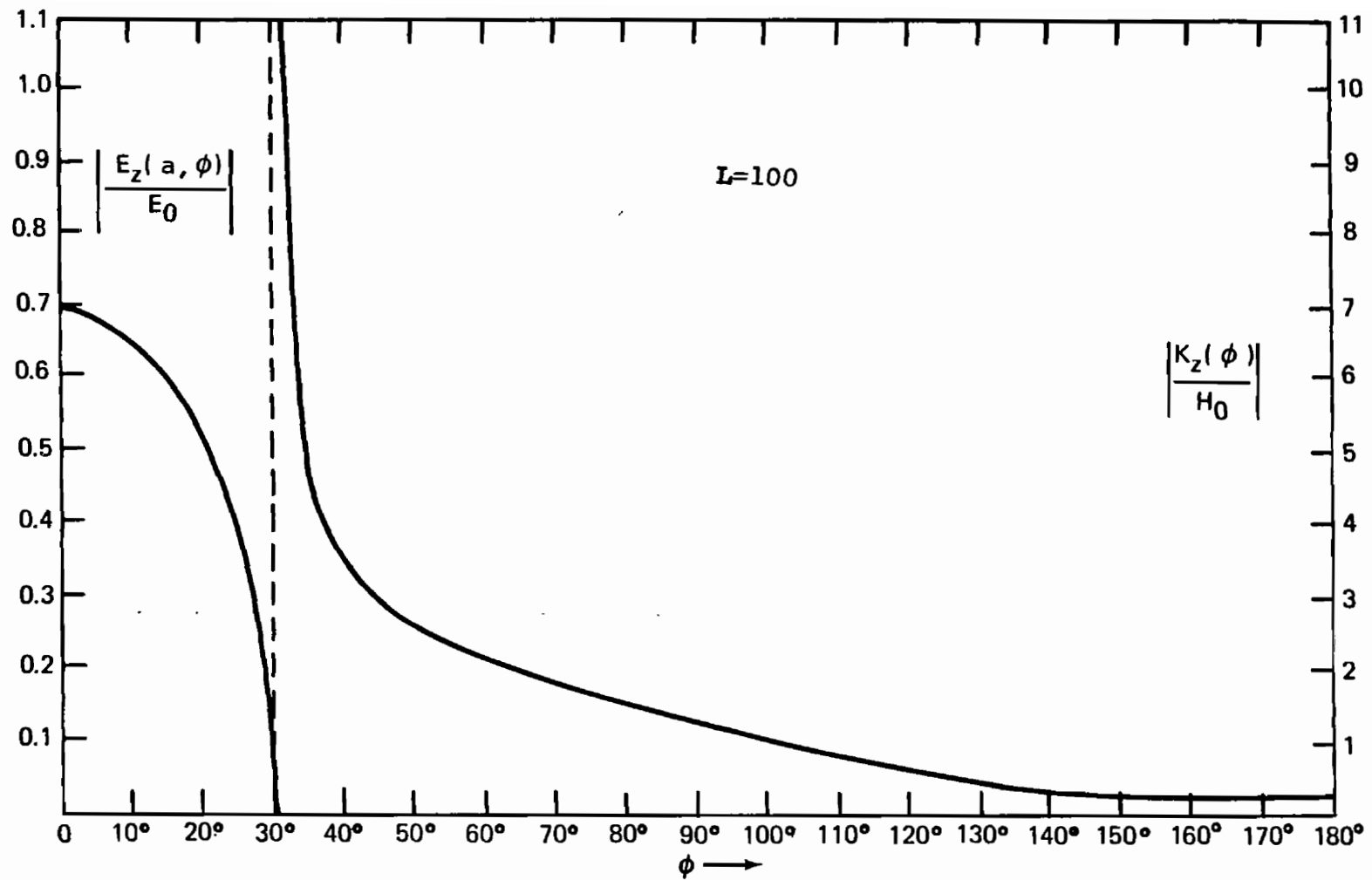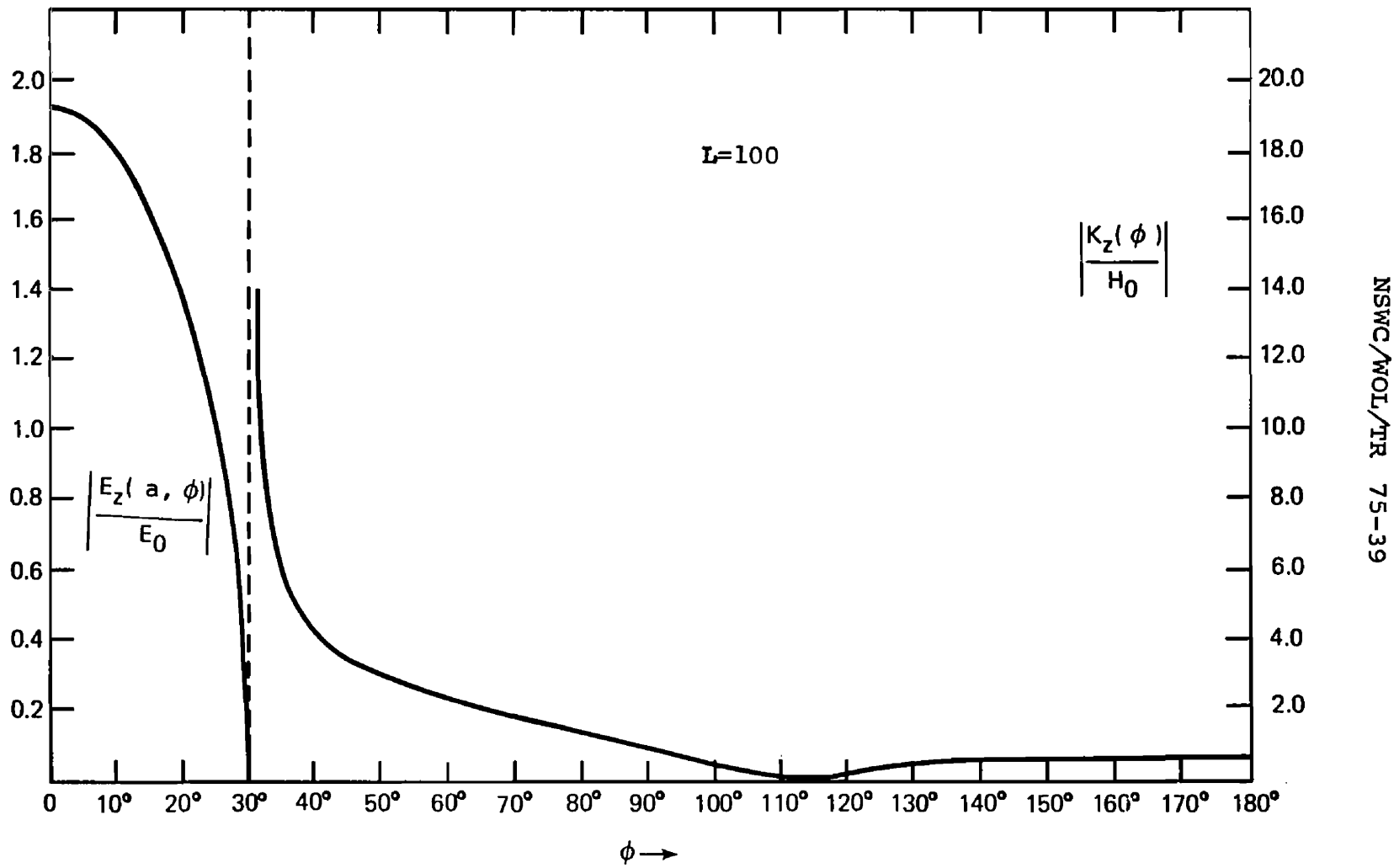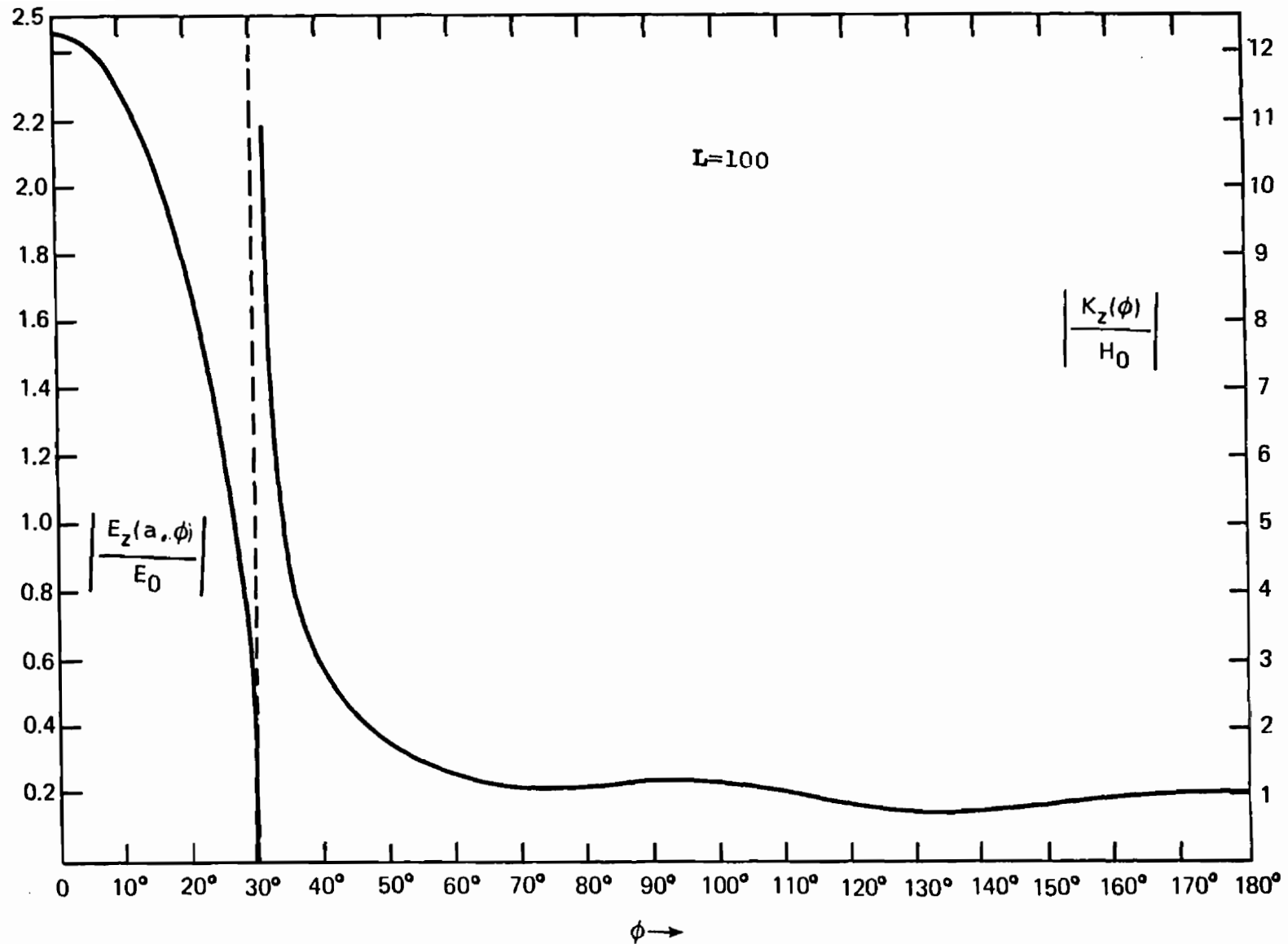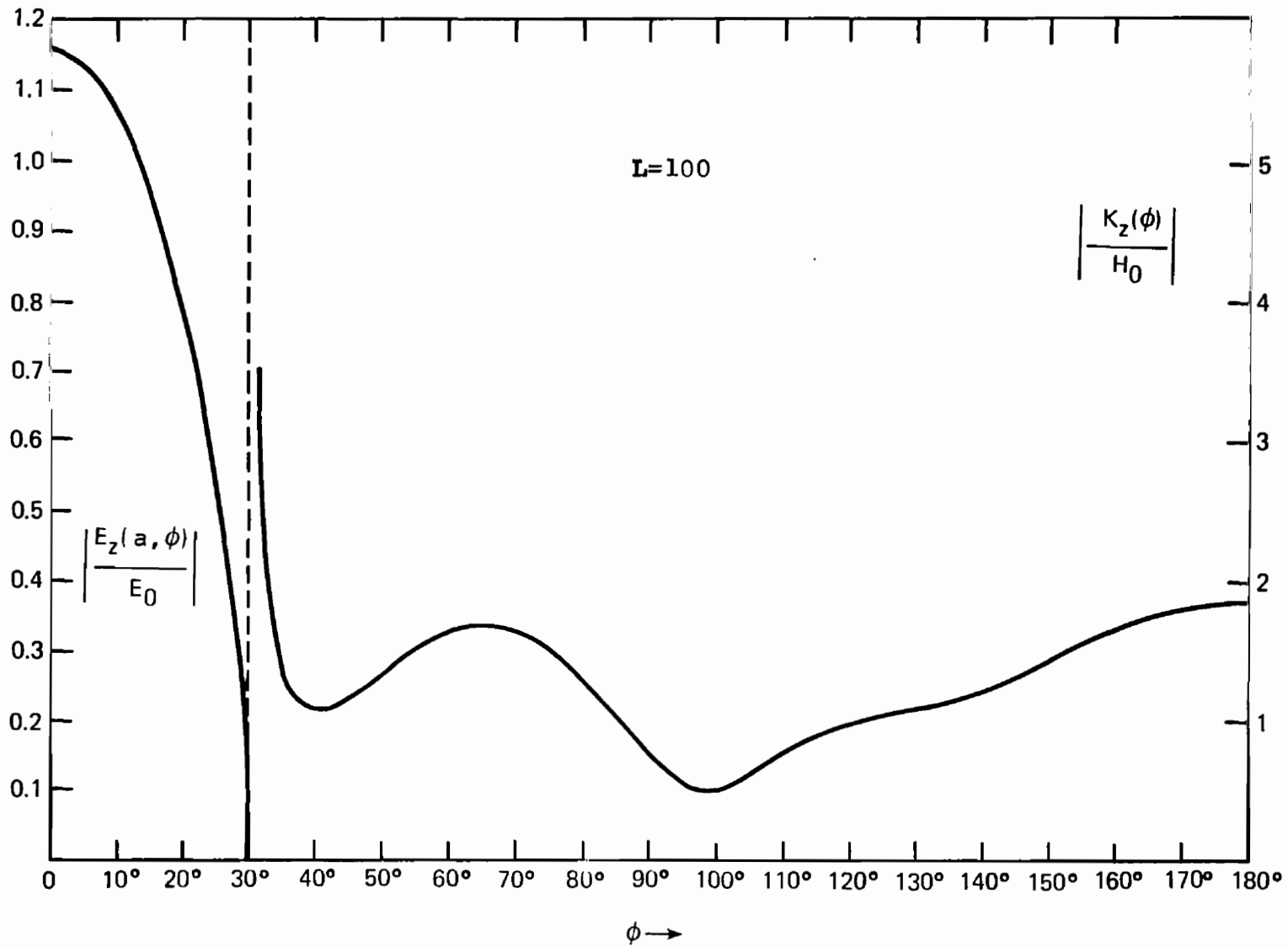
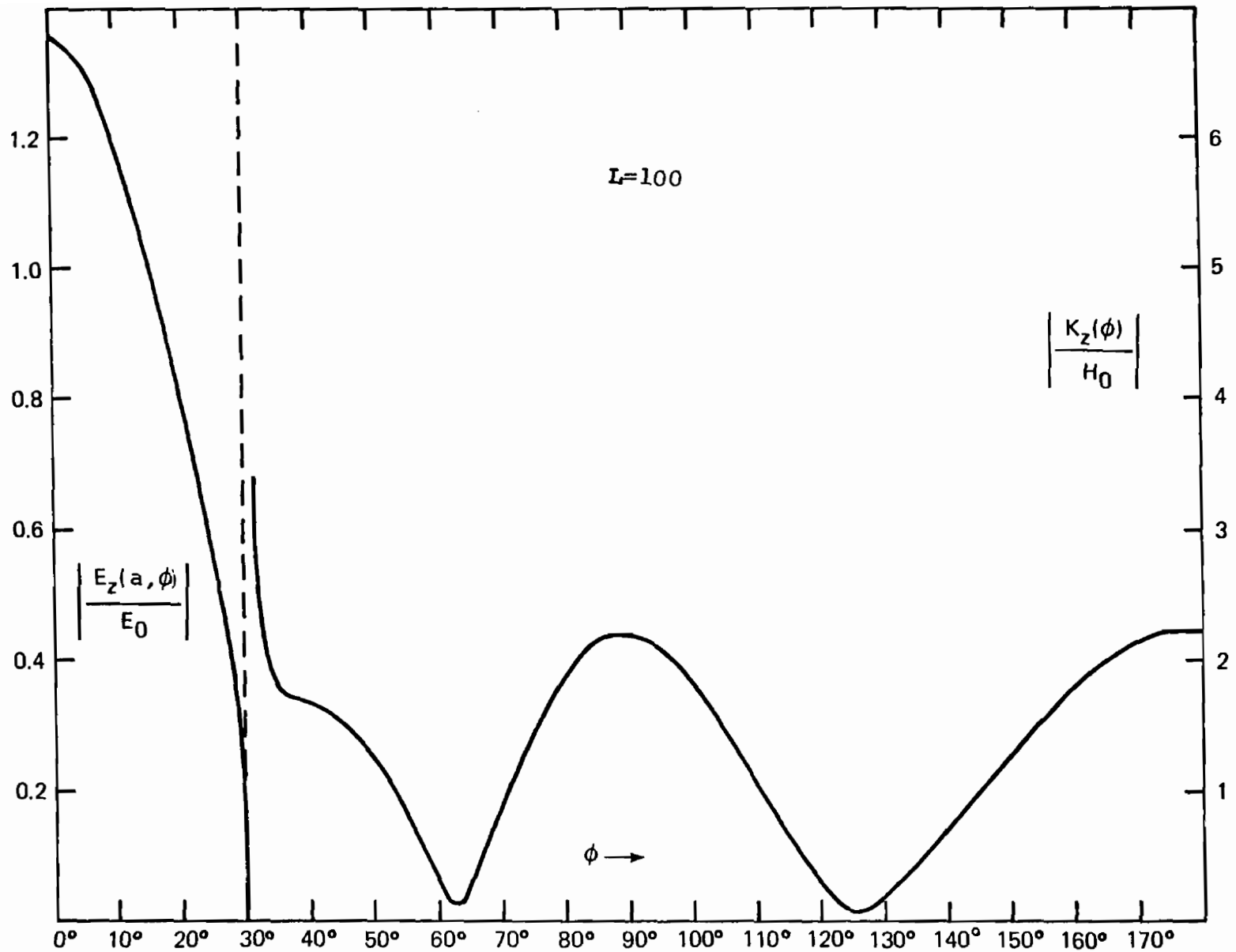Figure 7. Electric Field In The Slot, Surface Current On The Conductor; $\eta=4$, $\varphi_o=30°$

Figure 8. Electric Field In The Slot, Surface Current On The Conductor; $\eta=5$, $\varphi_0=30°$

speaking a very narrow slot it is not too surprising to find this

qualitative behaviour for the electric field. We can in fact inject

at this point experimental results that were obtained at a somewhat

later date. than the calculations being reported here. Measurements[32]

for the same size slot of the electric field component parallel to

the cylinder axis for axially polarized normally symmetric incident

radiation were made on a 12-inch long, open ended, cylinder for

$\eta = 3.84$. In the plane normally bisecting the cylinder axis this

electric field component was found to be qualitatively the same as

those calculated by the present authors. In fact the results for the

axial slot electric field distributions are quantitatively in fairly

close agreement. The results for the finite cylinder problem will be

presented in a subsequent report in substantial detail.

One should not be too hasty and be too strongly tempted to

assume that the long-wavelength approximation is adequate for

describing the $\varphi_0 = 30°$ slot electric field distribution over the

entire range of η considered. A quick preview glance at Figure 39

where the $\varphi_0 = 30°$ slot electric field at slot center is shown as a

function of η should indeed arouse some serious doubt as to the reli-

ability of the electrostatic approximation in this case. Certainly

this should arouse suspicion near the internal circular waveguide

32.   D. P. Margolis, C. L. Andrews, J. Heckl and L. Libelo, "Plane
      Wave Scattering by An Open-Ended Cylinder With An Axial-Slot",
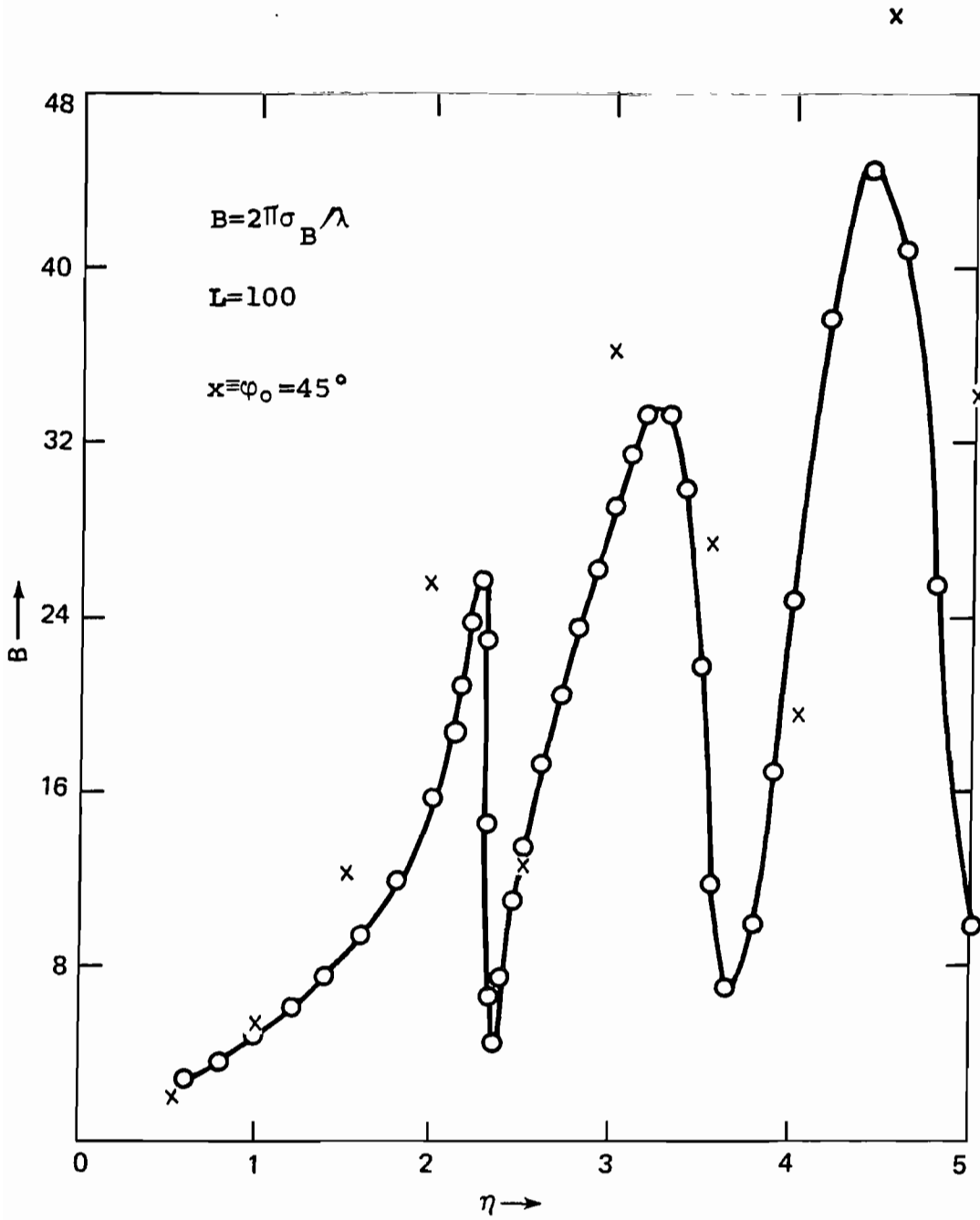   Bull. Am. Phys. Soc. Vol. 20, No. 1, p 101, 1975

Figure 9. Back-Scattering Cross-Section, $\varphi_0 = 30°$

resonances for $\varphi_0 = 30°$. We again repeat for emphasis that $\varphi_0 = 30°$ implies a slot such that 1/6 of the conducting cylinder is missing. This can hardly be considered to be an approximately _narrow_ slot.

All things considered then the infinite cylinder results for $\varphi_0 = 30°$ as shown in Figures 4 through 8 are quite accurate values for the range of η they represent. The back-scattering cross-section vs. η for $\varphi_0 = 30°$ is shown in Figure 9. The sharp minima that occur at $\eta \approx 2.40$ and $\eta \approx 3.83$ correspond to the two lowest internal TM modes for the circular cylindrical waveguide which are

$$\eta_{01} = 2.405 \text{ and } \eta_{11} = 3.832$$

This behaviour is reasonably consistent with the Morse and Feshbach[6] prediction for very narrow slots at internal resonances. Otherwise the calculated results are about as should be expected. This result lends additional support to the credence of the values obtained for the surface current density for $\varphi_0 = 30°$.

3. The $\varphi_0 = 45°$ Slot Characteristics

Next we consider the situation where the half-slot angle is increased to $\varphi_0 = 45°$. Now we are investigating the characteristics of a cylinder for which 1/4 of the conductor is missing. The calculations were performed assuming L = 100, i.e. the conductor is assumed approximately described by 100 strips each carrying its own

---

6. P. M. Morse and H. Feshbach, "Methods of Theoretical Physics", Part II, 1387-1398 McGraw-Hill, New York, 1953

uniform current density. Thus for the range of azimuth $\varphi_0 < \varphi < \pi$ we

have 50 such strips where the ratio of the angular width of each

strip to the half-slot angle is

$$\frac{\Delta\varphi}{\varphi_0} = \frac{(\pi - \pi/4)/50}{\pi/4} = \frac{3}{50} = .06$$

The ratio of arclength of each such strip to the smallest wavelength,

or largest η, considered is

$$\frac{a\Delta\varphi}{\lambda} = \frac{2\pi a}{\lambda} \frac{\Delta\varphi}{2\pi} = \eta \frac{\Delta\varphi}{2\pi} = \frac{3}{80} = .0375$$

Thus the accuracy of the numerical results for this case should be

about the same and probably a slight bit better than we obtained for

$\varphi_0 = 30°$. In Figures 10 through 14 we show respectively the aperture

electric field and surface current density distributions for the

circumference to incident wavelength ratios $\eta = 1,2,3,4$ and 5. For

L = 100 the numerical approximation technique utilized probably

yielded results good, to within one or two per cent in this case. To

fail to recognize the very close resemblance of the surface current

density distributions at $\eta = 1,2,3$ for $\varphi_0 = 45°$ as shown in Figures

10, 11 and 12 to the corresponding ones of $\eta = 1,2,3$ for $\varphi_0 = 30°$ in

Figures 4, 5 and 6 is virtually impossible. The same number of

maxima and minima occur for each η for both $\varphi_0 = 30°$ and $\varphi_0 = 45°$,

i.e. the $\varphi_0 = 45°$ distribution appears to be merely that for $\varphi_0 = 30°$

compressed to fit over a smaller range of angle. For $\eta = 2, \varphi_0 = 45°$

we find a slow decrease in surface current density as we move away
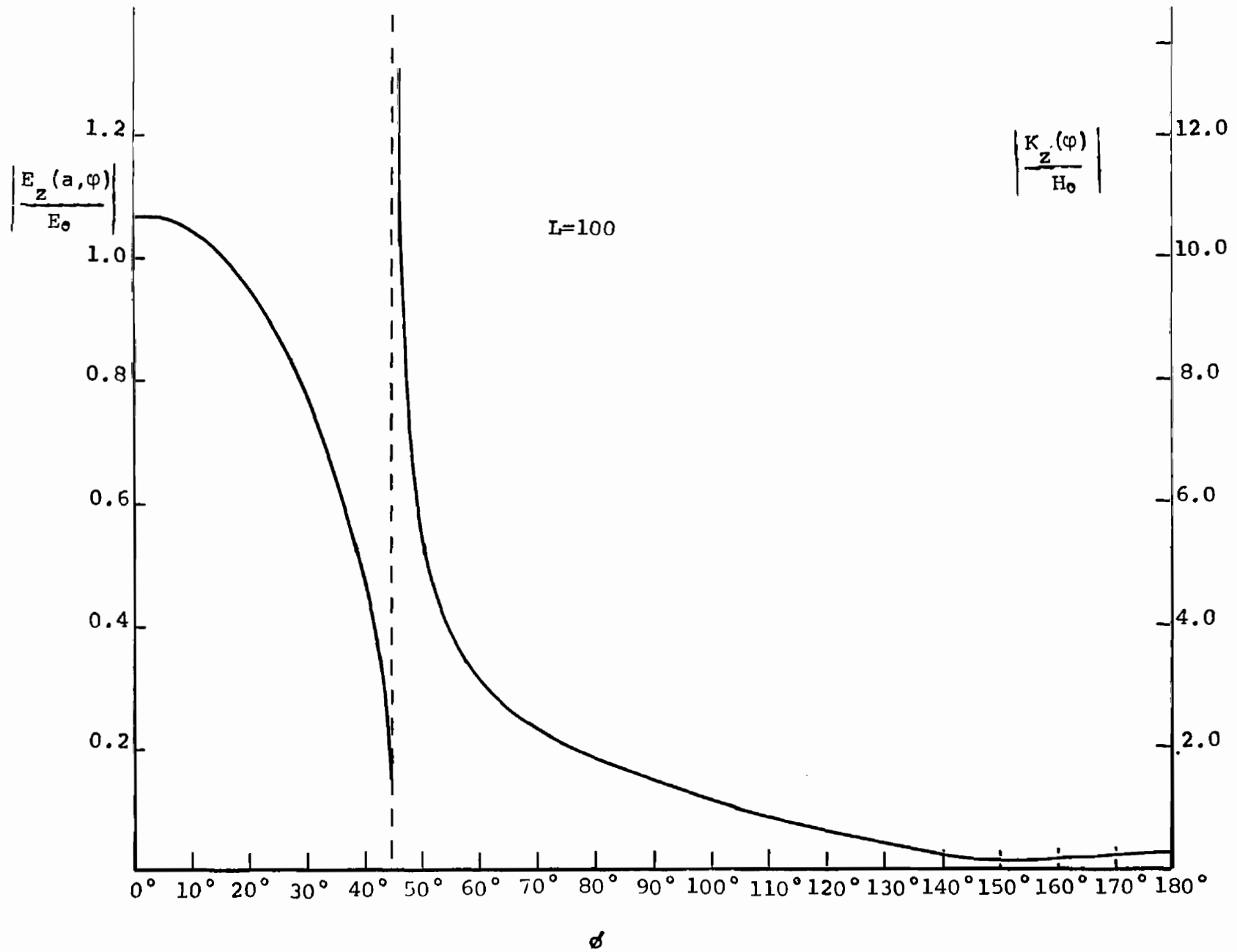
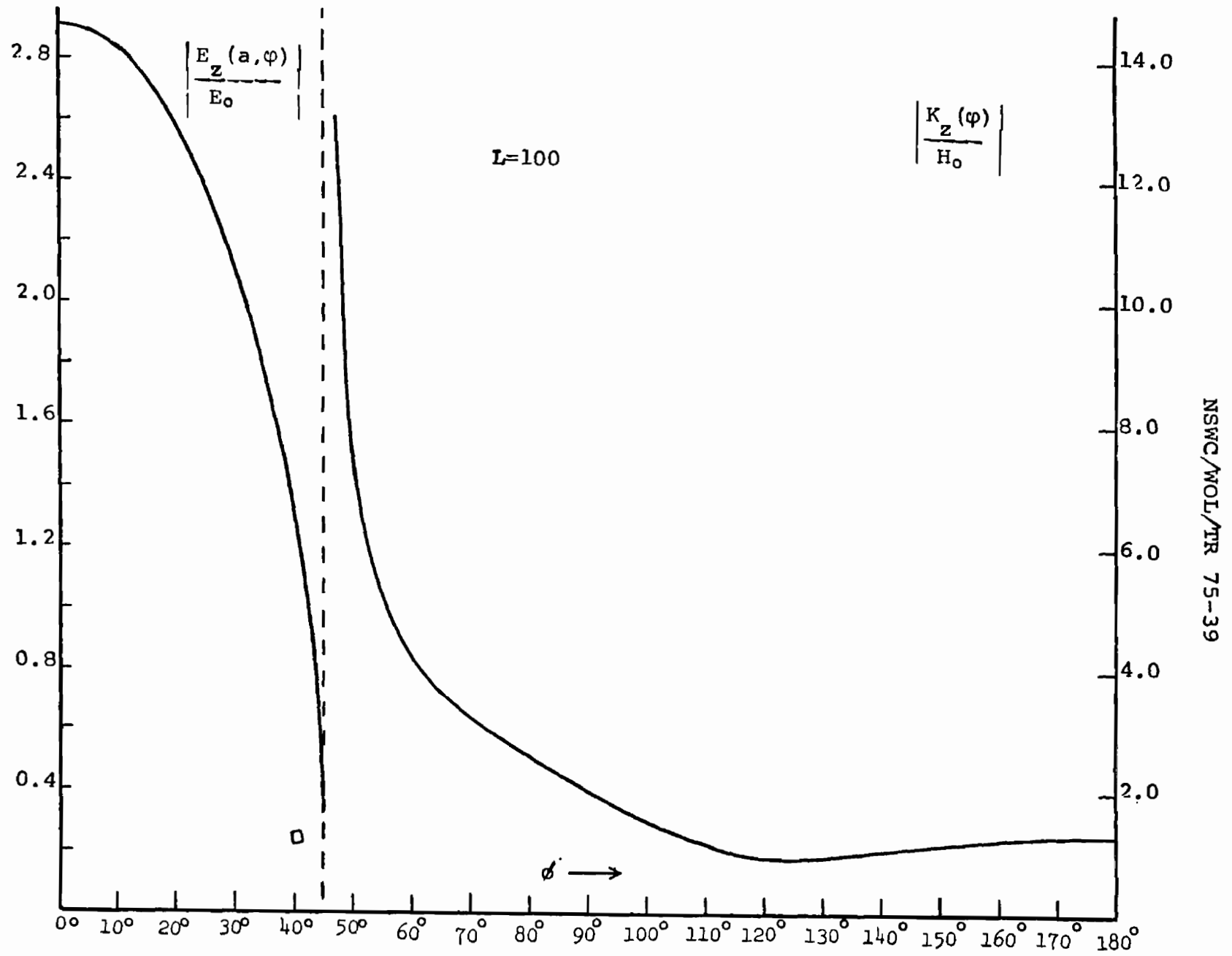Figure 10. Electric Field In The Slot, Surface Current On The Conductor; $\eta = 1$, $\varphi_0 = 45°$

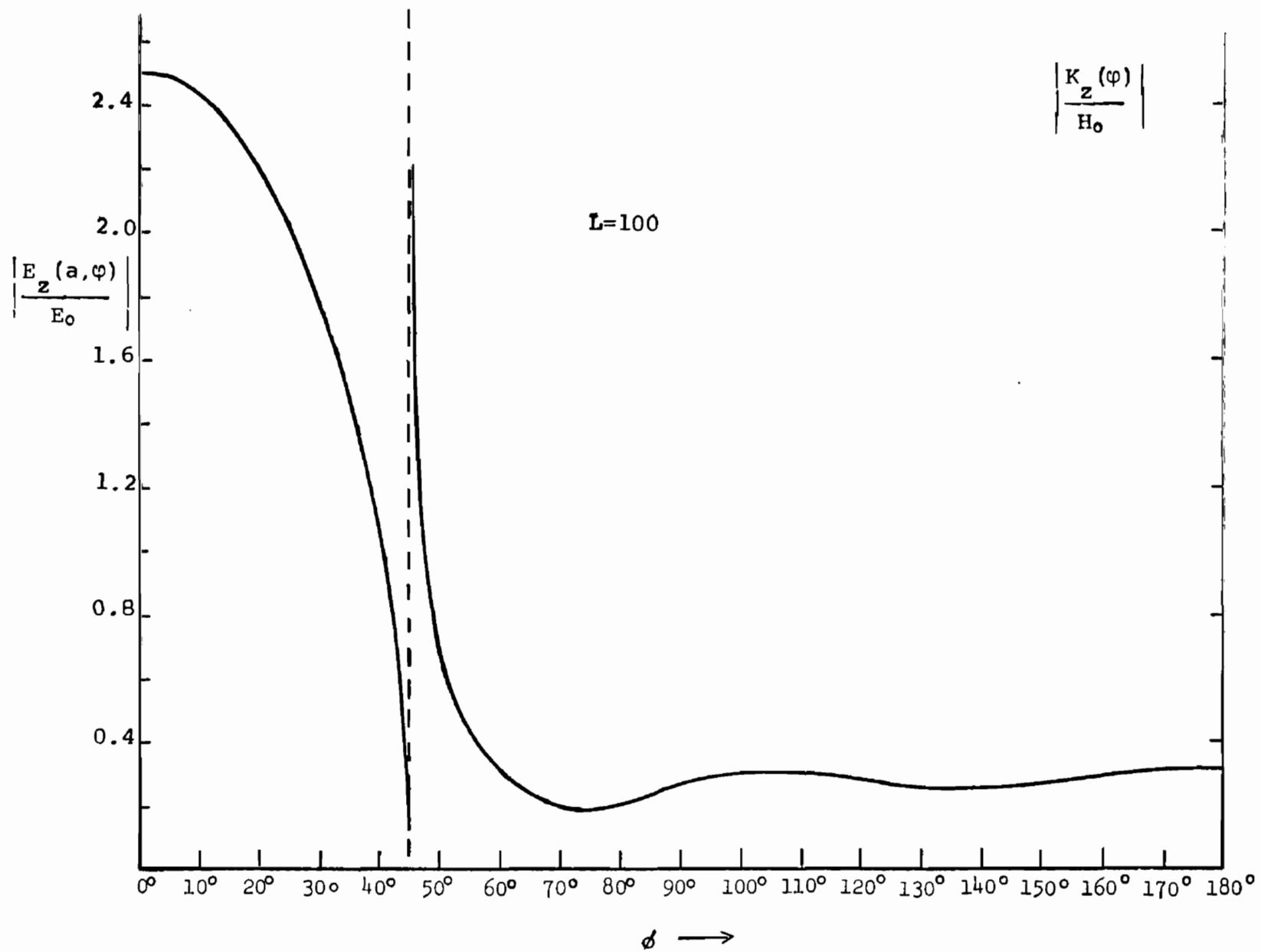Figure 11. Electric Field In The Slot, Surface Current On The Conductor; $\eta=2$. $\varphi_0=45°$

Figure 12. Electric Field In The Slot, Surface Current On The Conductor; $\eta = 3$, $\varphi_0 = 45°$

from the maximum at $\varphi = \pi$ to a minimum at about $\varphi = 122°$. Further

decrease in φ results in monotonically increasing current distribu-

tion. This is the same qualitative behaviour found for $\eta = 2$, $\varphi_o = 30°$.

In the latter case though the amplitude is lower and the minimum

occurs at about 115°. For $\eta = 3$ and $\varphi_0 = 45°$ the current density

amplitude follows that for $\eta = 3$ and $\varphi_0 = 30°$ fairly closely. The

principal difference is in the locations of the turning points (other

than at $\varphi = \pi$). For $\varphi_0 = 45°$ a maximum occurs at about $\varphi = 105°$

whereas for $\varphi_0 = 30°$ it appears near $\varphi = 95°$. Minima occur for

$\varphi_0 = 45°$ near 72° and 137° and near 70° and 132° for $\varphi_0 = 30°$.

Figures 13 and 14 give the surface current distributions for $\varphi_0 = 45°$

and $\eta = 4$ and $\eta = 5$. Again a very close resemblance to the corre-

sponding characteristics for $\varphi_0 = 30°$ is most clearly evident. Thus

for $\eta = 4$ we see from Figures 13 and 17 a maximum occurs at $\varphi = \pi$.

The amplitude of this maximum in the surface current density is

approximately 1.8 for $\varphi_0 = 30°$ and 2.1 for $\varphi_0 = 45°$. In both slotted

cylinder cases the current density falls monotonically as we move

away from the rear of the cylinder. For $\varphi_0 = 45°$ we pass through an

inflexion point at about 135° whereas the inflexion point occurs at

about 132° for $\varphi_0 = 30°$. Again both current distributions decrease

monotonically as we move away from the inflexion point toward smaller

values of φ. Note that the amplitudes are about 1.25 for $\varphi_0 = 45°$

and 1.15 for $\varphi_0 = 30°$ at the inflexion points. In the $\varphi_0 = 45°$ case

the first minimum occurs at about $\varphi = 90°$ with amplitude 0.5. For

$\varphi_0 = 30°$ this first minimum is at about $99°$ with the same amplitude. As we proceed further around towards the slot we find a monotonically increasing surface current density until a maximum is reached. This occurs for both $\varphi_0 = 45°$ and $\varphi_0 = 30°$ at about $\varphi = 65°$ with an amplitude of 1.7 for the narrower slot and is only very slightly higher for $\varphi_0 = 45°$. Proceeding further toward the slot both cases exhibit monotonically decreasing behaviour until a minimum at $\varphi = 53°$ and amplitude 1.7 is reached for $\varphi_0 = 45°$, while this occurs at $\varphi = 41°$ with amplitude 1.1 for $\varphi_0 = 30°$. Since both cases are thereafter close to the slot they both proceed rapidly to exhibit the strong influence of the slot edge as φ continues to decrease further. For $\eta = 5$ examination of Figure 14 for $\varphi_0 = 45°$ and comparison with Figure 8 for $\varphi_0 = 30°$ shows very plainly that from $\varphi = \pi$ around to about $\varphi = 62°$ both surface current distributions are very nearly the same. The principal difference over this range is merely the sharpening of the rate of change in surface current near the minima. Both surface current distributions have a maximum at $\varphi = \pi$ with amplitude of about 2.25 and a second maximum at about $\varphi = 91°$ with amplitude of about 2.25 for $\varphi_0 = 30°$ and 2.1 for $\varphi_0 = 45°$. They both have a deep lying minima at about $\varphi = 125°$ with amplitude of about 0.1. They further have a second deep minimum at $\varphi = 65°$ for $\varphi_0 = 45°$ and $\varphi = 63°$ for $\varphi = 30°$. At both of these second minima the current densities have an amplitude of about 0.1. As the slot edge is approached after passing through the second minimum the $\varphi_0 = 45°$

surface current density distribution possesses a shoulder at about $\varphi = 54°$ and with an amplitude of about 1.5. The $\psi_0 = 30°$ current distribution also exhibits a shoulder. This occurs at about $\varphi = \,7°$ is somewhat broader and has an amplitude of about 1.4. In summary then we note a gradual evolution in the surface current density distribution as we increase from $\varphi_0 = 30°$ to $\varphi_0 = 45°$. Next consider the $\varphi_0 = 45°$ slot electric field distributions as shown in Figures 10 through 14. For $\eta = 1,2,3$ we see these distributions as qualitatively what should be expected in the long-wavelength-narrow-slot width limit. This is somewhat remarkable since for $\varphi_0 = 45°$ as we noted earlier, 1/4 of the cylinder has been removed. In the $\eta = 2$ case for example the slot width is approximately equal to 1/2 a wavelength. For $\eta = 4$, $\varphi_0 = 45°$ the slot electric field is clearly deviating from the long-wavelength limit behaviour. In fact the field for this case resembles that shown in Figure 8 for $\eta = 5$ and $\varphi_0 = 30°$. Figure 14 for $\eta = 5$ and $\varphi_0 = 45°$ shows very simply that the electrostatic or long-wavelength or narrow-slot approximation cannot reliably be used to describe the slot electric field distribution except when safely in the limiting region $a\Delta\varphi/\lambda \ll 1$. For $\eta = 5$ the slot width is comparable to the wavelength. The electric field distribution over the slot for $\eta = 5$ displays a maximum at the slot center followed by a minimum and in turn another slightly higher maximum as the edge is approached. This of course then ends by a monotonically decreasing field amplitude which vanishes as the slot
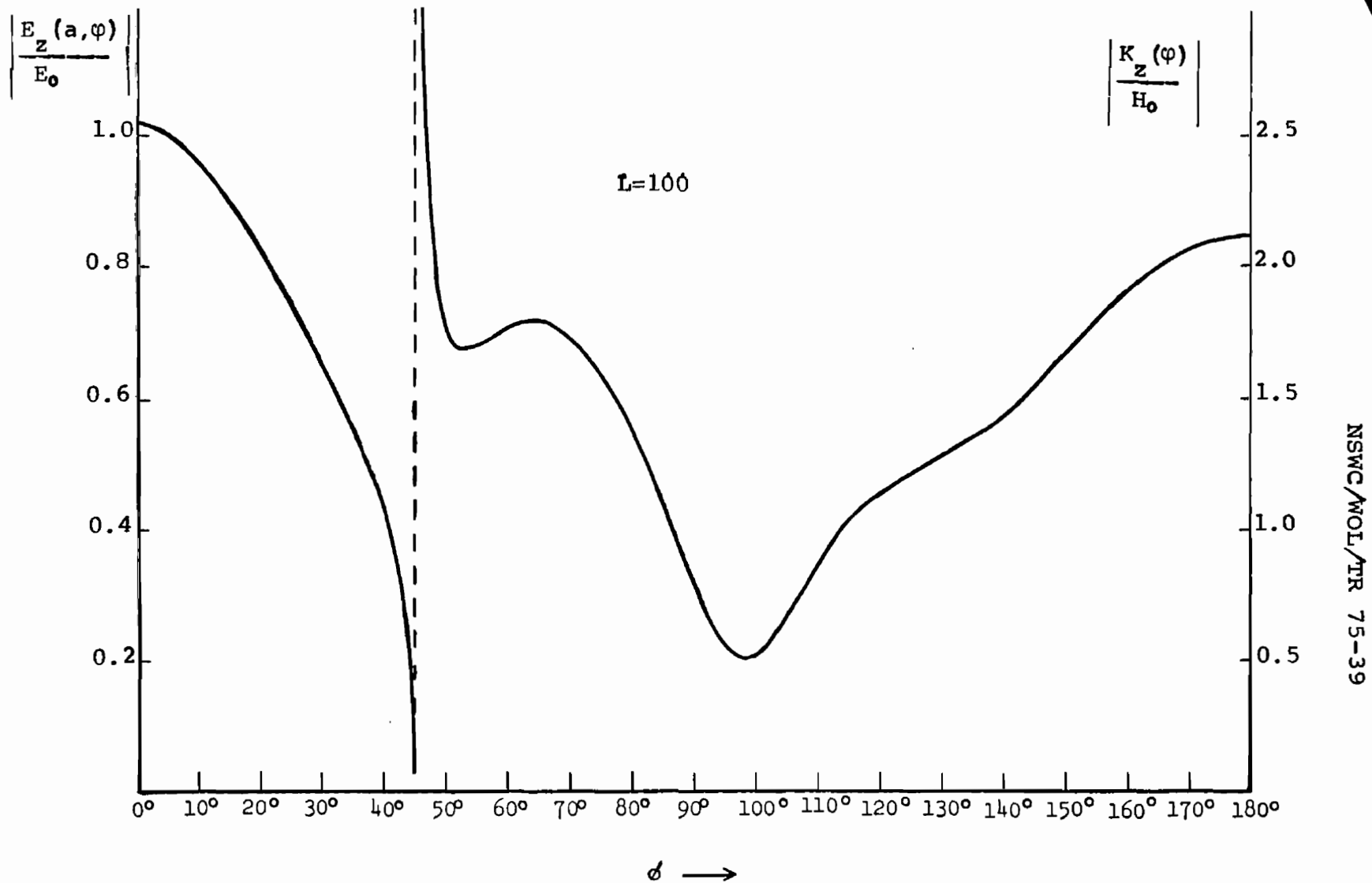
Figure 13. Electric Field In The Slot, Surface Current On The Conductor; $\eta=4$, $\varphi_0=45°$
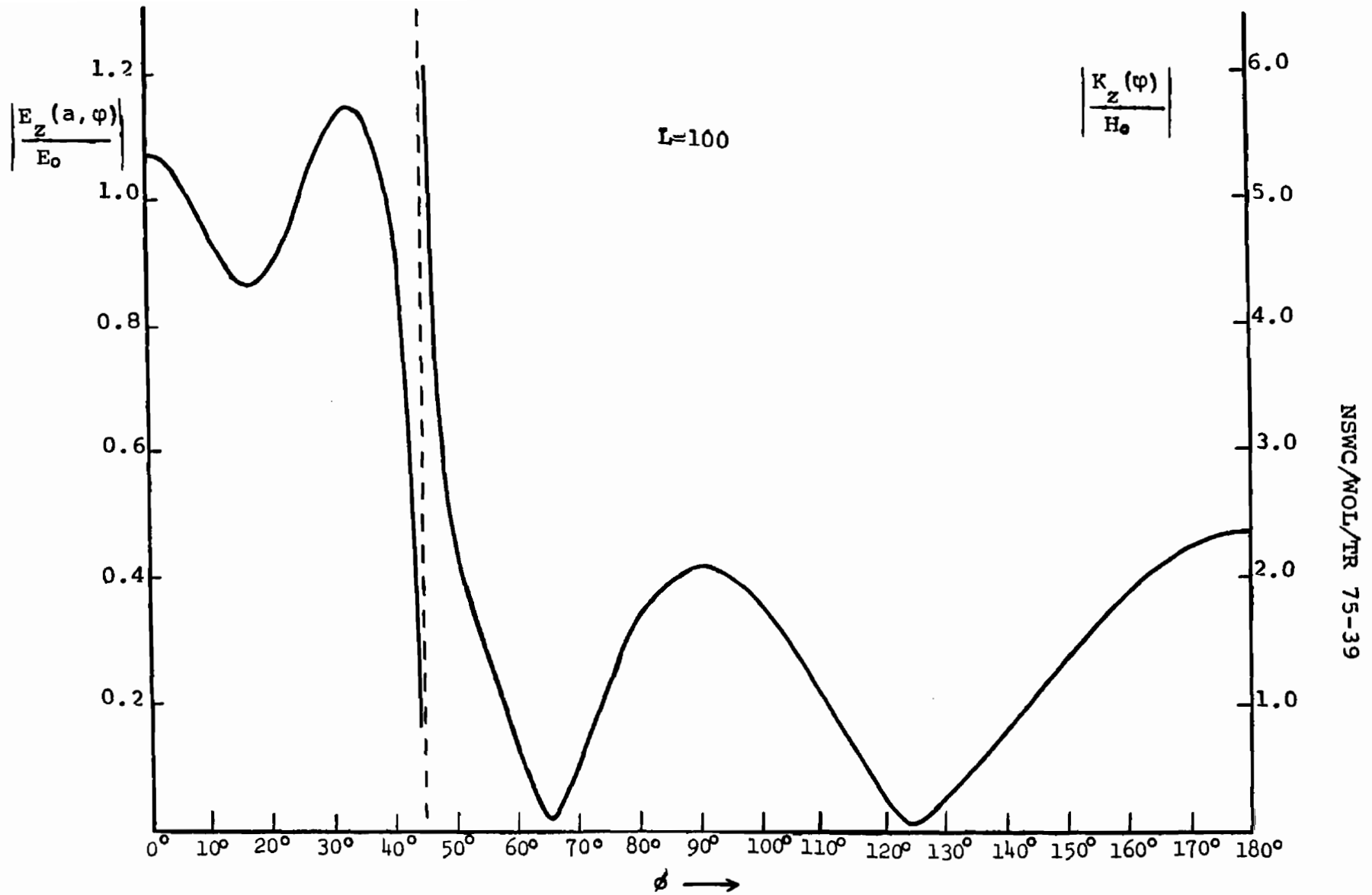
Figure 14. Electric Field In The Slot, Surface Current On The Conductor; $\eta=5$, $\varphi_0=45°$

edge is reached. The $\varphi_0 = 45°$, $\eta = 5$ slot electric field behaviour is radically different from that for $\varphi_0 = 30°$, $\eta = 5$ even though the latter also involves a slot width comparable to the wavelength.

We have superposed, using small crosses, the back-scattering cross-section for $\varphi_0 = 45°$ on the corresponding curves for $\varphi_0 = 30°$ in Figure 9 and $\varphi_0 = 60°$ in Figure 20. From an examination of these curves we observe the gradual evolution of the back-scattering cross-section characteristics as the slot is widened.

4. The $\varphi_0 = 60°$ Slot Characteristics

For this case the same order of approximation was taken in the range $\varphi_0 < \varphi < \pi$ namely 50 points. This leads to the conducting portion of the slotted cylinder being approximated by L = 100 zones of equal arclength each carrying a uniform current density. Note that in this case we have

$$(\Delta\varphi)/\varphi_0 = \frac{(\pi - \pi/3)/50}{\pi/3} = .04$$

and the ratio of the arclength of each constant current zone to the incident wavelength at the largest η considered is

$$\frac{a\Delta\varphi}{\lambda} = \eta \frac{\Delta\varphi}{2\pi} = 5 \times \frac{1}{150} = \frac{1}{30} \approx .03$$

Again we emphasize that this is the largest ratio of arclength to wavelength considered for this particular slotted cylinder. The results obtained for this case should be somewhat more accurate than for the previous slotted cylinder. Figures 15 through 19 show

89

respectively for $\eta = 1,2,3,4$ and 5 the slot electric field distribution and simultaneously the surface current density distribution on the conductor for the $\varphi_0 = 60°$ slotted cylinder. Upon examination of Figures 15, 16 and 17 for $\eta = 1,2,3$ respectively we see that the slot electric field, not unexpectedly, is still evolving from the narrow-slot electrostatic type distribution. Simultaneous with this the corresponding large angle range of the surface current distribution for the $\varphi_0 = 60°$ slotted cylinder still possesses the $\varphi_0 = 0$, or slot-less, cylinder character. But this quantity is also undergoing increasing deviation for the $\varphi_0 = 60°$ case for $\eta = 1,2,3$. It is certainly obvious as η takes on larger values as can be seen in Figures 18 and 19 that $\varphi_0 = 60°$ cannot be described by the narrow-slot approximation. Considerable structure is now evident in both the surface current density distribution and the slot electric field distribution. Note however that the qualitative behaviour of the current distributions for $\eta = 1,2,3$ are somewhat similar for $\varphi_0 = 30°$, $\varphi_0 = 45°$ and for $\varphi_0 = 60°$. Figures 7, 13 and 18 make it quite plain that for the larger slot angle the current distributions can be significantly different for the slotted cylinders. The changes are apparently gradually evolving as one can observe by comparing the $\eta = 5$ situation for the surface currents. Figures 8, 14 and 19 respectively for the $\varphi_0 = 30°$, $\varphi_0 = 45°$ and $\varphi_0 = 60°$ slots exhibit maxims at or near $\varphi = 90°$ and $\varphi_0 = 180°$ and a minimum in the neighborhood of $\varphi = 120°$. They show the occurrence of another minimum

90

Figure 15. Electric Field In The Slot, Surface Current On The Conductor; $\eta=1, \varphi_0=60°$

Figure 16. Electric Field In The Slot, Surface Current On The Conductor; $\eta=2$, $\varphi_0=60°$
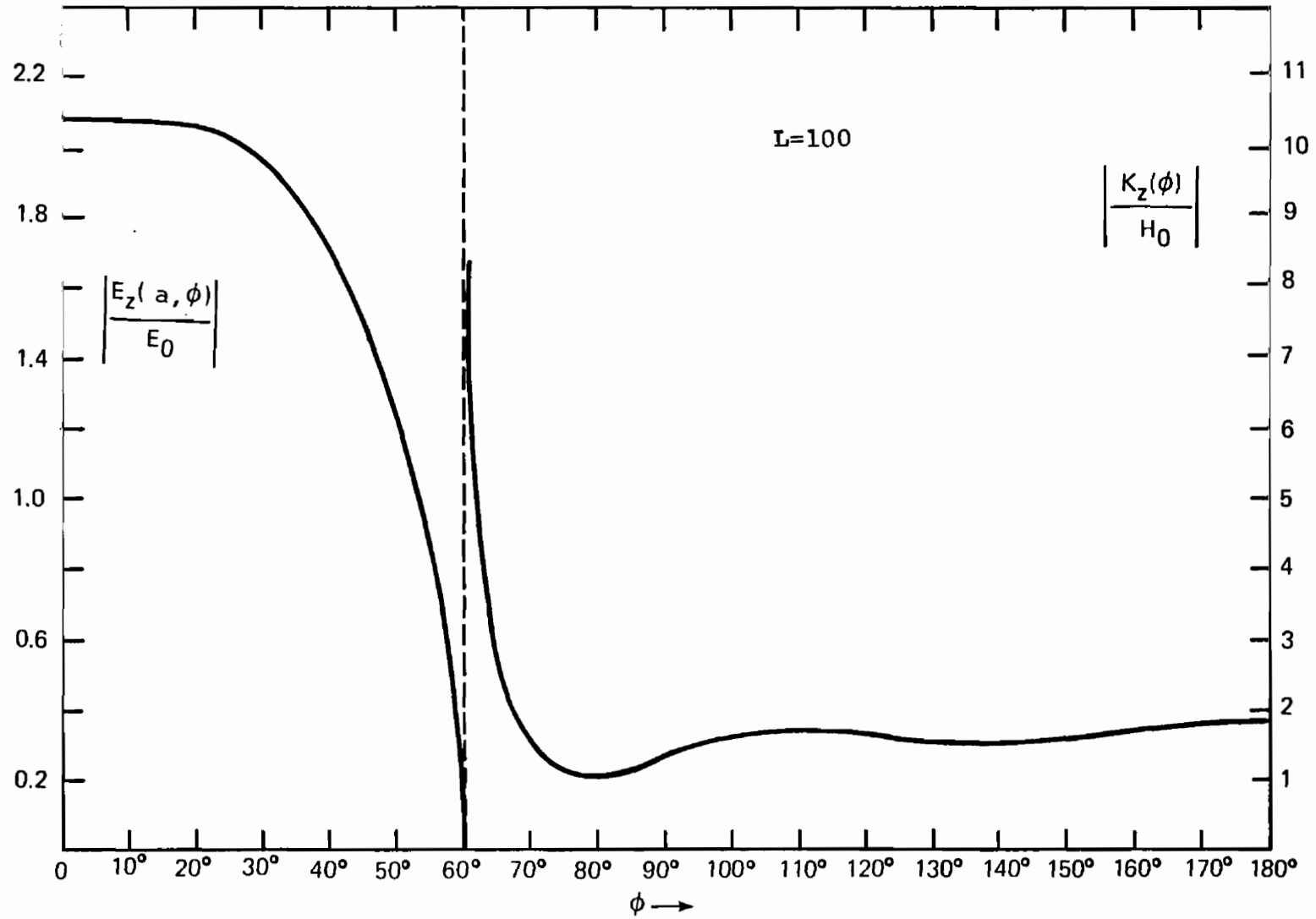
Figure 17. Electric Field In The Slot, Surface Current On The Conductor; $\eta=3$, $\varphi_0=60°$
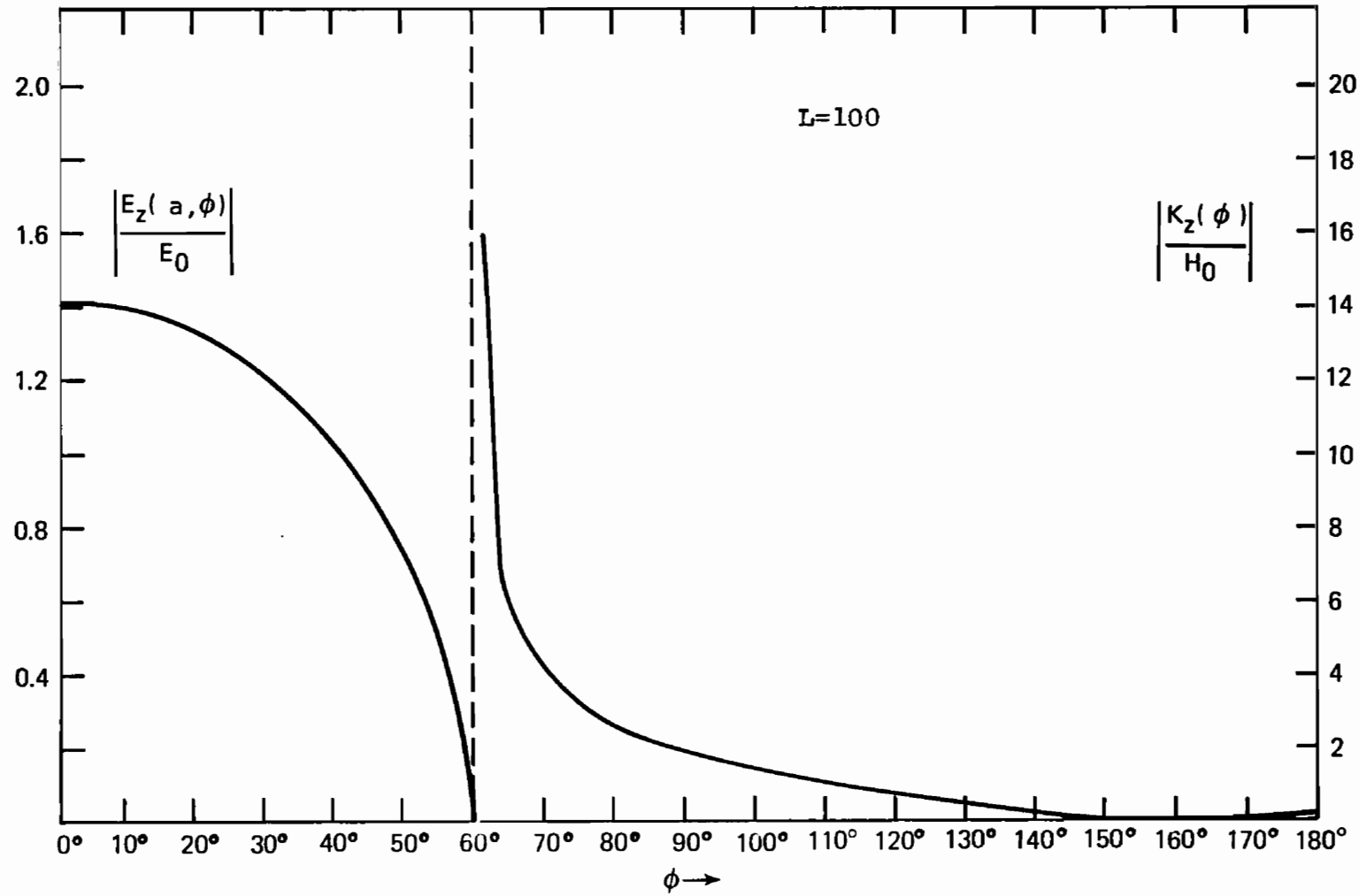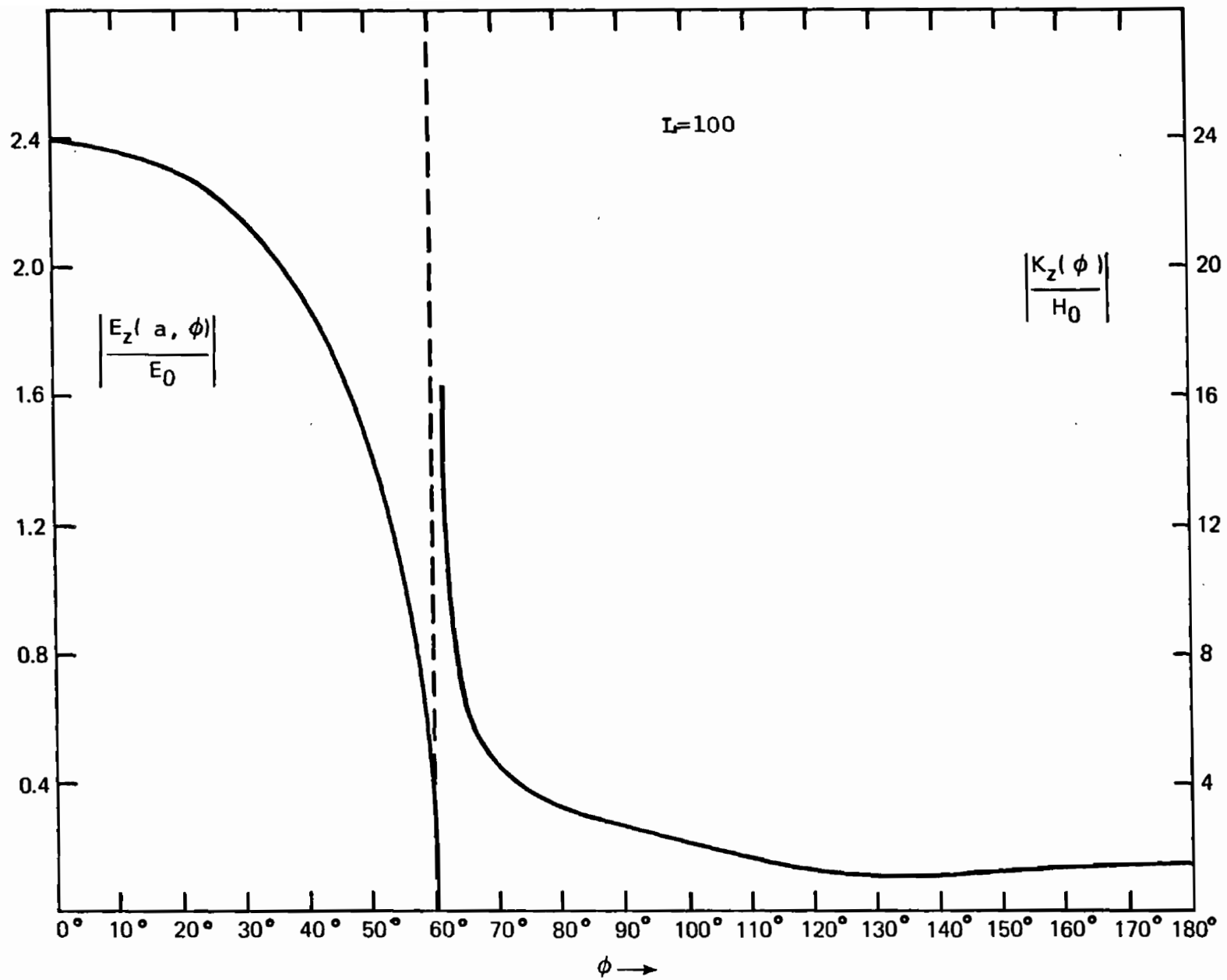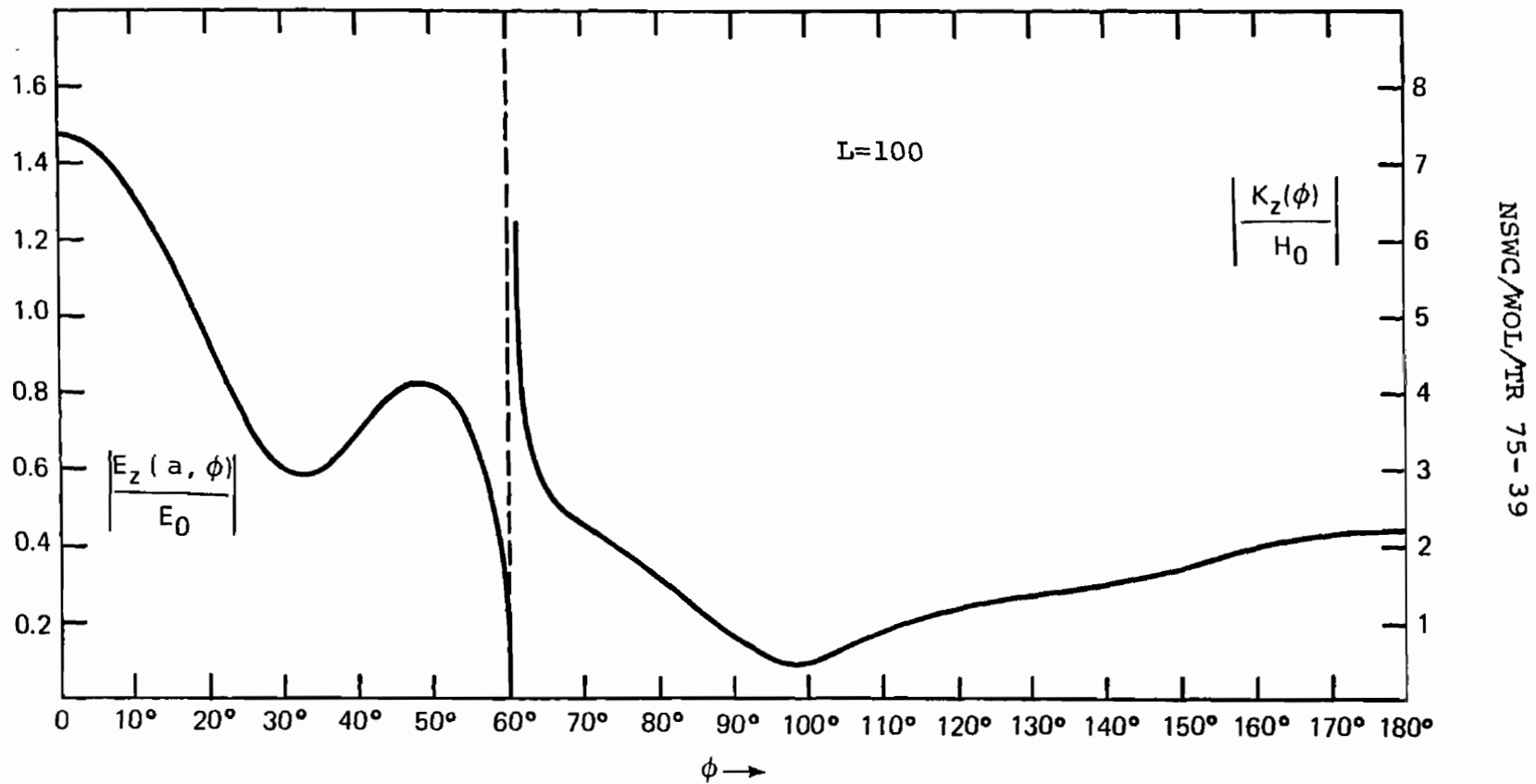
Figure 18. Electric Field In The Slot, Surface Current On The Conductor; $\eta=4$, $\varphi_0=60°$
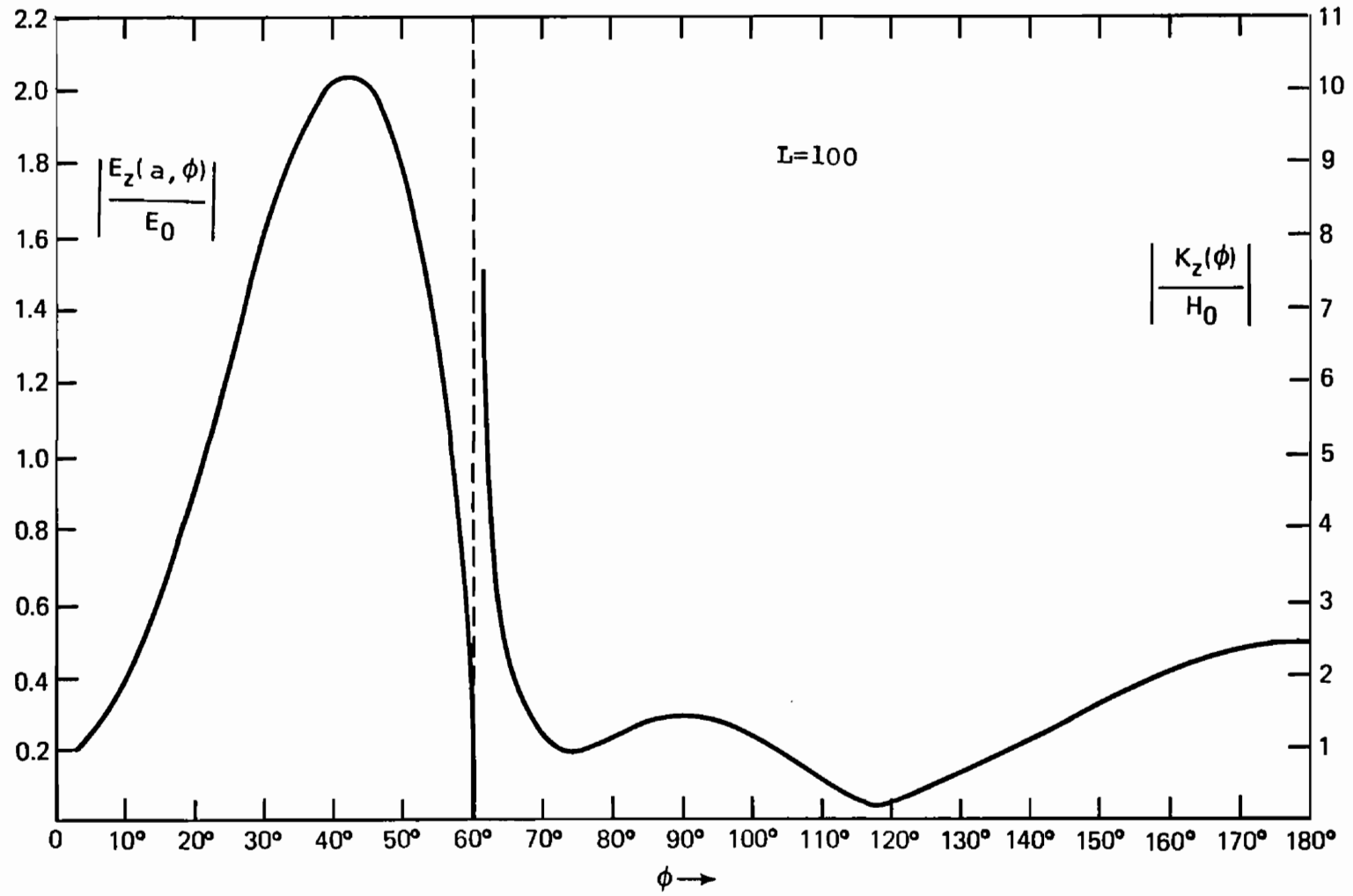
Figure 19. Electric Field In The Slot, Surface Current On The Conductor; $\eta=5$, $\varphi_0=60°$

Figure 20. Back-Scattering Cross-Section, $\varphi_0 = 60°$

$B = 2\pi\sigma_B/\lambda$

$L = 100$

$x \equiv \varphi_0 = 45°$
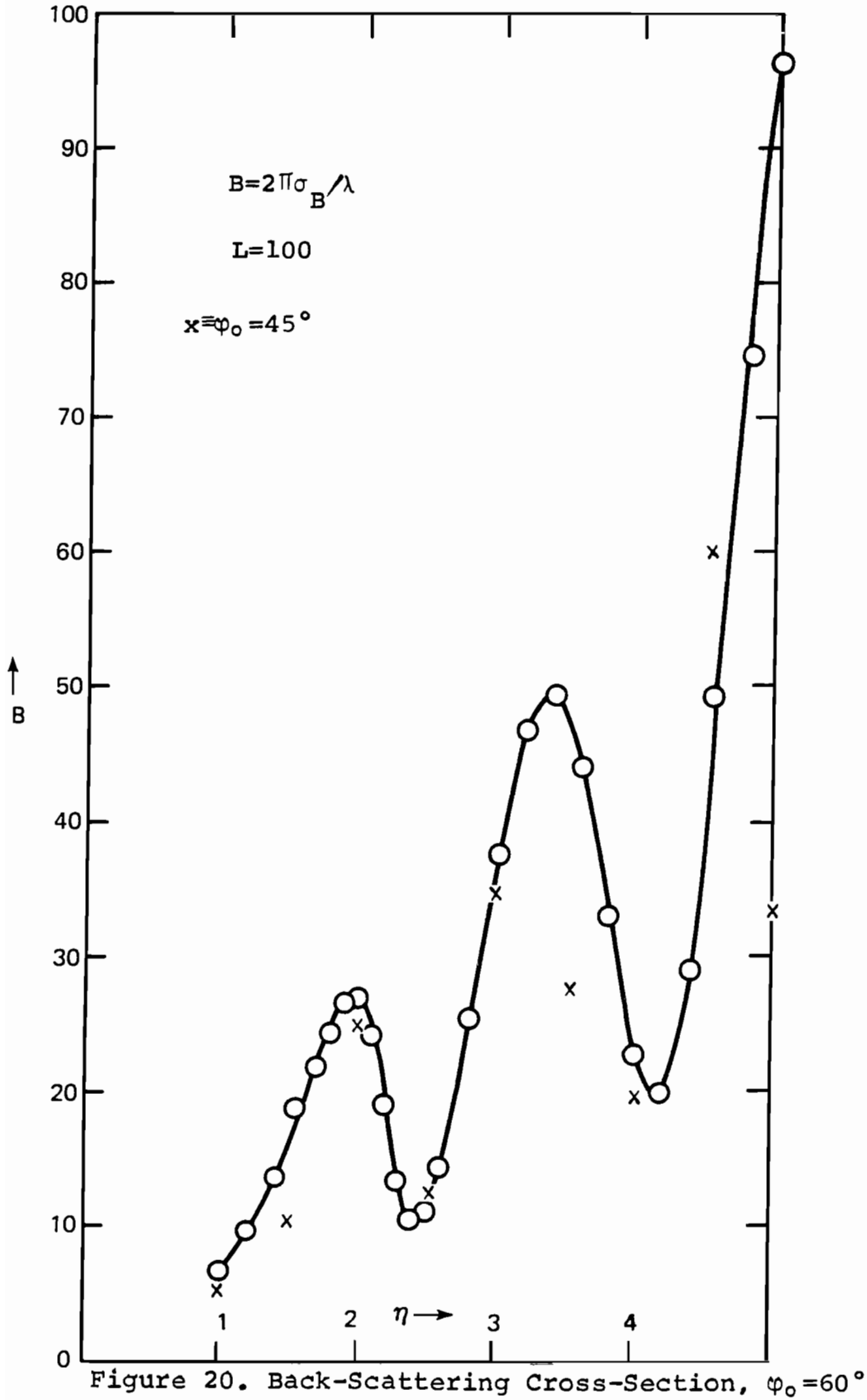
and a shoulder near the slot edge. These latter occur at different angles in each case. Furthermore the shoulder is barely perceptible for the $\eta = 5$, $\varphi_0 = 45°$ and $\varphi_0 = 60°$ cases and quite boldly evident for $\eta = 5$, $\varphi_0 = 30°$ case. Finally we should note the back-scattering cross-section for the $\varphi_0 = 60°$ slotted cylinder. This is given in Figure 20. It still shows the existence of two relatively sharp minima. But these now occur at about $\eta = 2.4$ and $\eta = 4.2$. This is essentially the predicted behaviour one should anticipate. It is a consequence of the physical fact that the cylinder is becoming less clearly defined as a cylinder. At $\varphi_0 = 60°$ one third of the conductor has been removed. As a result it should be expected that the resonances for the slotted cylinder should wander from those for a cylindrical waveguide and in addition they should display broadened oscillations when plotted against wavelength. This indeed occurs as can be seen by comparing Figures 20 and 9. Otherwise the overall behaviour is the usual one as η increases from the Rayleigh limit.

5. The $\varphi_0 = 90°$ Slot Characteristics (Half-Cylinder)

This slotted cylinder configuration is the so-called "half-cylindrical mirror". Again the same order of approximation was taken for the range of azimuth $\varphi_0 < \varphi < \pi$. We consider again the conducting portion of the slotted cylinder to be approximated by L = 100 zones of equal arclength. Each such zone it is assumed carries a uniform surface current density. In this case we have

$$(\Delta\varphi)/\varphi_0 \;=\; \frac{(\pi-\pi/2)/50}{\pi/2} \;=\; 1/50 \;=\; 0.02$$

The ratio of the arclength of each constant surface current element to the wavelength of the incident radiation for the largest value of η considered in this case is

$$\frac{a\Delta\varphi}{\lambda} \;=\; \eta \,\frac{\Delta\varphi}{2\pi} \;=\; 5 \times \frac{1}{200} \;=\; \frac{1}{40} \;=\; 0.025$$

Just as we stated in the previous case we expect the calculated surface current distribution to be a bit more accurate for this slotted cylinder than for the preceding slotted cylinder. Figures 21 through 25 respectively present the surface current distribution on the conductor and the distribution of the electric field in the aperture for values at $\eta = 1,2,3,4$ and 5. Now if we examine Figures 21 and 22 and 2 we note that in the shadow region, i.e. near $\varphi = \pi$ we have roughly speaking qualitatively similar behaviour in the current density for the half-cylindrical mirror and for the slot-less circular cylinder. By this we are referring to the occurrence of a maximum at π for both $\eta = 1$, and $\eta = 2$ and $\varphi_0 = 0$ and $\varphi_0 = \pi/2$. This maximum is accompanied by a slightly lower minimum in the surface current density at a smaller value of φ but roughly in the neighborhood of $\varphi = 160°$ in all four cases being compared. This is followed by monotonically increasing behaviour of the current density as φ decreases. For the $\varphi_0 = 90°$ case, of course, the singularity of the edge behaviour soon dominates and we get the anticipated marked
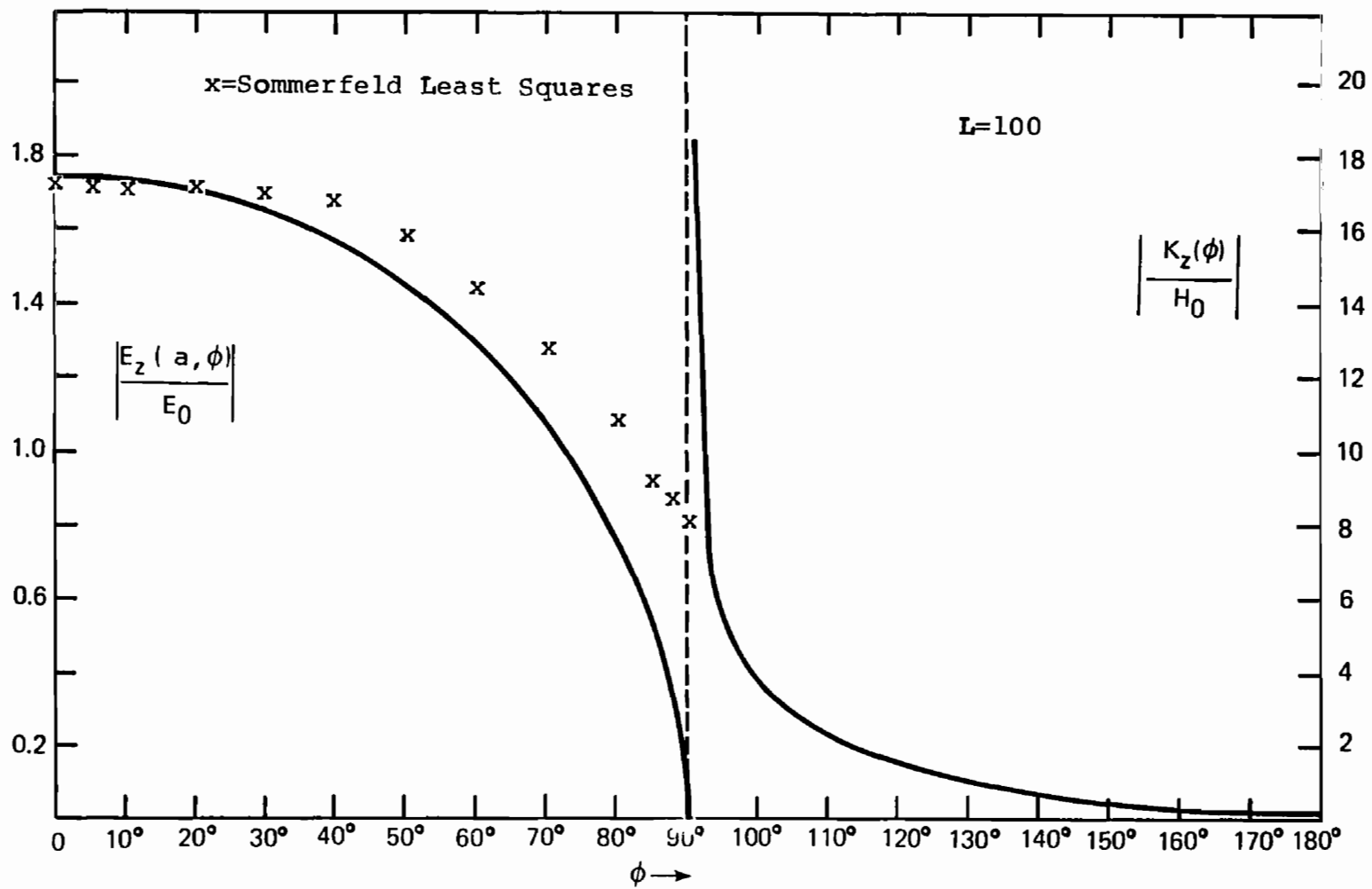
Figure 21. Electric Field In The Slot-By Method of Moments and by Sommerfeld Least Squares, Surface Current On The Conductor; $\eta=1$, $\varphi_0=90°$
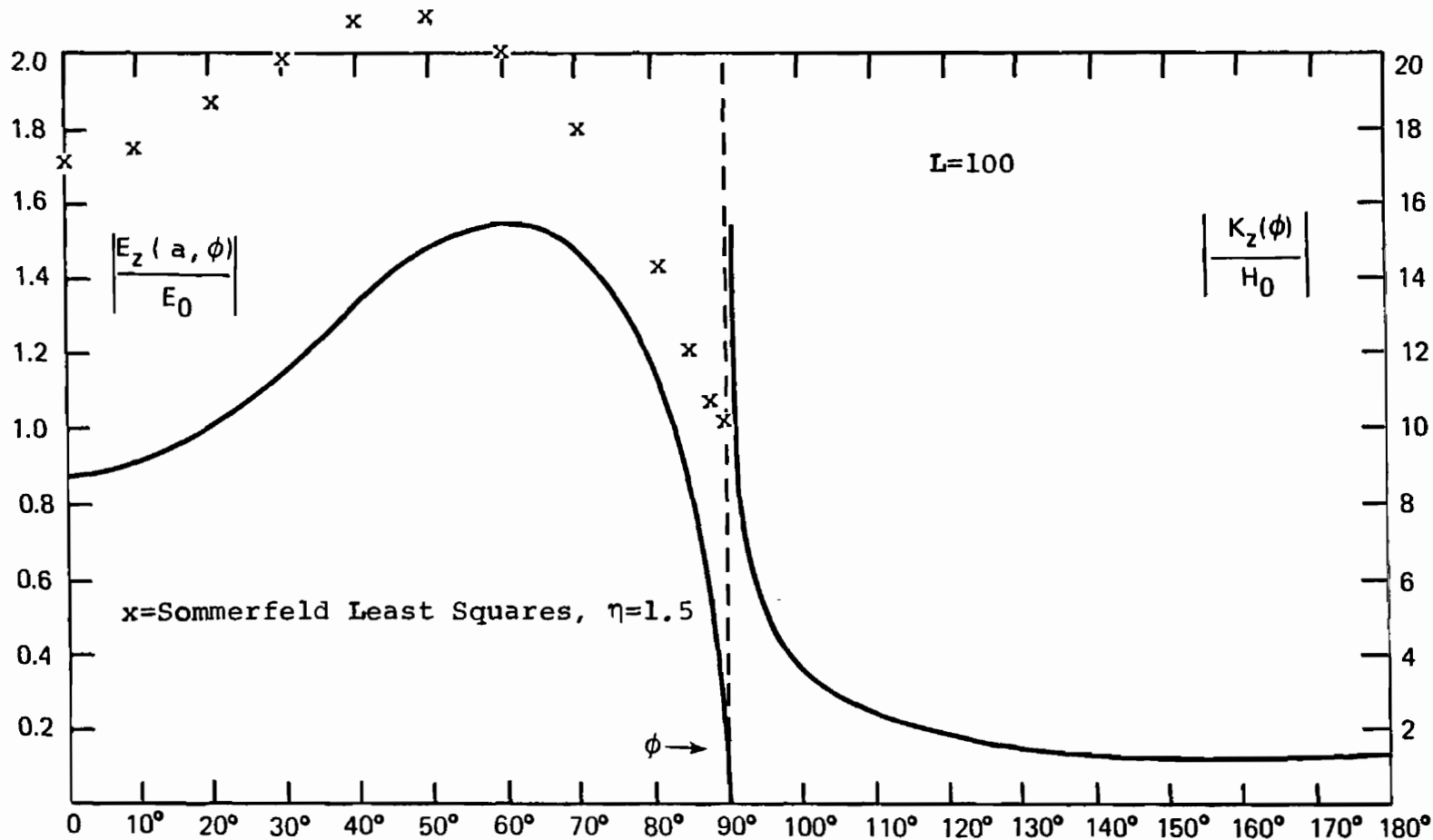
Figure 22. Electric Field In The Slot – By Method of Moments η=2,
And By Sommerfeld Least Squares, η=1.5, Surface Current On The Conductor, η=2; φ₀=90°

deviation from the $\varphi_0 = 0°$ behaviour as we get further away from

$\varphi = \pi$. It must be emphasized that vestiges of the characteristics of

the slot-less cylinder may continue to appear for the $\varphi_0 = 90°$ case.

Nevertheless we should expect greater deviation from the $\varphi_0 = 0°$

case. After all one should recall we now have only half the cylinder

remaining in the present diffraction problem. Thus, the $\eta = 3$ situa-

tion as shown in Figure 23 is a rather familiar type of behaviour

which actually is somewhat surprising for the half-cylinder. Con-

tinuing we see the $\eta = 4$ and $\eta = 5$ tangential electric field results

of Figures 24 and 25 are now departing very radically from the long

wavelength cylinder limit behaviour. Accompanying this behaviour of

the slot electric field we observe growing departure of the surface

current density distribution from the full cylinder (i.e. $\varphi_0 = 0$)

characteristic as shown in Figure 3. Again we anticipate a later

report on measurements[32] on a 12-inch long cylinder open at both ends,

for $\varphi_0 = 90°$ and $\eta = 3.84$. These results showed a slot electric

field distribution, in the plane that divides the cylinder in half

lengthwise, with maxima at $\varphi = 0°$ and about $70°$ and a sharp minimum

at about $\varphi = 40°$ much like the behaviour exhibited by the infinite

half cylinder in Figure 24 for $\eta = 4$.

In the half-cylindrical mirror case we have results obtained

---

32. D. P. Margolis, C. L. Andrews, J. Heckl and L. Libelo, "Plane
    Wave Scattering by An Open-Ended Cylinder With An Axial-Slot",
    Bull. Am. Phys. Soc. Vol. 20, No. 1, p 101, 1975
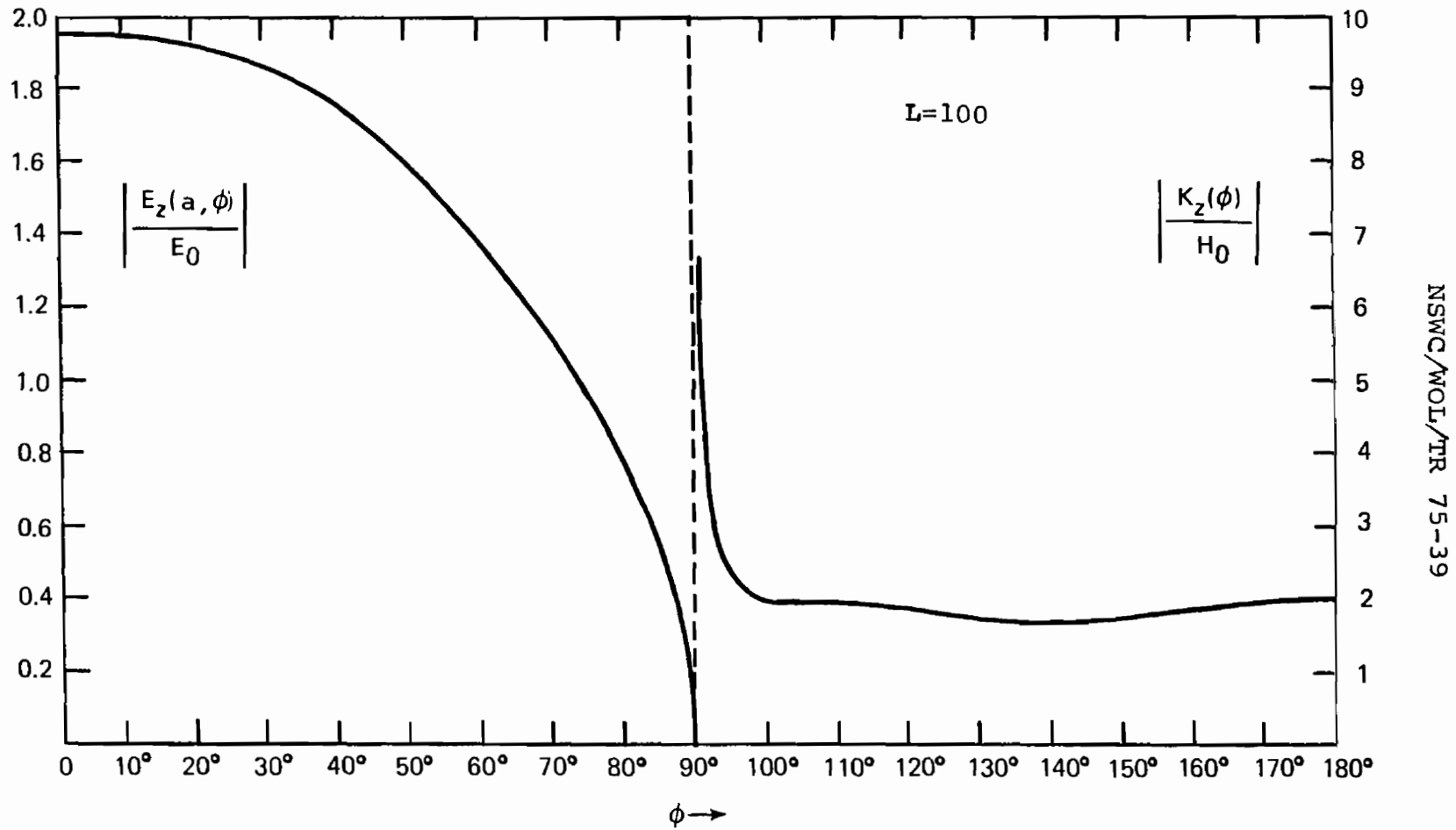
Figure 23. Electric Field In The Slot, Surface Current On The Conductor; $\eta=3$, $\varphi_0=90°$

from an earlier attempt to solve this problem namely that of Barakat
and Levin[9] using the Sommerfeld least squares method[5]. We have cal-
culated the aperture electric field distribution using the tabulated
coefficients of Barakat and Levin for $\eta = 1$ and 1.5. In Figure 21 we
show their results for $\eta = 1$ using a four-term approximation for an
infinite series representation of the field. Clearly the behaviour
close to the slot edge can't be expected to be predicted too well in
this order of approximation. As can be seen by comparison with the
L = 100 solution this is indeed the case. Surprisingly though the
Barakat-Levin results are not too far off in amplitude from the
center of the slot almost to the slot edge itself. However, the
qualitative behaviour predicted by the four-term approximation fails
abysmally both in the central region of the slot and at the edge.
The Barakat and Levin electric field for $\eta = 1$ predicts a minimum at
the slot center then a very slow rise to a maximum at about $\varphi = 20°$.
The amplitude over this range rises from 1.7 at $\varphi = 0$ to about 1.71
at the maximum. From there on the electric field monotonically
decreases as we proceed toward the edge of the conductor. Unfortu-
nately the Barakat-Levin approximation leads to a non-zero tangential

5. A Sommerfeld, "Partial Differential Equation", p 29-31
    Academic Press, New York, 1949

9. R. Barakat and E. Levin, "Diffraction of Plane Electromagnetic
    Waves by a Perfectly Conducting Cylindrical Lamina", Jour. Opt.
    Soc. of Amer. 54, 1089-1094, September 1964

component of electric field at the slot edge. This is fundamentally
incorrect physically. The only other set of data published by
Barakat and Levin that we could use for purposes of comparison is the
case for η = 1.5. Using their five-term approximation for the
infinite series for the slotted cylinder field we calculated the
corresponding electric field amplitude over the slot region. Upon
examination of Figure 22 we can only guess that the qualitative
behaviour they predict is probably not too far off except very near
the slot itself. Truncation of the infinite series beyond the fifth-
term probably accounts for the non-vanishing tangential component of
electric field at the slot edge itself. In fact they predict the
field at the slot edge is about half that at the slot center. Note
that the Barakat-Levin five-term approximation for η = 1.5 predicts
the occurrence of a minimum in the slot electric field at the slot
center followed by a maximum at about φ = 50° and a steady falloff in
amplitude thereafter as we proceed around the cylinder toward the
slot edge. This behaviour is very similar to that for η = 2 in our
method-of-moments calculation. The difference in amplitudes between
the two solutions probably is due to the difference in the value of η
they represent.

The radical change in the slot electric field distribution as η
increases from 4 to η = 5 results from the somewhat less remarkable
change in the surface current density over the half-cylinder for the
same pair of values of η. We observe in Figure 24 for η = 4 the
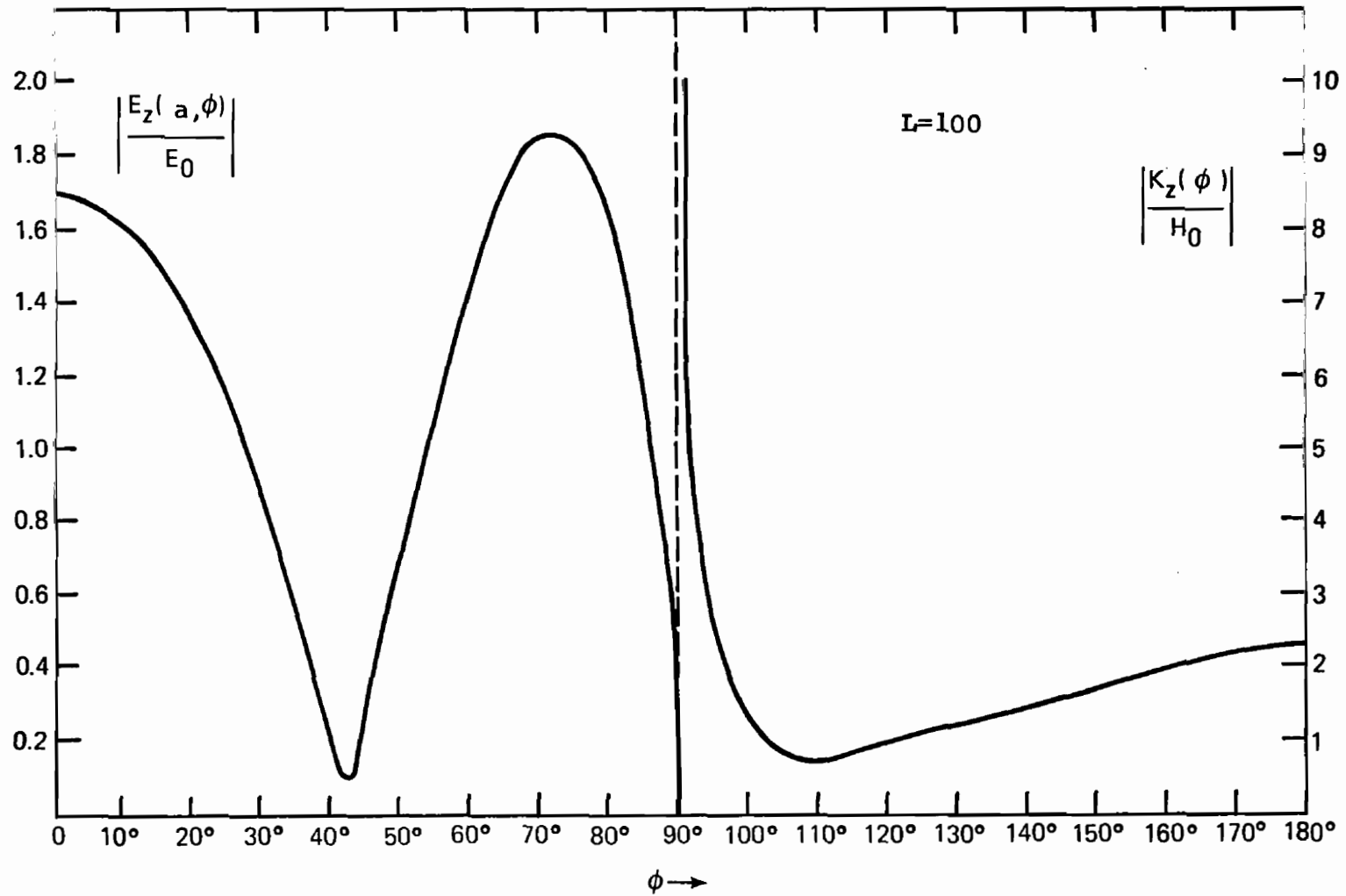
Figure 24. Electric Field In The Slot, Surface Current On The Conductor; $\eta=4$, $\varphi_0=90°$
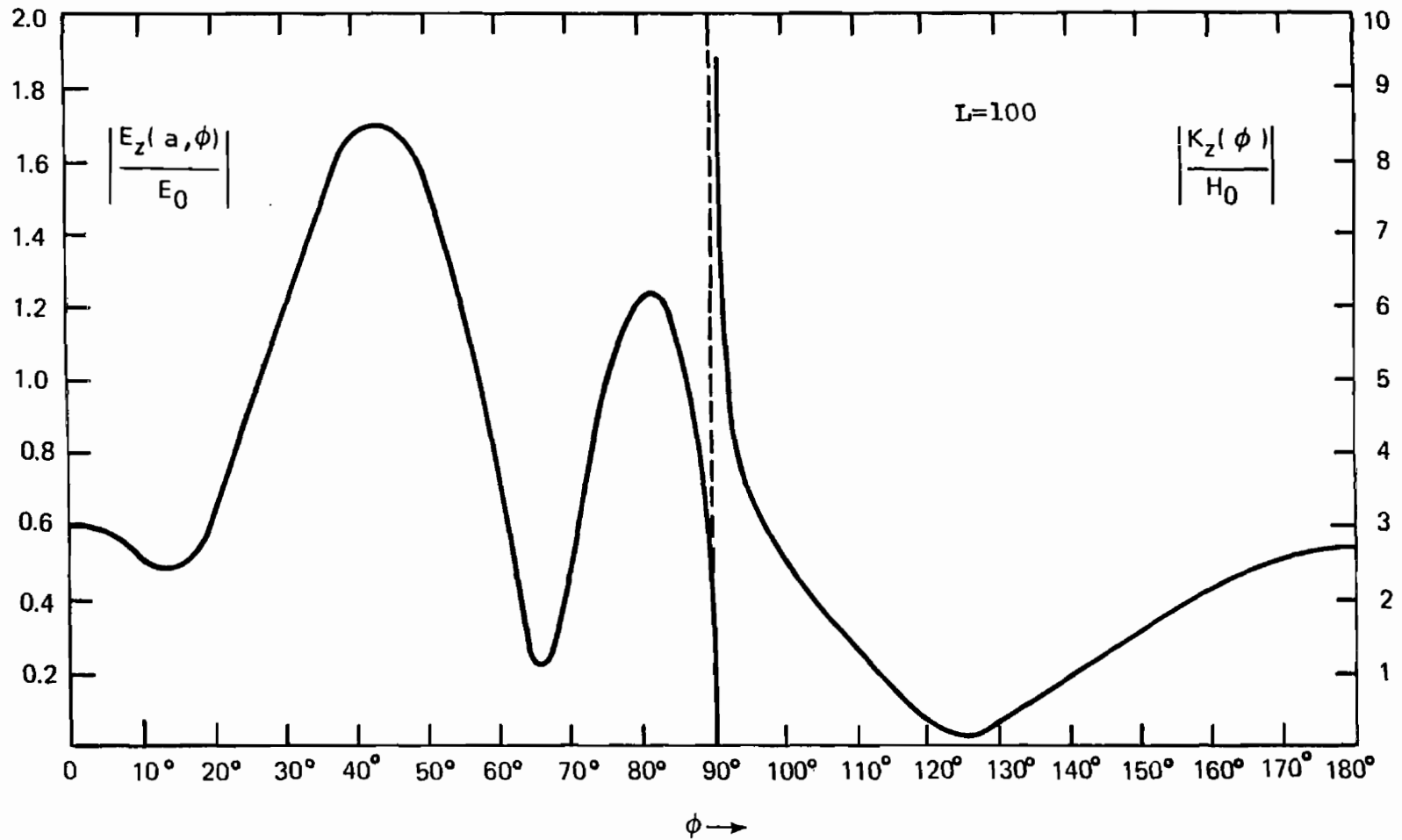
Figure 25. Electric Field In The Slot, Surface Current On The Conductor; $\eta=5$, $\varphi_0=90°$

electric field has a <u>maximum</u> at the slot center with an amplitude of 1.68 followed by a sharply reduced minimum of amplitude 0.85 at $\varphi = 43°$. This in turn is followed by a sharp rise to a second maximum with amplitude of 1.86 at $\varphi = 72°$ and then a sharp drop to zero at the slot edge. Figure 25 for $\eta = 5$ displays a low lying <u>maximum</u> of amplitude 0.6 at the slot center then falls off slightly to a minimum at $\varphi = 13°$ with amplitude of 0.5. Proceeding around the slot we find a rapid rise to a maximum of amplitude 1.7 at $\varphi = 44°$ then a rapid decrease to a second minimum at $\varphi = 66°$ with amplitude 0.22. This is then followed by a sharp rise to a third maximum of amplitude 1.23 at $\varphi = 82°$ and then a very sharp drop to zero at the slot edge. We thus have observed two very different but very interesting distributions of electric field distributions over the slot due to a change of just 25% in the incident wavelength. Note that for both $\eta = 4$ and $\eta = 5$ very little resemblance to the long-wavelength approximation persists in the slot electric field distribution. Simultaneous with this we observe that the corresponding surface current densities are quite similar for these two values of η.

Figure 26 shows the back-scattering cross-section as a function of a/λ or η for the half-cylinder. The calculated behaviour shows the further shifting of the resonances and the broadening of the spectrum with increasing slot size. Only one minimum is now evident in the range of η up to $\eta = 5$. The second minimum occurs somewhere beyond $\eta = 5$. This curve is consistent with the pattern evolving as
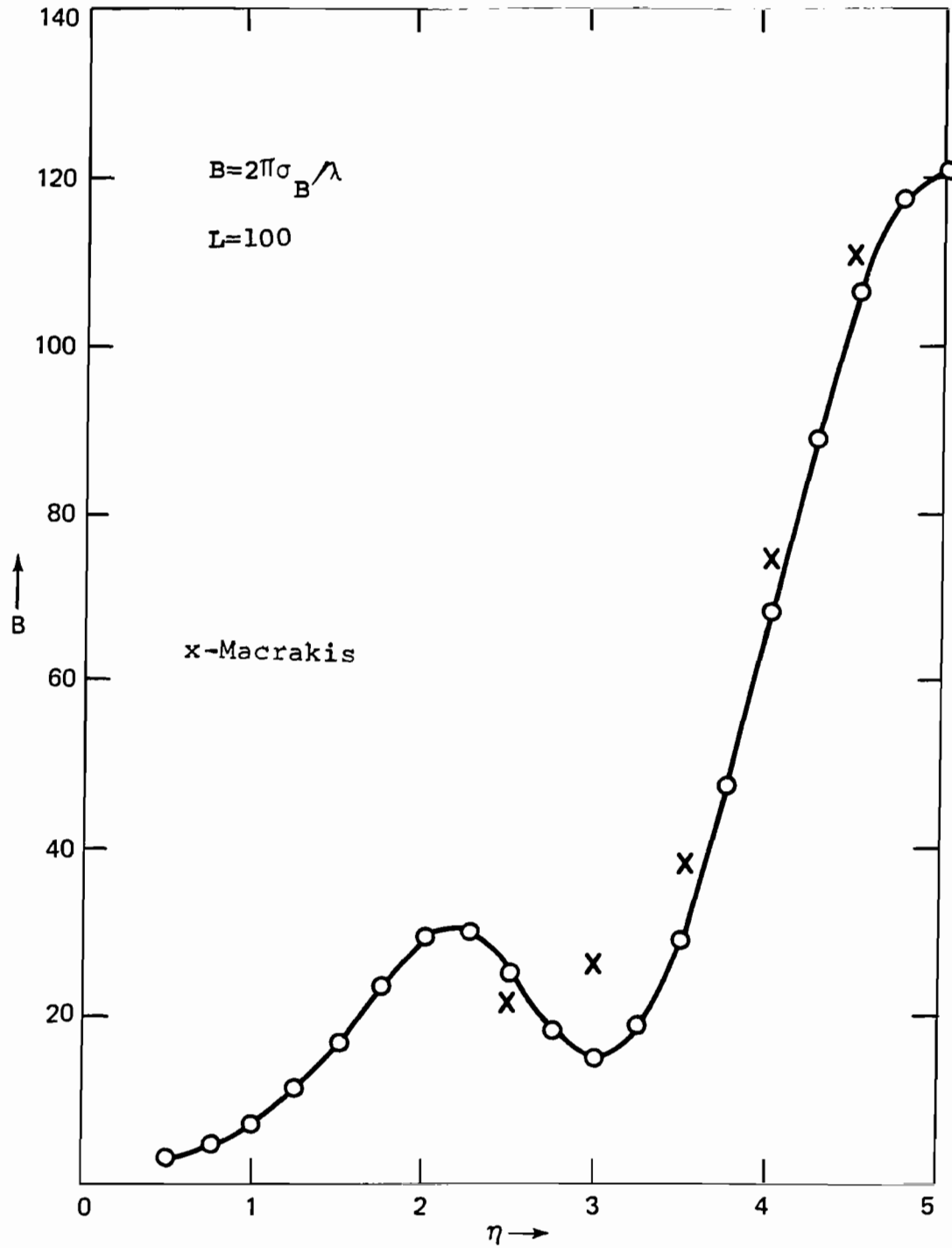
Figure 26. Calculated and Measured Back-Scattering
Cross-Sections; $\varphi_0 = 90°$, The Half Cylindrical Mirror

the slot increases. In Figure 26 we also have included the results

obtained by Macrakis[13] in his attempt to experimentally investigate

the back-scattering of the concave half-cylindrical mirror. From

about $\eta = 3.5$ on to $\eta = 5$ his experimental results are in fairly good

agreement with our theoretical results. His measurements should

coincide with the Rayleigh limit type of behaviour for small η. For

this to be the case if we try to extrapolate down from his result for

the smallest η of his experiment, namely, $\eta = 2.5$ a maximum would

have to exist below $\eta = 2.5$. This agrees at least qualitatively with

our theoretically predicted behaviour. His lack of more precise

agreement with our calculations is very probably rooted in the

limitation of his experimental accuracy. This latter unfortunate

characteristic arises as he himself has observed from the difficul-

ties of modeling in the laboratory an infinite slotted cylinder by

finite slotted cylinders.

6. The $\varphi_0 = 120°$ Slot Characteristics (120° Cylindrical Ribbon)

In this case we have 2/3 of the metallic cylinder missing. We

can consider this problem, as we stated in Part I of this report, as

the scattering by a cylindrical strip subtending an angle of $2\pi/3$ at

the axis. The incoming radiation is of course incident from the con-

cave side of the strip. For this case we again show the results for

---

13. M. S. Macrakis, "Backscattering Cross-Section of Slotted Cylinders", Ph.D. Dissertation, Harvard University, Cambridge, MA, 1958

L = 100. The ratio of angle subtended by each of the 100 approximating uniform current strips to the half-slot angle is

$$\frac{\Delta\varphi}{\varphi_0} = \frac{\pi - 2\pi/3}{2\pi/3} \times \frac{1}{50} = \frac{1}{100} = .01$$

The ratio of the arclength of each of those strips to the shortest wavelength considered is

$$\frac{a\Delta\varphi}{\lambda} = \frac{2\pi a}{\lambda} \frac{\Delta\varphi}{2\pi} = \eta \frac{\Delta\varphi}{2\pi} \approx 0.017$$

These strips are quite small relative to the smallest wavelength considered and hence should be expected to give us quite good results for the calculated quantities. Figure 27 displays the slot electric field distribution and surface current density distribution for $\eta = 1$. The results for the electric field distribution are indeed quite surprising in that we find the characteristic behaviour for the narrow-slot limit approximation. Clearly the slot in the cylinder is not small by any stretch of the imagination. On the other hand the conductor width is about 1/3 the incident wavelength. Clearly we have made a transition. It is now more appropriate to consider how close an approximation to the infinite plane strip our conductor is rather than inquiring as to how narrow a slot we have. We emphasize that we have nevertheless calculated the electric field over the cylindrical surface of radius a not occupied by conducting material. The surface current distribution for $\eta = 1$ has a minimum at $\varphi = \pi$.
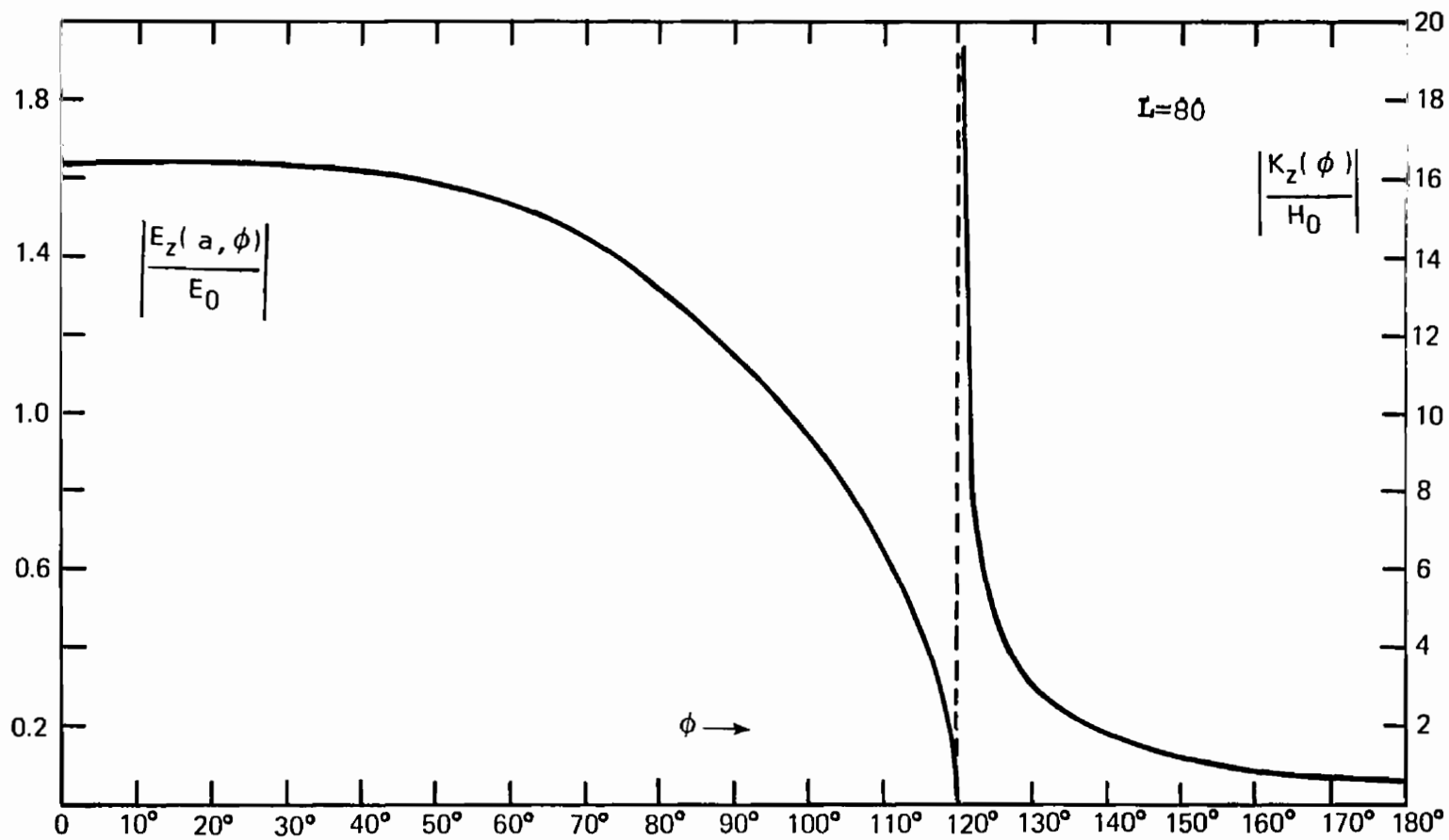
Figure 27. Electric Field In The Slot, Surface Current On The Conductor; $\eta=1$, $\varphi_0=120°$

This is the first slotted cylinder case in which this characteristic
appears. As we move away from the strip center the current density
slowly and steadily increases until near the edge where it rises much
more rapidly. In Figure 28 the electric field distribution over the
slot, not surprisingly, no longer resembles the long-wavelength
behaviour. We now observe a small amplitude maximum at the center of
the slot followed by a minimum of about half the amplitude at the
slot center. The electric field then gradually increases to a much
larger maximum not too far from the slot edge and then, as it must,
sharply falls to zero as the edge is approached. Simultaneously the
surface current density has a slightly higher value at the strip
center than exhibited by the $\eta = 1$ case. Actually the current at the
strip center is a maximum. About 1/3 of the way toward the edge a
minimum a just slightly lower amplitude than at the strip center can
be seen. Continuing from the minimum the surface current density
slowly increases until the rapid rise near the slot edge takes over.
Qualitatively the surface current density away from the edge is
roughly similar to the slot-less distribution. In fact for $\eta = 2$ we
have about the same behaviour of surface current for all the previous
cases considered, $\varphi_0 = 0$, 30°, 45°, 60° and 90°. In Figure 29 we
have the slot electric field and surface current density for $\eta = 3$.
In this case the arclength of the conductor is precisely one wave-
length long. This case presents some very noteworthy behaviour for
the electric field distribution. Note in particular that the slot

center, $\varphi = 0$, is an electric field minimum with amplitude 1.91. The electric field remains nearly constant as we move away from the slot center and only gradually rises to a maximum at about $\varphi = 26°$ with amplitude of 1.96. This is about 2 - 3% higher than the minimum at the slot center. Proceeding around we find the amplitude of the electric field continuing to fall off until another minimum is reached at $\varphi = 78°$ with amplitude 0.64 i.e. about 1/3 that over the neighborhood of the slot center. As φ increases further the electric field in the slot steadily increases to a second maximum at $\varphi = 102°$. Here the amplitude is 1.16, about twice that at the preceeding minimum. Continuing around the cylindrical slot the electric field thereafter falls sharply until it vanishes at the slot edge. The surface current density distribution is almost exactly the same as we saw in Figure 28 for $\eta = 2$, $\varphi_0 = 120°$. The only essential difference is an enhancement of the maximum at the rear of the strip and the minimum which now occurs at $\varphi = 153°$ instead of at $\varphi = 160°$ for $\eta = 2$. Recall that the slot electric field distribution has been calculated from the surface current density on the strip. We then conclude that the former is obviously quite sensitive to the latter since only relatively small variations in current distribution over the strip can clearly generate significant changes in the electric field distribution. Compare the slot electric field distribution and surface current density distribution in Figure 30 for $\eta = 4$ with the corresponding quantities in Figure 29 for $\eta = 3$. The result of this
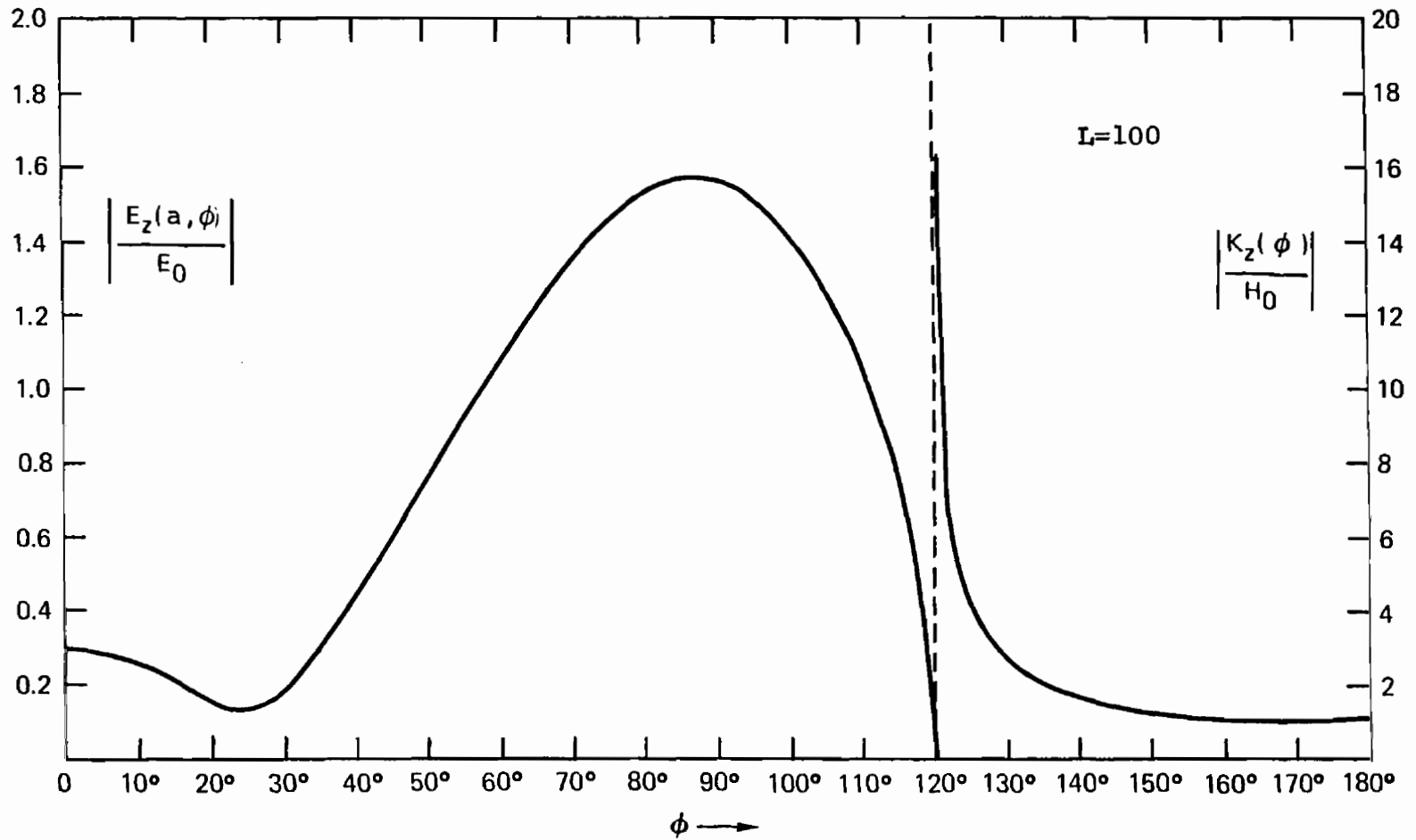
Figure 28. Electric Field In The Slot, Surface Current On The Conductor; $\eta=2. \varphi_0=120°$
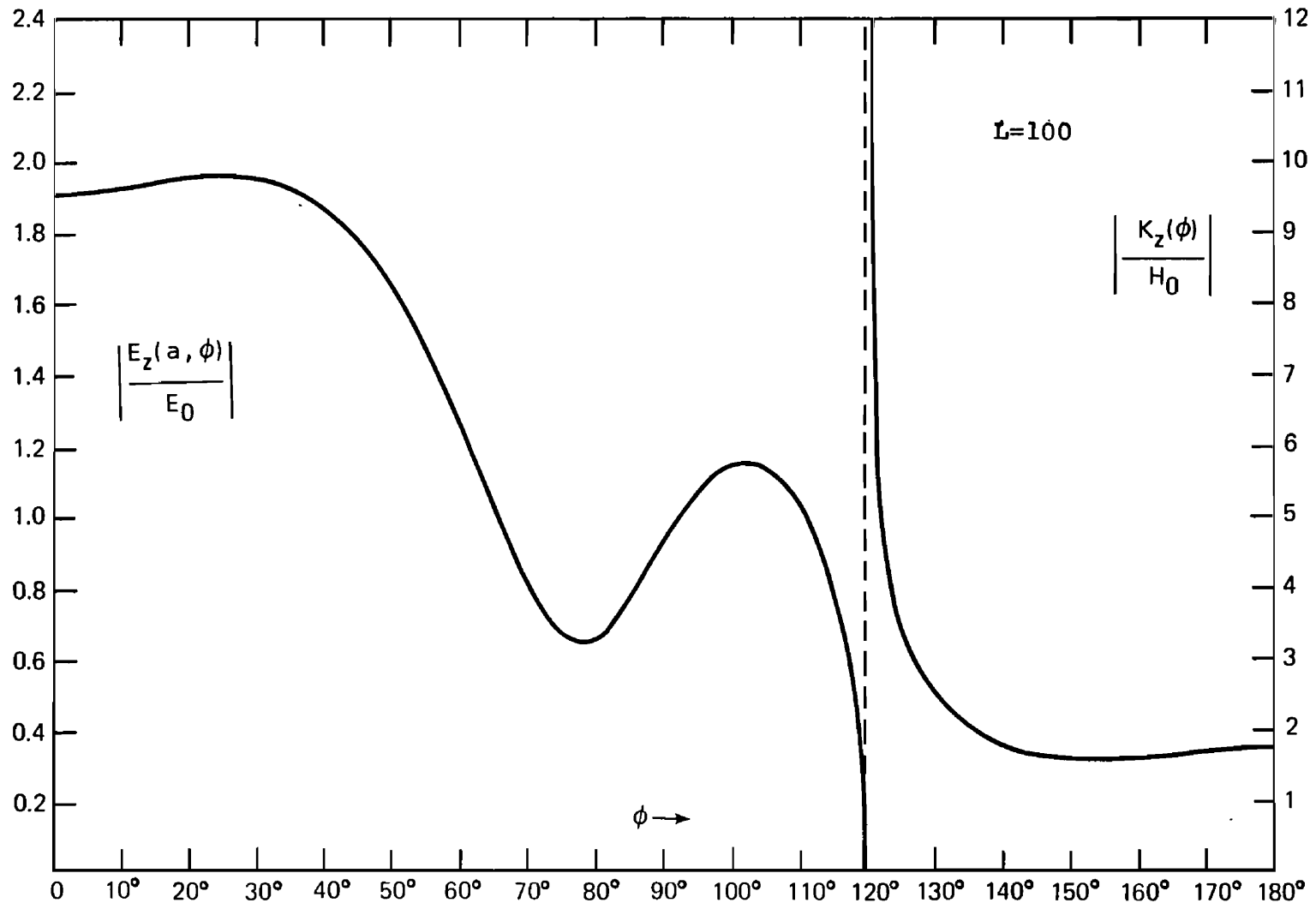
Figure 29. Electric Field In The Slot, Surface Current On The Conductor; $\eta=3, \varphi_o=120°$

comparison is to lend further emphasis to the conclusion just cited

that small changes in the surface current distribution can induce

quite remarkable variations in the electric field distribution. For

the current on the strip when $\eta = 4$ we note that there is a maximum

at the strip center of amplitude 2.1. For $\eta = 3$ the maximum at the

strip center had an amplitude of about 1.8. For $\eta = 4$ there is a

minimum at $\varphi = 143°$ with an amplitude of about 1.5. The correspond-

ing minimum is at $\varphi = 153°$ for $\eta = 3$ with an amplitude of 1.6.

Essentially the only difference in surface current on the strip for

$\eta = 3$ and $\eta = 4$ consists merely of a further enhancement of the maxi-

mum and minimum. Similarly the $\eta = 4$ and $\eta = 2$ surface currents on

the strip differ, basically, in the same manner. As a consequence of

these relatively small changes in surface current on the strip as η

varies from 2 to 4 we find in the latter case a maximum for the

electric field at the slot center. The amplitude of this maximum

field at the slot center is 1.48. Moving around the cylindrical slot

from the center the field decreases steadily to a minimum of ampli-

tude 0.34 at $\varphi = 46°$. It then continues to increase with increasing

φ to another maximum of amplitude 1.32 at $\varphi = 93°$ and thereafter

rapidly decreases to finally vanish at the slot edge at $\varphi = 120°$. We

emphasize that the relatively unremarkable change in current distri-

bution on the strip in going from $\eta = 3$ to $\eta = 4$ has induced very

markedly different electric field distributions. This strong sensi-

tivity exhibited in the slot electric field distribution to

relatively small changes in the strip current distribution is again

shown in Figure 31 for $\eta = 5$, $\varphi_o = 120°$. The surface current maximum

at the strip center for $\eta = 5$ has an amplitude of 2.2 which is not

too different than the corresponding amplitude of 2.1 for $\eta = 4$. The

strip current minimum for $\eta = 5$ is at $\varphi = 138°$ and has amplitude of

1. For $\eta = 4$ this minimum occurred at 143° with the amplitude of

1.5. Again the only essential differences between surface current on

the conducting strip for $\eta = 4$ and $\eta = 5$ are a further sharpening of

the maximum and minimum and a shift in location of the minimum. This

latter behaviour is not an unanticipated result. Also the $\eta = 5$

current distribution on the strip is quite similar to that for $\eta = 3$.

As a result of the surface current density distribution on the strip

for $\eta = 5$ we find the very different electric field distribution on

the cylindrical slot shown in Figure 31. A _minimum_ of amplitude 0.68

occurs at the center of the slot. This is followed by a long range

of azimuth φ during which the electric field monotonically increases

to a maximum at $\varphi = 56°$ with the amplitude of 1.68. This amplitude

is more than double that of the minimum at the slot center. Further

increase in φ shows a continuing decrease in electric field until a

second minimum appears at $\varphi = 83°$ with amplitude 0.3. The deep mini-

mum in electric field has an amplitude less than half that of the

slot center. Proceeding further around the cylindrical slot we note

a rapid rise in electric field amplitude to a maximum with amplitude

1.64 at $\varphi = 105°$. The second maximum has an amplitude almost equal
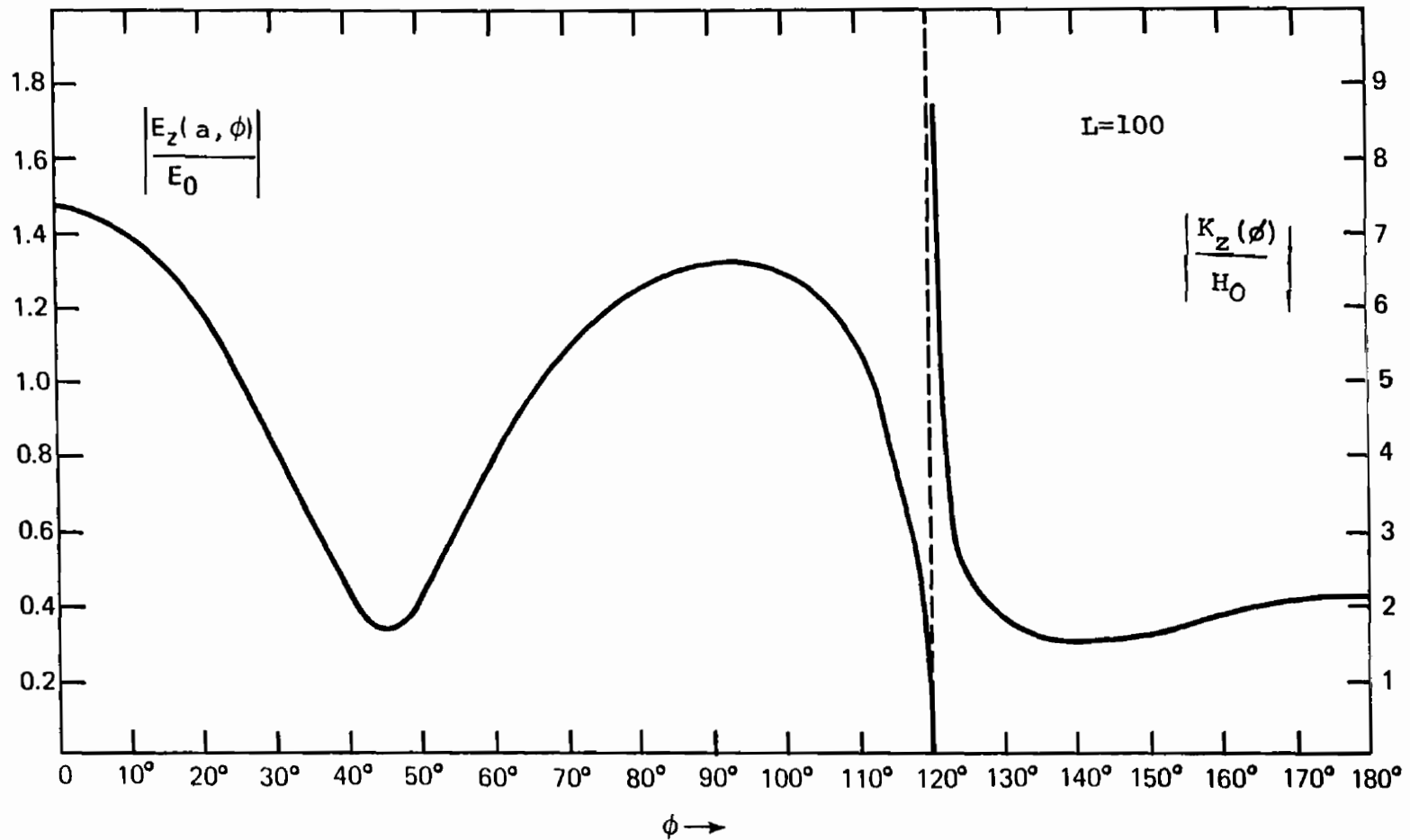
Figure 30. Electric Field In The Slot, Surface Current On The Conductor; $\eta=4, \varphi_0=120°$

$$\left|\frac{E_z(a,\phi)}{E_0}\right|$$

L=100

$$\left|\frac{K_z(\phi)}{H_0}\right|$$

$\phi \longrightarrow$
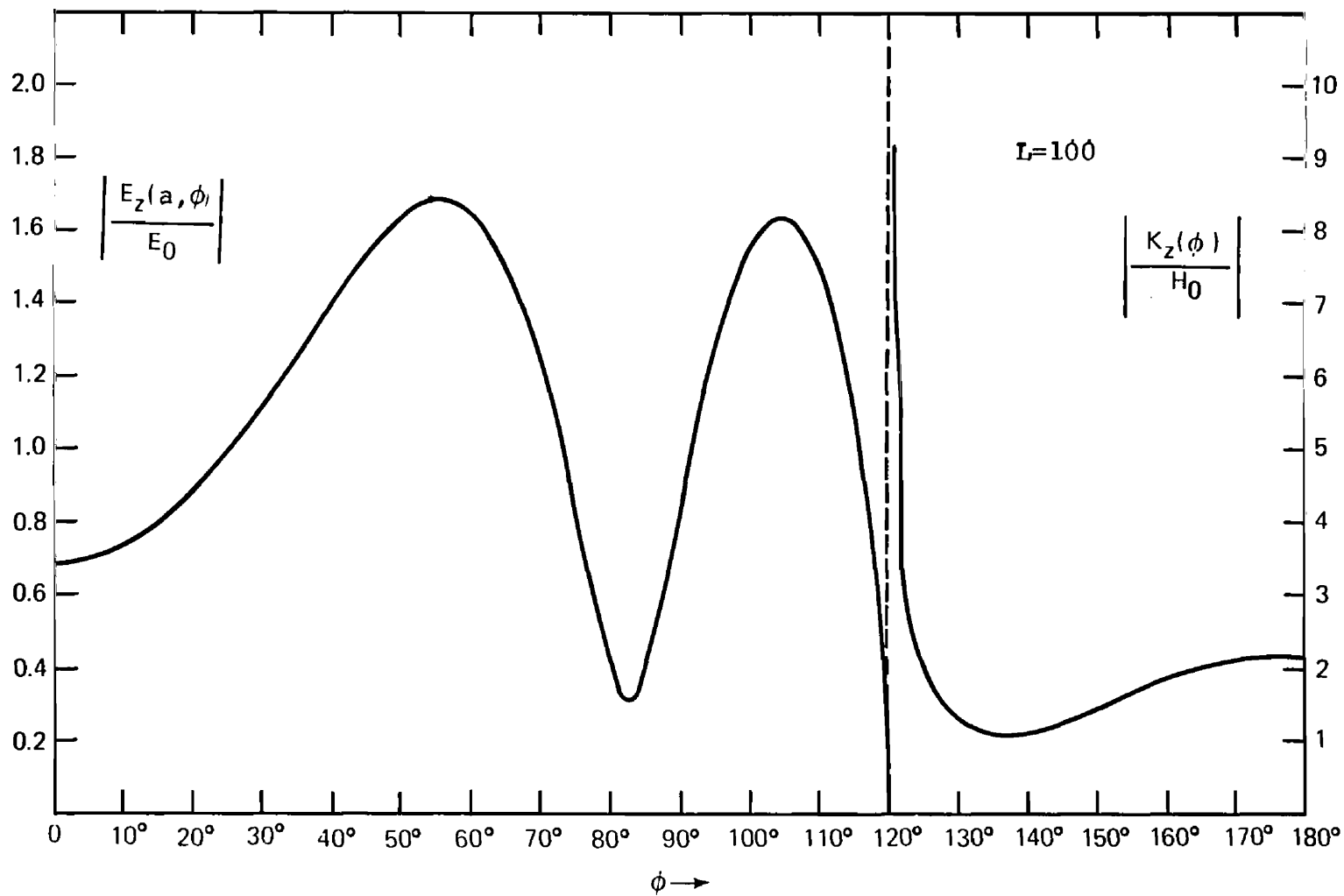
Figure 31. Electric Field In The Slot, Surface Current On The Conductor; $\eta=5$, $\varphi_0=120°$
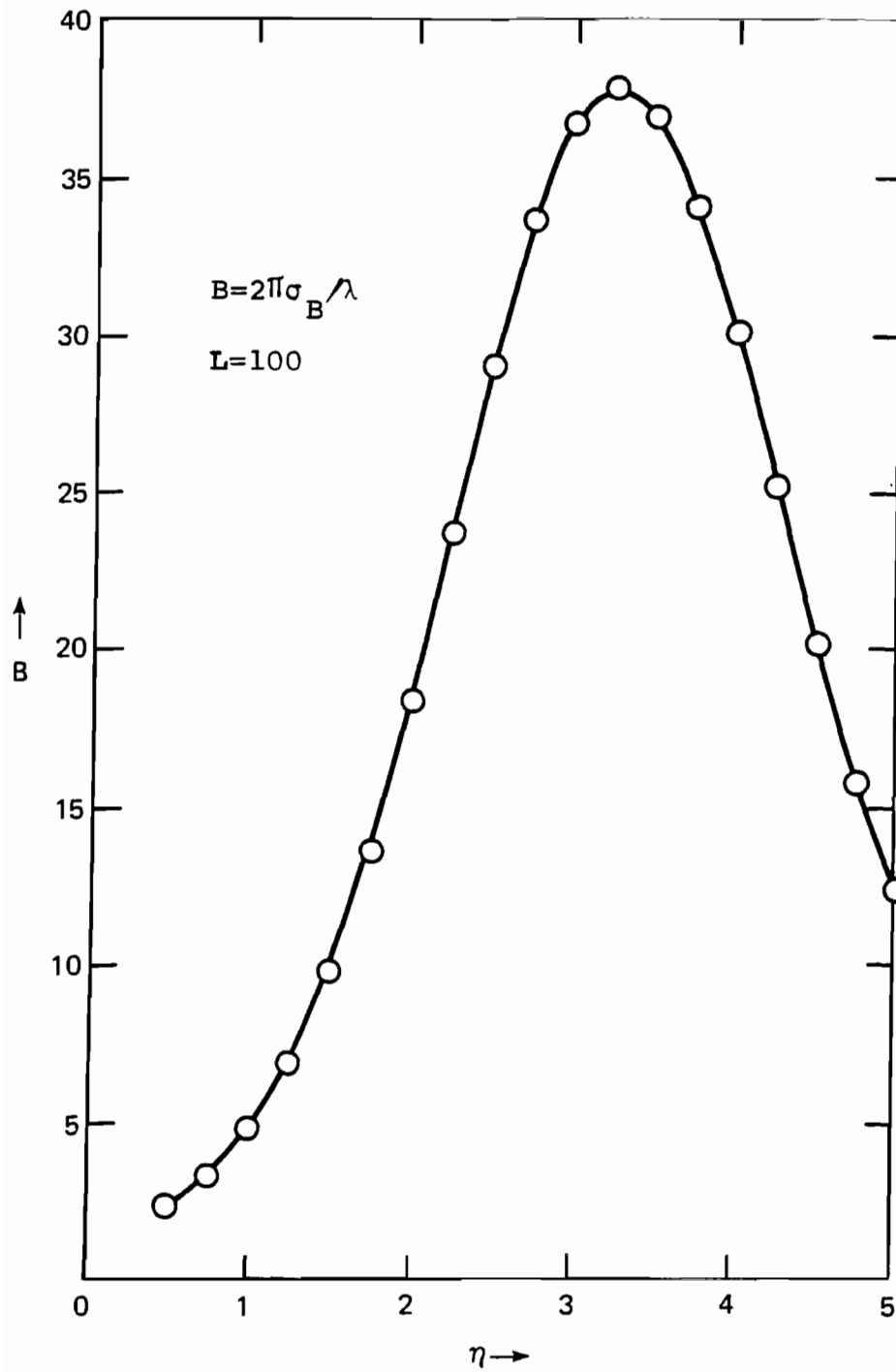
Figure 32. Back-Scattering Cross Section $\varphi_0 = 120°$

to that at the first maximum. This is then followed by rapid decrease in the electric field amplitude to zero at $\varphi = 120°$ i.e. at the slot edge. All of this remarkable variation in the slot electric field with relatively mild variation in the surface current density distribution over the strip is rather subtly concealed in the character of the back-scattering cross-section for the strip when considered as a function of the ratio of circumference to wavelength i.e. η. Figure 32 exhibits this b.s.c.s. as a function of η. What we find is not surprising. For small η we have the usual Rayleigh region behaviour. For larger η we note only one turning point occurs over the range of η we considered. Essentially we are still witnessing the transition that should occur as the slot widens further. The slot-less cylinder resonance frequencies have become considerably less reliable as resonances for the large slot situation. Continuous shifting of resonances from those for $\varphi_0 = 0$, i.e. no slot and further broadening of the lines of the spectrum with increasing slot width result in our problem for $\varphi_0 = 120°$ in the occurrence of only one broad line in the b.s.c.s. and a resonance that lies somewhere just beyond $\eta = 5$.

7. The $\varphi_0 = 150°$ Slot Characteristics (60° Cylindrical Ribbon)

As the final slotted cylinder, or cylindrical strip, case we calculated the surface current density on a conducting strip that subtends a total angle of 60° at the axis and the slot electric field over the cylindrical slot surface that subtends a half angle $\varphi_0 = 150°$

at the axis. In this case we approximated the conducting cylindrical
strip by 80 substrips each carrying its own constant uniform current
density. This means the ratio of the angle each such zone subtends
at the axis to the half slot angle is

$$\frac{\Delta\varphi}{\varphi_0} = \frac{\pi - 5\pi/6}{5\pi/6} \times \frac{1}{40} = \frac{1}{200} = .005$$

The second characteristic size parameter for this case, namely the
ratio of the arclength of the zones to the smallest wavelength con-
sidered, is

$$\frac{a\Delta\varphi}{\lambda} = \eta \frac{\Delta\varphi}{2\pi} = 5 \times \frac{1}{480} = \frac{1}{96} \approx 0.01$$

Noting that each approximating subdivision on the conducting strip is
about one one-hundredth of the incident wavelength we should expect
the numerical method of calculation to yield very accurate results.
These results for the surface current density over the conducting
cylindrical strip and the electric field distribution around the
cylindrical slot are shown in Figures 33 through 37 for $\eta = 1,2,3,4$
and 5 respectively. Consider the current density as displayed in
Figures 33, 34 and 35. In those cases i.e. for $\eta = 1$, 2 and $\eta = 3$
there is a minimum at the strip center. The amplitudes for the
current densities at $\varphi = \pi$ are respectively 1.4, 1.0 and 1.2. Moving
away from the strip center in each ease the current on the strip
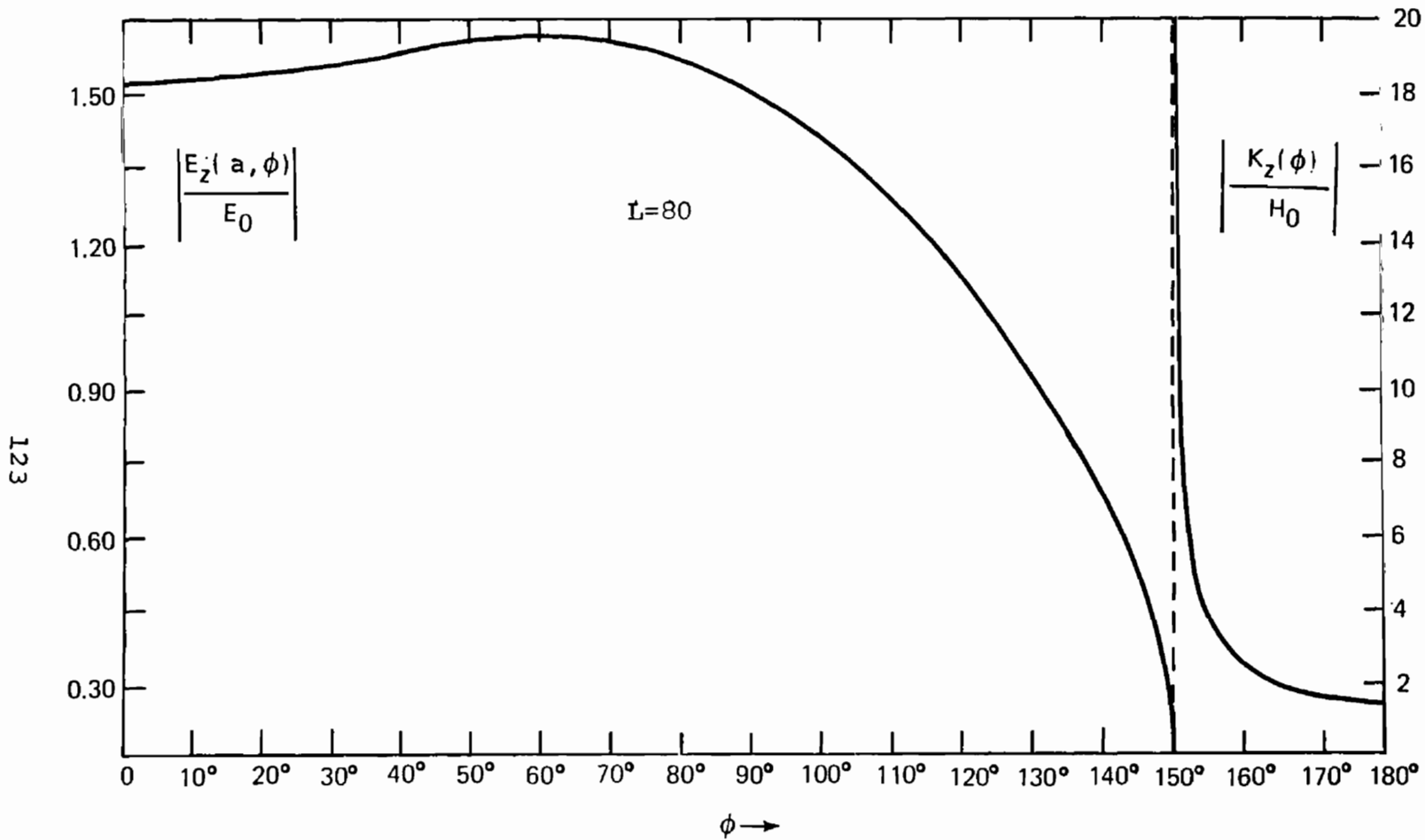
Figure 33. Electric Field In The Slot, Surface Current On The Conductor; $\eta=1$, $\varphi_0=150°$
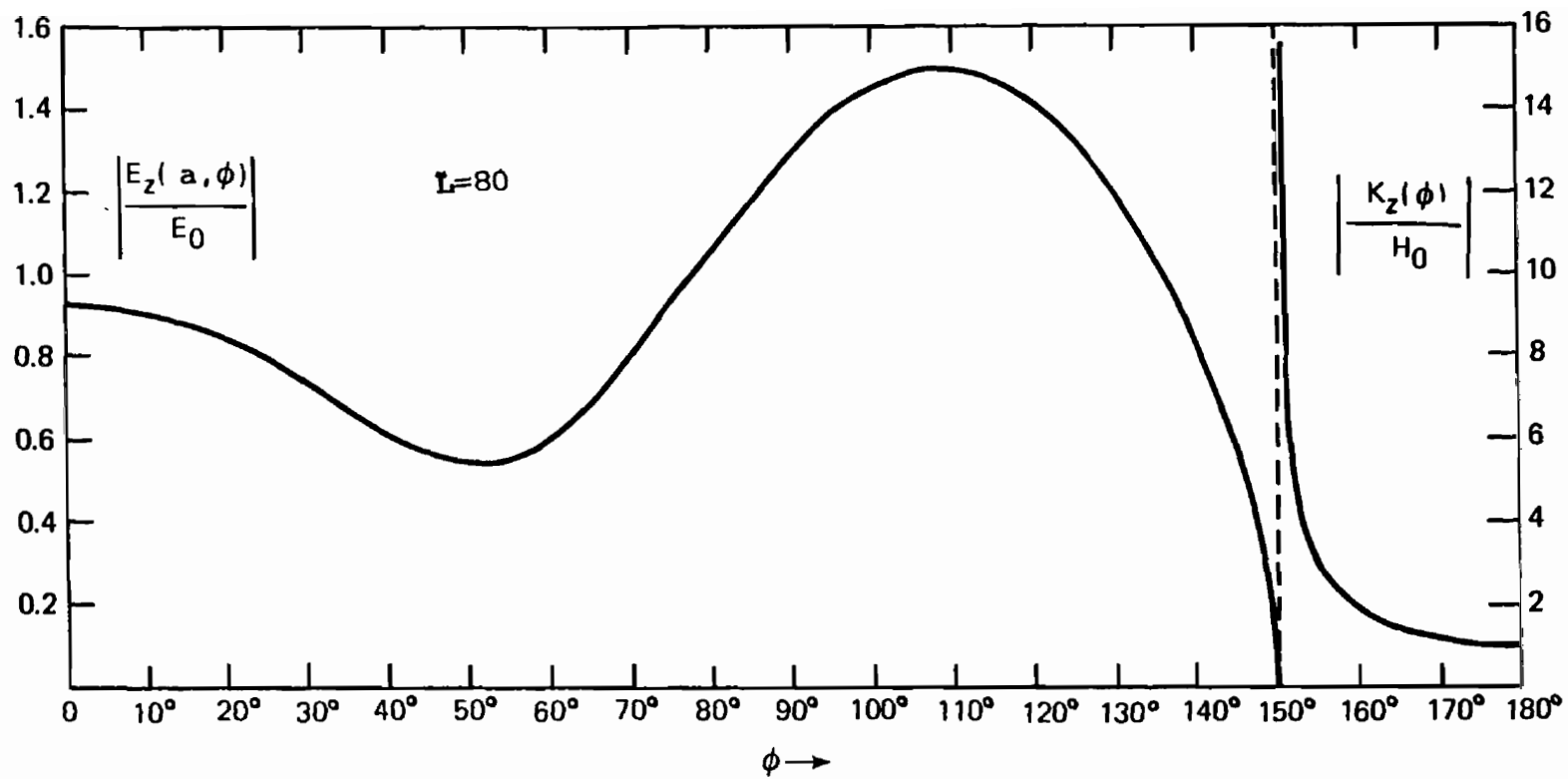
Figure 34. Electric Field In The Slot, Surface Current On The Conductor; $\eta=2$, $\varphi_0=150°$
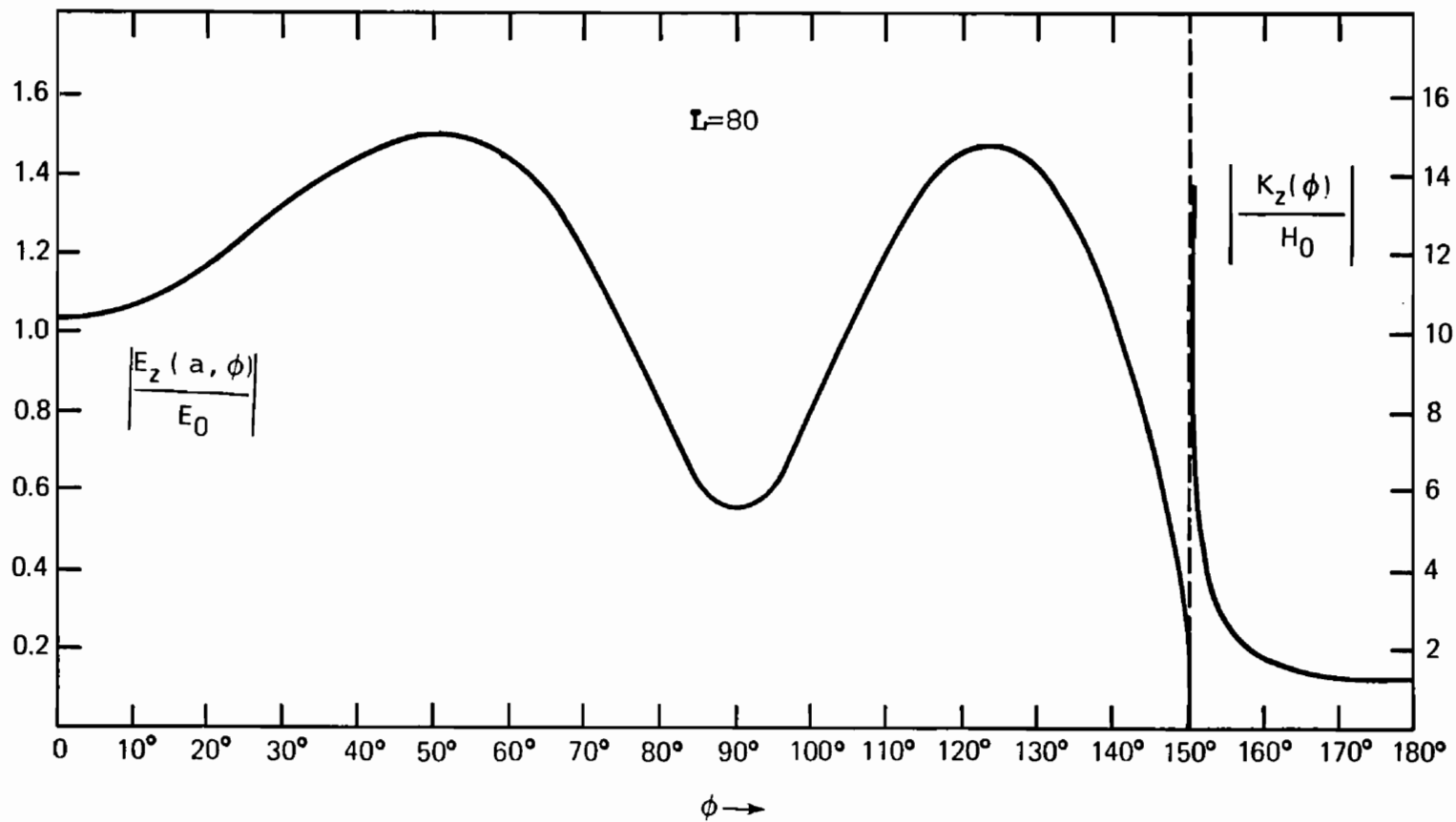
Figure 35. Electric Field In The Slot, Surface Current On The Conductor; $\eta=3$, $\varphi_0=150°$

gradually increases but at successively slower rates as η increases

from 1 through 2 to η = 3. In the last of the three cases under

discussion the surface current is nearly constant for about 1/3 of

the way from the center to the edge. In all three situations the

current increases very rapidly from about 8° away from the edge.

Once again we observe the very sensitive dependence of the electric

field distribution on the current distribution around the cylindrical

conducting strip. This surface current variation as η goes from 1 to

3 hardly exhibits any remarkable change in behaviour. Actually the

behaviour is pretty much that shown for the η = 1 and η = 2 situa-

tions for φ_0 = 120°. The electric field distributions, on the other

hand, show clearly and quite obviously some very fascinating varia-

tion in behaviour as η changes. Figure 33 for η = 1 shows a minimum

for the electric field at the slot center with an amplitude of about

1.34 and then an ensuing very slow rate of increase to a maximum at

63° with amplitude of about 1.46. This is only an increase of about

10% over about half the way from the slot center to the slot edge.

Beyond this maximum the electric field falls off at an increasing

rate to vanish at the strip edge. This electric field distribution

is very roughly similar to that shown in Figure 22 for η = 2 and

φ_0 = 90°. In Figure 34 we note a maximum in the electric field at

the slot center with amplitude of 0.92 followed by a minimum at

φ = 52° with amplitude of 0.54 and then another maximum at φ = 109°

with the larger amplitude of 1.5. Thereafter for about the remaining

1/3 of the range of φ from center to edge the electric field decreases with growing rapidity all the way to the strip edge where it vanishes. This electric field behaviour is similar to that for $\eta = 4$, $\varphi_0 = 120°$ of Figure 30, and roughly that of $\eta = 4$, $\varphi_0 = 90°$ of Figure 24, and for $\eta = 5$, $\varphi_0 = 45°$ of Figure 14. It should be noted that the current distribution in all of these other situations is of significantly varying character. For $\eta = 3$ and $\varphi_0 = 150°$ the electric field again displays a minimum at the center of the slot where the amplitude is 1.4. The field then increases to a maximum of amplitude 1.5 at $\varphi = 52°$ (note for $\eta = 2$ this is the location of a minimum in the electric field distribution). Further progress away from the slot center results in a decreasing electric field until a minimum of amplitude 0.54 appears at $\varphi = 91°$. Proceeding further around the cylinder the field rises more rapidly to a second maximum at $\varphi = 124°$ with amplitude 1.48. Continuing the electric field falls off ever more rapidly and finally vanishes at the edge of the conducting strip. Although the current distributions are clearly quite different the electric field behaviour is again roughly similar to that for $\eta = 5$, $\varphi_0 = 120°$ as shown in Figure 31. The surface current density for $\eta = 4$, $\varphi_0 = 150°$ exhibits a maximum of amplitude 1.6 at the strip center and then a barely recognizable minimum at about $\varphi = 172°$ of very nearly the same amplitude. This can be seen in Figure 36. With the appearance of this minimum we find the slot electric field distribution it generates has three clearly defined

maxima from $\varphi = 0$ to $\varphi = 150°$. These occur at $\varphi = 0$ with amplitude 1.55, $\varphi = 82°$ with amplitude 1.44 and $\varphi = 132°$ with amplitude 1.4. Minima in the electric field occur between these maxima. These are at $\varphi = 53°$ (note this is the location of a maximum in the slot electric field distribution for $\eta = 3$, cf. Figure 35) with an amplitude of 0.46, and at $\varphi = 107°$ with amplitude of 0.62. The only other case we have considered that exhibited an electric field distribution even remotely resembling the one presently under discussion is shown in Figure 25 for $\eta = 5$, $\varphi_0 = 90°$. Again the corresponding current distributions over the conductor are quite different. In Figure 37 we note that for $\eta = 5$ the surface current density on the strip differs from that for the lower values of η merely by a slightly more enhanced behaviour near the maximum at the strip center and near the minimum at $\varphi = 164°$. The resulting slot electric field distribution now shows two additional turning points. For $\eta = 5$ there are maxima at the slot center with amplitude 0.29, at $\varphi = 53°$, (note this is a minimum for $\eta = 4$ and a maximum for $\eta = 3$) amplitude 1.54 and at $\varphi = 98°$ with amplitude of 1.30 and finally at $\varphi = 135°$ with the amplitude 1.32 (this almost coincides with the third maximum for $\eta = 4$). Between these maxima lie minima at $\varphi = 8°$ amplitude 0.28, at $\varphi = 78°$ (nearly coincident with the maxima for $\eta = 4$) with an amplitude of 0.59, and at $\varphi = 116°$ where the amplitude is 0.74.

The back-scattering cross-section for the $\varphi_0 = 150°$ slot (or conducting cylindrical strip of 60°) is shown in Figure 38 as a

128
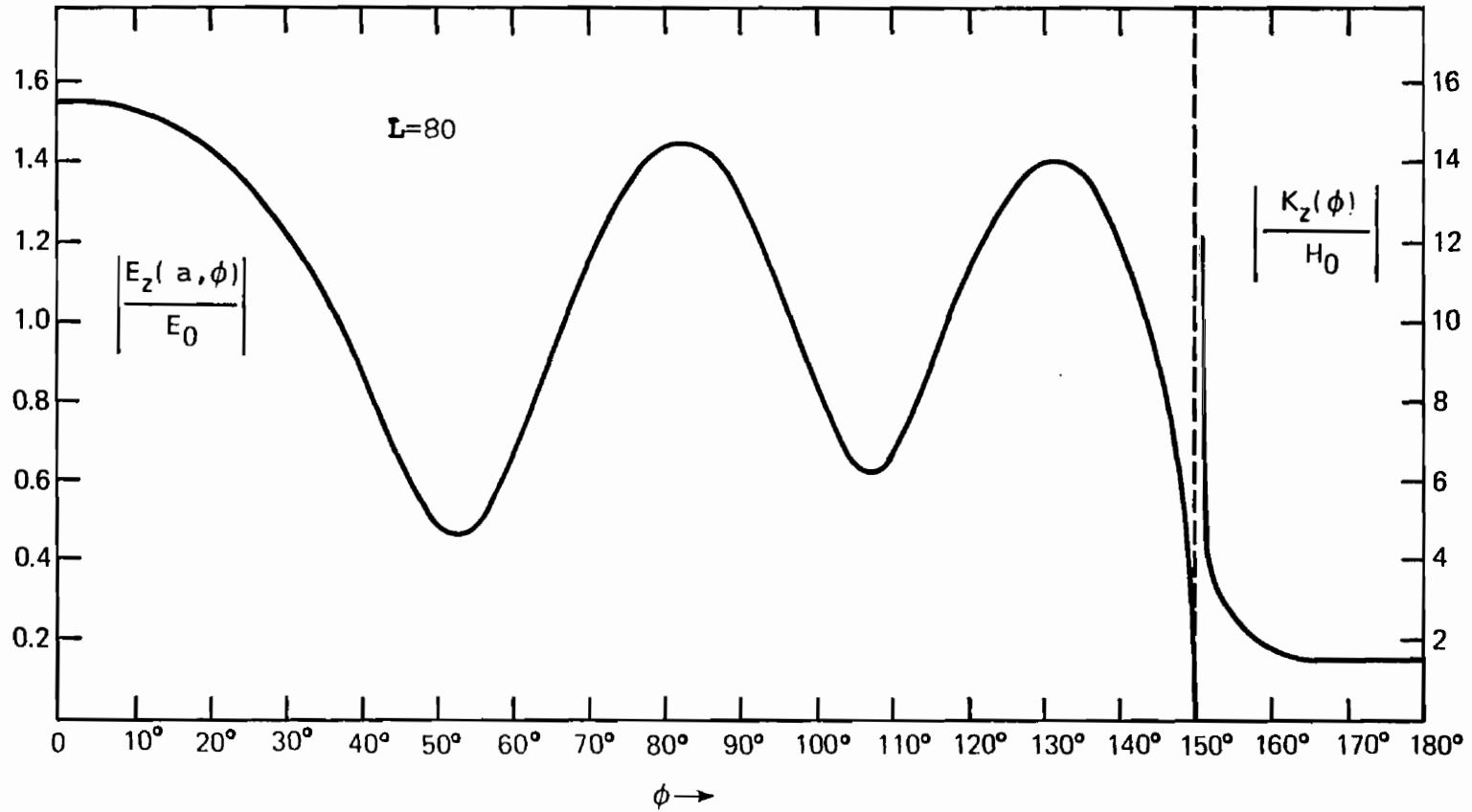
Figure 36. Electric Field In The Slot, Surface Current On The Conductor; $\eta=4$, $\varphi_0=150°$
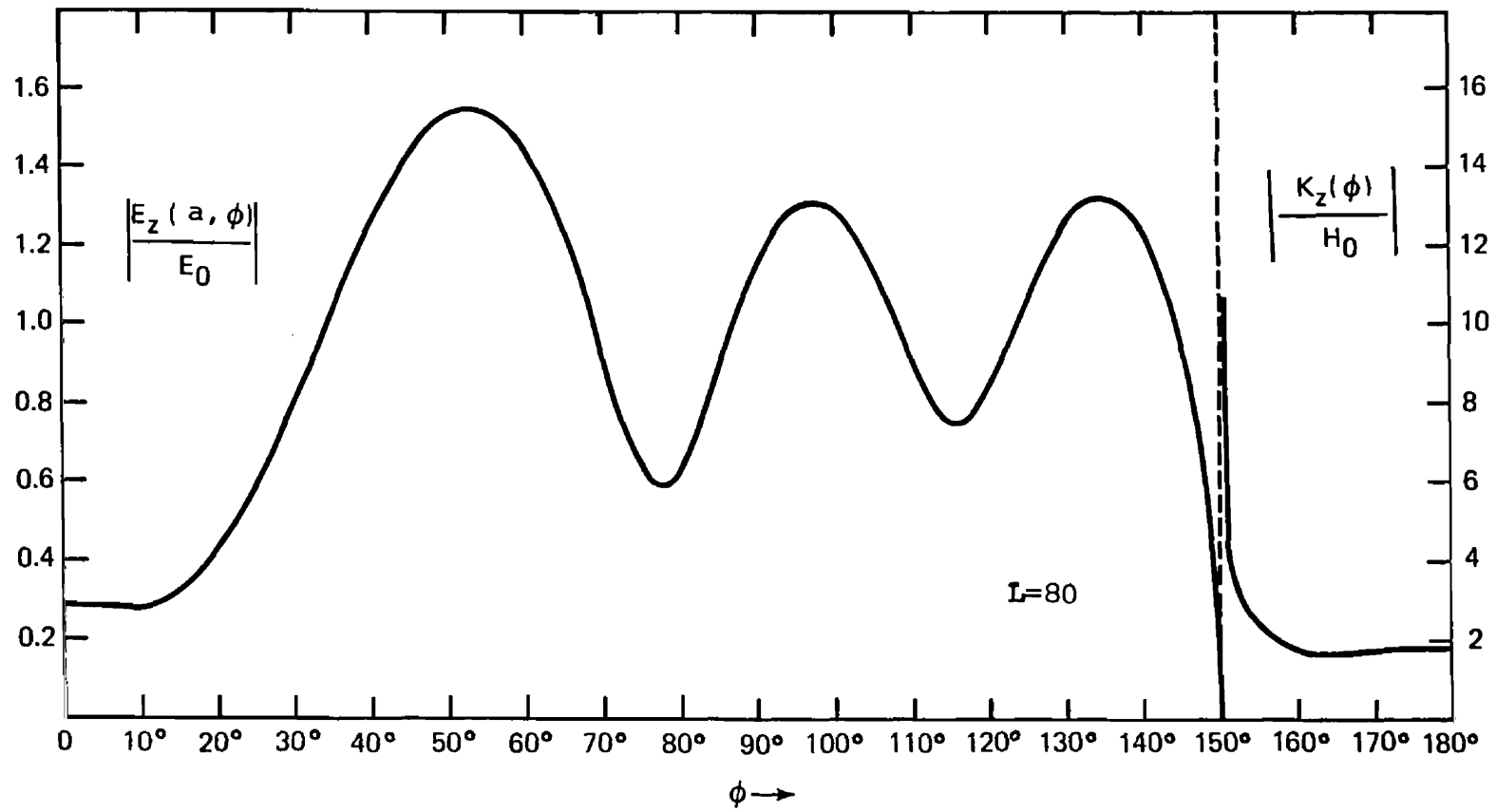
Figure 37. Electric Field In The Slot, Surface Current On The Conductor; $\eta=5$, $\varphi_0=150°$
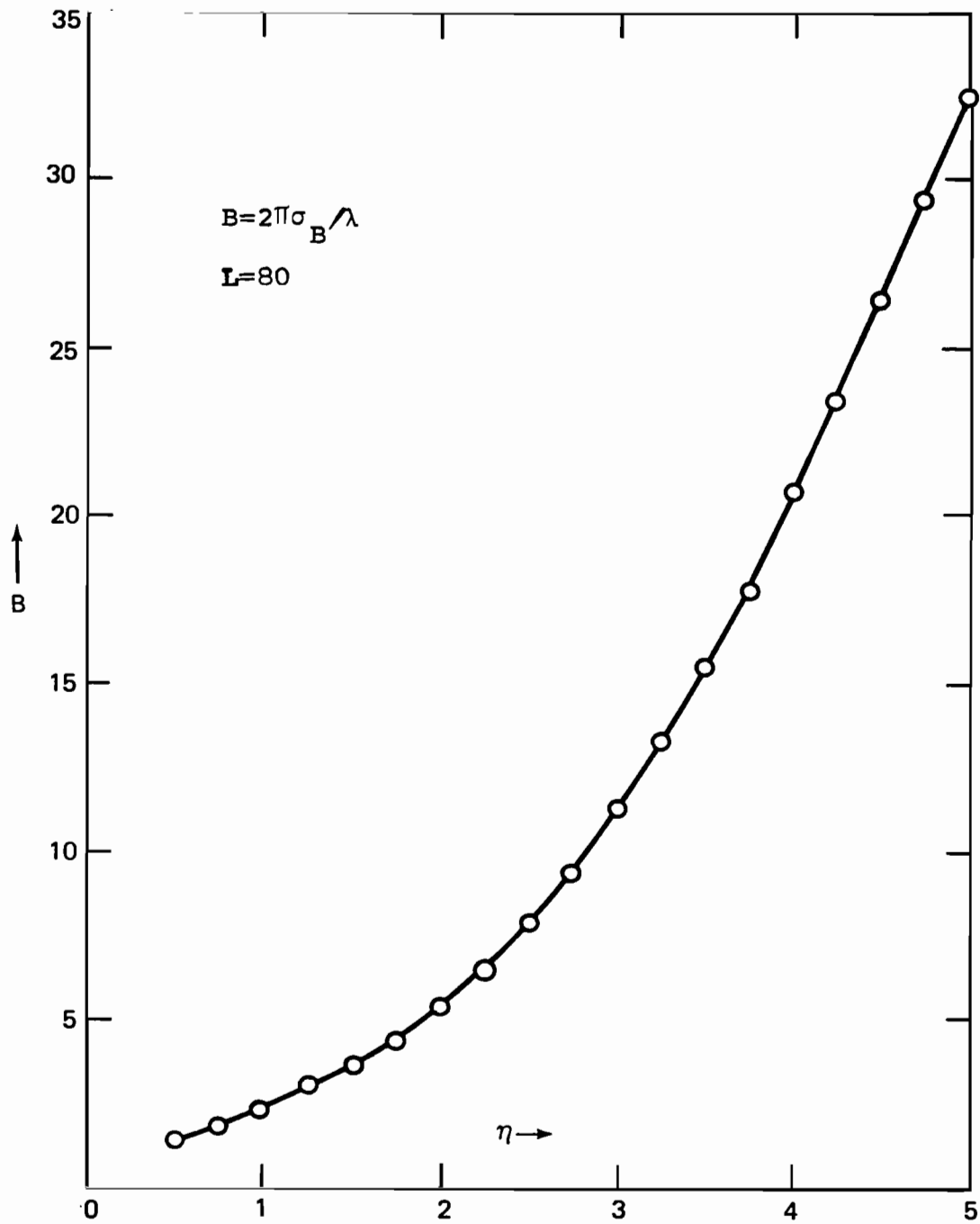
Figure 38. Back-Scattering Cross-Section, $\varphi_0 = 150°$

function of η. Now the resonances for the cylindrical system occur well beyond $\eta = 5$. The b.s.c.s. more appropriately is now evolving towards that for an infinite flat strip. This latter quantity was calculated by Morse and Rubenstein[33] using the limiting form of solution for an elliptic cylinder as it shrinks in thickness. One glaring observation can be made after viewing Figure 38 and thinking back over the above discussion. This is that the far field behaviour displayed in the back-scattering cross-section thoroughly masks, almost misleadingly, the very rich and fascinating variation in behaviour of the near fields.

33. P. M. Morse, P. J. Rubenstein, "The Diffraction of Waves by Ribbons and by Slits", Phys. Rev. 54, 895 (1938)

IX. EFFECTS OF INTERIOR RESONANCES ON SCATTERING BEHAVIOUR

1. Constraints on The Aperture Electric Field

The electric field in the interior of the slotted cylinder, i.e. for $\rho < a$, was given in eq. (8) as

$$E_z^{(1)}(\rho,\varphi) = \sum_{m=0}^{\infty} \frac{J_m(k\rho)}{J_m(\eta)} A_m \cos m\varphi$$

where the expansion coefficient is that given by eq. (16) namely

$$A_m = \frac{\epsilon_m}{2\pi} \int_{-\varphi_0}^{\varphi_0} d\varphi \; e(\varphi) \cos m\varphi$$

It is a physical fact that the electric field in the interior must be finite at all frequencies for any value of slot angle φ_0. Consequently we must have some requirements that constrain the electric field over the slot at frequencies for the incident radiation that coincide with internal resonances. These frequencies in the present problem are defined by the roots of the Bessel functions $J_m(\eta)$. Denoting the n-th root of the m-th order Bessel function by η_{mn} we have as the internal resonances frequencies defined by $\eta = \eta_{mn}$ where

(95) $$J_m(\eta_{mn}) = 0$$

Note that the frequencies associated with the η_{mn} values are the only ones which can be sustained in a TM mode of a circular waveguide.

We conclude then that the coefficient A_m must approach zero as η approaches η_{mn} in such a manner that the quantity

$$(96) \quad \lim_{\eta \to \eta_{mn}} \left[A_m / J_m(\eta) \right]$$

remains finite and well-behaved. Several requirements on the electric field in the opening are compatible with this essential condition. The ways in which A_m can vanish at $\eta = \eta_{mn}$ are as follows

$$I. \quad \Re e \left[\mathcal{E}(\varphi) \right] = 0 \quad \text{and} \quad Im \left[\mathcal{E}(\varphi) \right] = 0$$

$$(97) \quad II. \quad \Re e \left[\mathcal{E}(\varphi) \right] = 0 \quad \text{and} \quad \int_0^{\varphi_0} d\varphi' \; Im \left[\mathcal{E}(\varphi') \right] \cos m\varphi' = 0$$

$$III. \quad \int_0^{\varphi_0} d\varphi' \; \Re e \left[\mathcal{E}(\varphi') \right] \cos m\varphi' = 0 \quad \text{and} \quad Im \left[\mathcal{E}(\varphi) \right] = 0$$

$$IV. \quad \int_0^{\varphi_0} d\varphi' \; \Re e \left[\mathcal{E}(\varphi') \right] \cos m\varphi' = 0 \quad \text{and} \quad \int_0^{\varphi_0} d\varphi' \; Im \left[\mathcal{E}(\varphi') \right] \cos m\varphi' = 0$$

where $\Re e[\;]$ and $Im[\;]$ as usual indicate respectively the real and imaginary parts of the quantity $[\;]$. The constraints I. through IV. as listed in eq. (97) on the slot electric field are essentially the only ones compatible with the condition that A_m vanishes at $\eta = \eta_{mn}$.

Two limiting forms for the slot electric field can be utilized to infer a relationship between the size of the opening, or slot, and the particular requirement which holds for the electric field in that

opening at a resonant frequency. To begin with the limiting case of

no opening implies

(98) $\lim_{\varphi_0 \to 0} \mathcal{E}(\varphi) \longrightarrow 0$

in such a way that we must have

(99) $\lim_{\substack{\varphi_0 \to 0 \\ \eta \to \eta_{mn}}} \text{Re}\,[\mathcal{E}(\varphi)] \longrightarrow 0$ and $\lim_{\substack{\varphi_0 \to 0 \\ \eta \to \eta_{mn}}} \text{Im}\,[\mathcal{E}(\varphi)] \longrightarrow 0$

From this we deduce that constraint relation I. of Eq. (97)

should be invoked at an internal resonance frequency whenever the

slot is a narrow slot, i.e. φ_0 is small. This certainly is true for

the lower order modes. The second limiting situation is that of no

conductor, which implies

(100) $\lim_{\varphi_0 \to \pi} \mathcal{E}(\varphi) \longrightarrow E_z^i(a,\varphi) = E_0\, e^{i\eta \cos\varphi}$

and in turn

$$\lim_{\varphi_0 \to \pi} \int_0^{\varphi_0} d\varphi'\, \mathcal{E}(\varphi')\, \cos m\varphi' \longrightarrow \pi E_0\, (-i)^m\, J_m(\eta)$$

or equivalently

$$(101) \qquad \lim_{\substack{\varphi_0 \to \pi \\ \eta \to \eta_{mn}}} \int_0^{\varphi_0} d\varphi' \; \Re e \, [\mathcal{E}(\varphi')] \; \cos m\varphi' \longrightarrow 0$$

and simultaneously

$$(102) \qquad \lim_{\substack{\varphi_0 \to \pi \\ \eta \to \eta_{mn}}} \int_0^{\varphi_0} d\varphi' \; Im \, [\mathcal{E}(\varphi')] \; \cos m\varphi' \longrightarrow 0$$

Our conclusion from this limiting situation is that constraint relation IV of eq. (97) should be invoked for the slot electric field at internal resonance whenever we have a very narrow cylindrical strip concave towards the incident radiation. This certainly holds for the lower order modes.

We pause to emphasize that the particular resonant frequency may also influence which requirement in eq. (97) applies to a particular aperture since the associated wavelength can be very small, comparable to, or much larger than the distance between the slot edges.

Morse and Feshbach[6] have considered a narrowly slotted cylinder where the wavelength of the incident radiation was assumed to be large compared to the distance between the slot edges. The wavelength was not, however, assumed to be long compared to the cylinder diameter. In the course of their analysis they state that the

---

6. P. M. Morse and H. Feshbach, "Methods of Theoretical Physics", Part II, 1387-1398 McGraw-Hill, New York 1953

electric field in the slot is required to vanish at the TM mode

eigenfrequencies. This results in complete absence of any evidence

of the existence of the narrow slot outside of the cylinder at the

corresponding internal TM mode resonances. Their analysis becomes

slightly less valid as the internal modes of high order are con-

sidered. Nevertheless for the regime they considered constraint con-

dition I. of eq. (97) was invoked by them. This leads to having all

of the expansion coefficients for the scattered field, due to the

presence of the opening, vanishing at any internal TM mode. Physi-

cally, of course, it is not likely that the very high order TM modes

will be excited with appreciably significant amplitudes. For the

range a/λ not too large they have probably a reasonably good approxi-

mation. It should be noted that thus far in the literature the

existence of only constraint I. seems to have been discussed or

acknowledged. Now the remaining constraint conditions i.e., II, III

and IV of eq. (97) are apparently entirely new ones for the slot

electric field. Each of these, it is important to point out, merely

require a single one of the set of expansion coefficients to vanish

at any given internal resonance frequency. It then follows immedi-

ately from this that constraint conditions II, III and IV allow for

the existence of a non-zero scattered field due to the presence of a

slot at the internal TM mode frequencies. We repeat for emphasis

constraint conditions II, III and IV of eq. (97) do not appear to

have been known in the literature prior to this investigation.

137

2. The Interior Electric Field In Terms of The Surface Current

The electric field in the interior of the slotted cylinder, i.e. for $\rho < a$, can be expressed in terms of the surface current density. This permits calculation of the interior electric field without explicit concern over the interior TM mode eigenfrequencies. To obtain this formulation of the interior electric field we utilize eq. (27) for the expansion coefficients and then rewrite it rearranged as follows

$$(103) \qquad A_m = E_0 \, \epsilon_m \, (-i)^m \, J_m(\eta) - B_m \, J_m(\eta) \, H_m^{(1)}(\eta)$$

Substitution of this into the defining series for the interior electric field, i.e. eq. (8), gives

$$(104) \quad E^{(1)}(\rho,\varphi) = E_0 \sum_{m=0}^{\infty} \epsilon_m (-i)^m \, J_m(k\rho) \, \cos m\varphi - \sum_{m=0}^{\infty} B_m J_m(k\rho) H_m^{(1)}(ka) \cos m\varphi$$

The first summation in eq. (104) is merely that for the incident electric field. Then substituting from eq. (30) for the B_m coefficients we obtain for the interior electric field

$$(105) \quad E_z^{(1)}(\rho,\varphi) = E_0 \, e^{-ik\rho\cos\varphi} - \left(\frac{\eta}{4}\right)\sqrt{\frac{\mu_0}{\epsilon_0}} \int_{\varphi_0}^{2\pi-\varphi_0} d\varphi' \; \mathcal{K}(\varphi') \; .$$

$$\cdot \sum_{m=0}^{\infty} \epsilon_m \, J_m(k\rho) \, H_m^{(1)}(ka) \, \cos m(\varphi'-\varphi)$$

138

With the help of the following identity[34]

$$(106) \quad \sum_{m=o}^{\infty} \epsilon_m J_m(k\rho) H_m^{(1)}(ka) \cos m(\varphi'-\varphi) - H_o^{(1)}\left\{k\sqrt{\rho^2+a^2-2\rho\rho_o\cos(\varphi'-\varphi)}\right\}$$

$$\text{for } \rho<a$$

we can rewrite eq. (105) in the more compact form

$$(107) \quad E_z^{(1)}(\rho,\varphi) = E_o e^{-ik\rho\cos\varphi} - \left(\frac{\eta}{4}\right)\sqrt{\frac{\mu_o}{\epsilon_o}} \int_{\varphi_o}^{2\pi-\varphi_o} d\varphi' \; \varkappa(\varphi') \cdot$$

$$\cdot \; H_o^{(1)}\left\{k\sqrt{\rho^2+a^2-2\rho a\cos(\varphi-\varphi')}\right\} \quad \text{for } \rho<a$$

This latter equation reduces to the defining equation for the surface current, namely eq. (34), when the azimuthal variable φ falls in the range $\varphi_o \le \varphi \le 2\pi-\varphi_o$ and simultaneously $\rho=a$. The expression for the interior electric field in the form displayed in eq. (107) is more readily interpreted physically. This is due to the fact that the internal field is represented as a linear superposition of the incident field and a field explicitly due to the total induced current density on the conducting wall of the slotted cylinder. Summing up then eq. (107) gives the internal electric field in terms of the total surface current density on the conducting portion of the

34. I. S. Gradshteyn, I. W. Ryzhik, "Tables of Integrals, Series and Products", eq. 2, Section 8.531 p 979, Academic Press, N. Y. 1965

slotted cylinder. We recall at this point that the surface current density is the basic quantity we calculate via the method-of-moments. Once this quantity is available we can determine all other physical quantities of interest such as the internal electric field as shown in eq. (107).

3. Consistency of the Aperture Field Constraint Conditions With Numerical Results

The constraint conditions on the aperture electric field distribution at internal resonances as given in eq. (97) can be corroborated by numerical calculation of the electric field in the slot at values of η over the range we investigated: $0.5 \leq \eta \leq 5$. This range of circumference to wavelength ratio includes two Bessel function zeros which correspond to the two lowest circular waveguide TM modes. These are, to three decimals,

$$
(108) \qquad \eta_{01} = 2.405
$$
$$
\eta_{11} = 3.832
$$

The roots of the Bessel functions are extensively tabulated and are readily available in many references e.g. the Jahnke-Emde tables[35] or the tables of Abramowitz and Stegun[36]. We have

35. E. Jahnke, F. Emde, "Tables of Functions", Chap. VIII, Dover Publications, New York, N. Y. 1945

36. M. Abramowitz, I. A. Stegun, "Handbook of Mathematical Functions" Table 9.5, U.S. Dept. of Commerce, National Bureau of Standards, Applied Mathematics Series-55, 3rd Printing 1965. U. S. Government Printing Office, Washington, D. C.

calculated the real and the imaginary parts of the electric field in the slot at each of the values given in eq. (108) for all the values of φ_0 in part VIII of this report. The results for all but the $\varphi_0 = 45°$ case are included in the following discussion. In Figure 39 we exhibit the wavelength dependence of the electric field at the center of the slot for the $\varphi_0 = 30°$ cylinder. As we noted in Figures 4 through 8 the electric field in the aperture displays maximum amplitude at $\varphi = 0$, i.e. at the center of the slot over the range $0.5 \leq \eta \leq 5$ for the $\varphi_0 = 30°$ case. Now examination of Figure 39 reveals that the electric field in the opening appears to approach zero as η approaches η_{01} and η_{11} . Figures 40 and 41 on the other hand show the distribution of the real and imaginary parts of the electric field over the aperture for the $\varphi_0 = 30°$ case for $\eta = 2.405 \approx \eta_{01}$ and $\eta = 3.832 \approx \eta_{11}$ respectively. We recall that the slot electric field distribution was calculated from a numerical approximation for the surface current density distribution and in addition values of η only closely approximating η_{01} and η_{11} were used in the calculation whose results are displayed in Figures 40 and 41. All things considered then we conclude that constraint requirement I of eq. (97) is the appropriate one at η_{01} and η_{11} for the slotted cylinder with $\varphi_0 = 30°$. This conclusion is further confirmed by the fact that the back-scattering cross-section for the $\varphi_0 = 30°$ case is nearly identical to the back-scattering cross-section for the $\varphi_0 = 0°$ (or no slot) case at both η_{01} and η_{11} . This can be seen by comparing the b.s.c.s. in

141
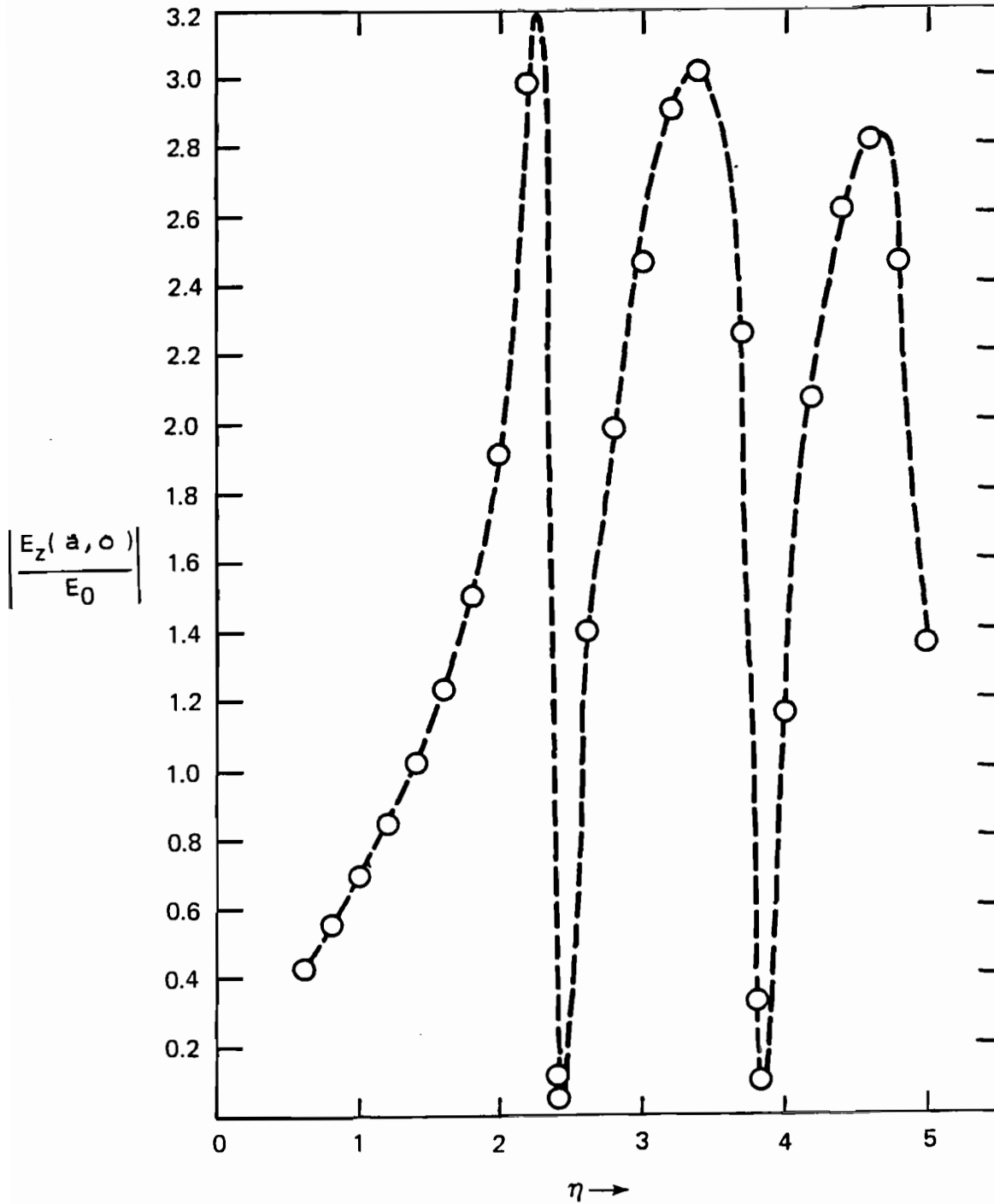
Figure 39. Amplitude of The Electric Field At The
Center Of The $\varphi_0 = 30°$ Slot
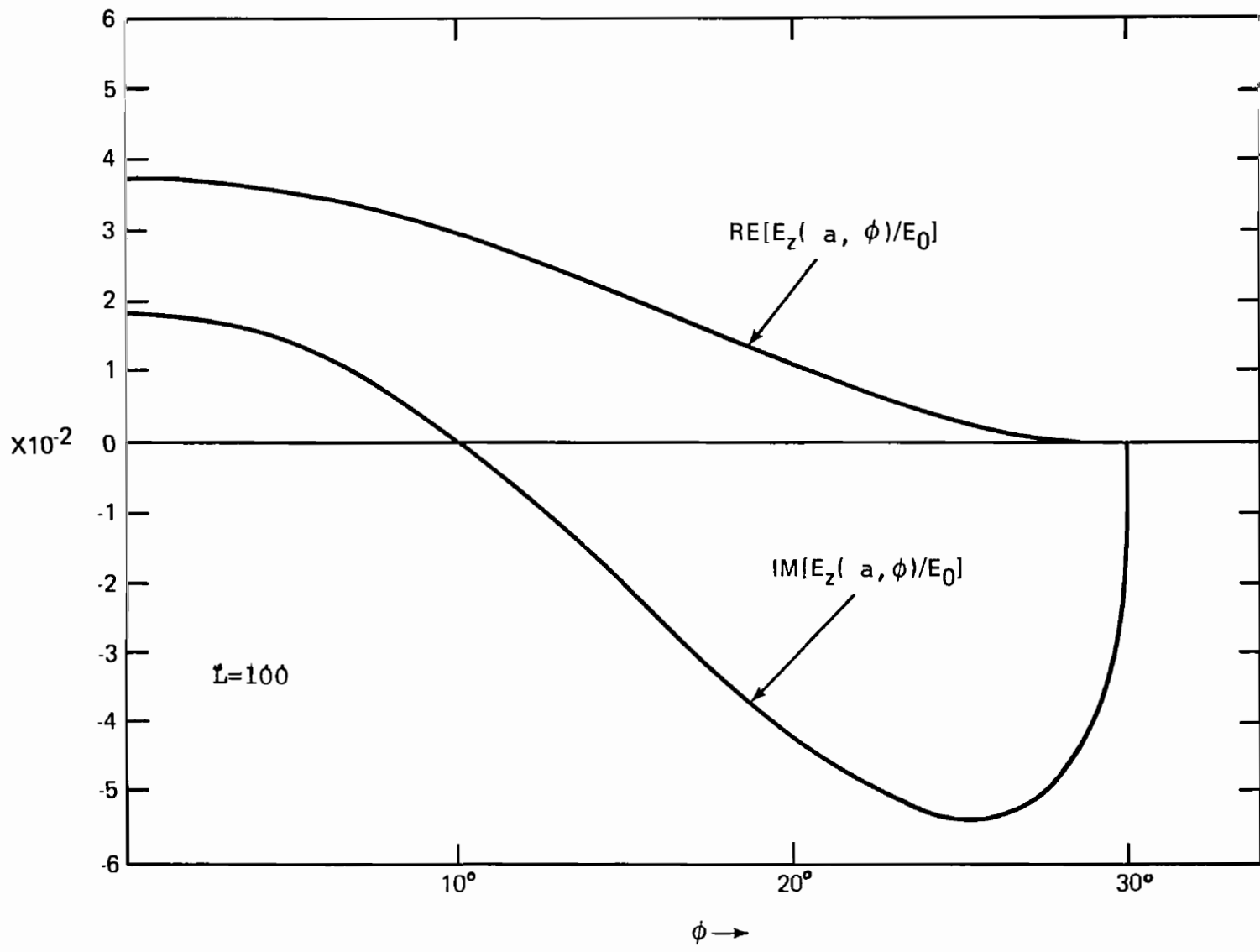
Figure 40. Real And Imaginary Parts Of The Slot Electric Field; $\eta=2.405, \varphi_0=30°$
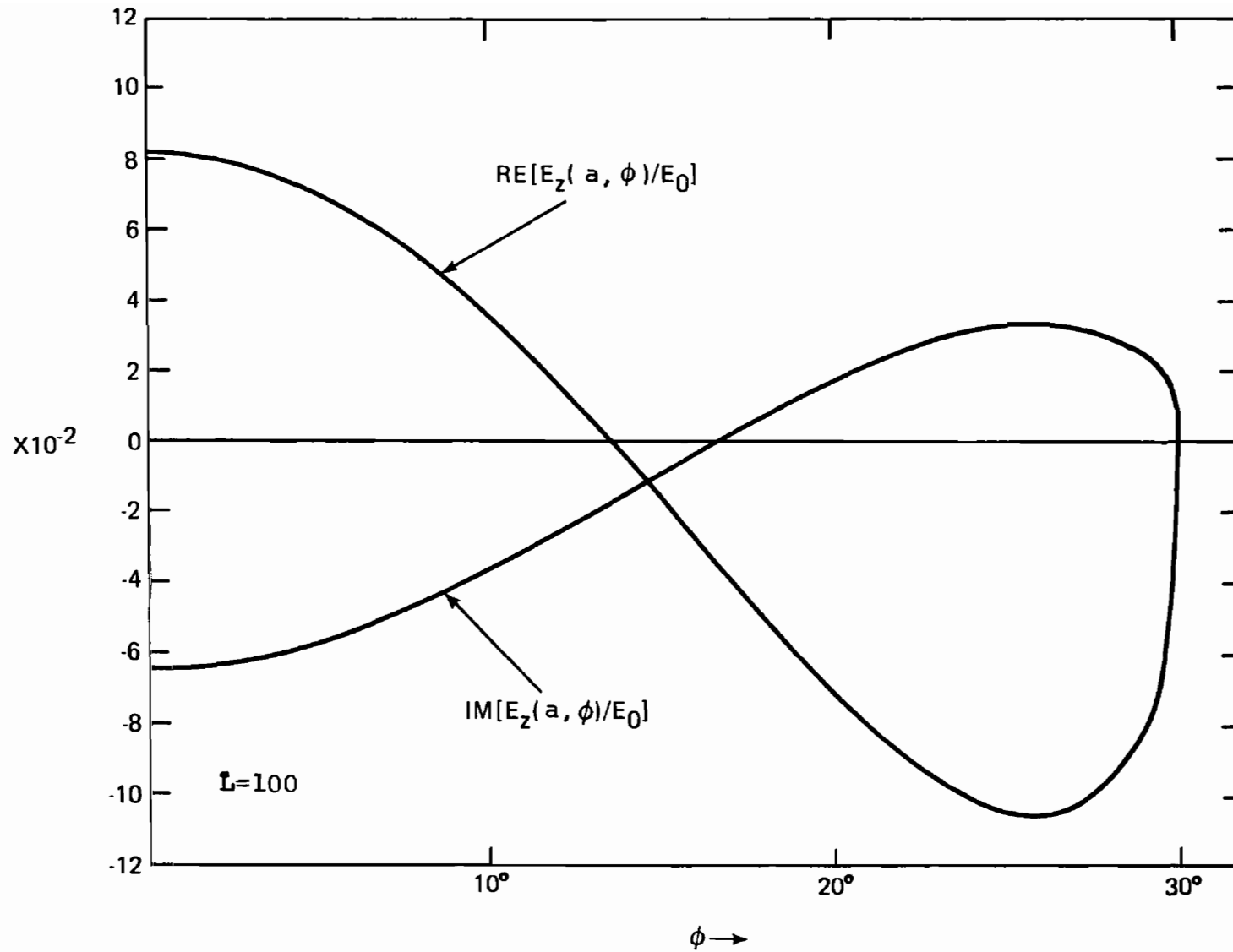
Figure 41. Real And Imaginary Parts Of The Slot Electric Field; $\eta=3.832$, $\varphi_0=30°$

Figure 9 for $\varphi_0 = 30°$ with interpolated values from Table 1 for the b.s.c.s. when $\varphi_0 = 0°$. Thus $\varphi_0 = 30°$ appears to be still exhibiting further narrow slot characteristics for $0.5 \leq \eta \leq 5$.

Figures 42 and 43 give respectively the distributions over the $\varphi_0 = 60°$ slot of the real and imaginary parts of the electric field for $\eta = \eta_{01}$ and $\eta = \eta_{11}$. Comparison of the back-scattering cross-sections at $\eta = \eta_{01}$ and η_{11} in Figure 20 for $\varphi_0 = 60°$ are far from identical with the b.s.c.s. at η_{01} and η_{11} for the $\varphi_0 = 0$ cylinder. This clearly indicates that the $\varphi_0 = 60°$ case is, as should be expected, very poorly described by the narrow slot approximation. This inadequacy of the narrow slot approximation is becoming more pronounced. It has been further confirmed by considering the frequencies corresponding to the very sharply defined two lowest internal TM circular waveguide modes (i.e. for η_{01} and η_{11}). The presence of the slot of half angle 60° has physically modified these eigenvalues for the closed cylinder so that they then correspond to broader lines centered at slightly shifted frequencies differing from the precise values of η_{01} and η_{11}. This phenomenon of evolution of line broadening and shifting of the centers of these lines is already discernible for the $\varphi_0 = 45°$ case of the slotted cylinder. This has been alluded to in section VIII for both $\varphi_0 = 45°$ and $\varphi_0 = 60°$ and again must be pointed out in this section where the resonance frequencies are being considered. For the $\varphi_0 = 45°$ case this can be seen by

inspecting Figures 9 and 20 which respectively permit comparison of

the $\varphi_0 = 30°$ and $\varphi_0 = 45°$ b.s.c.s. and the $\varphi_0 = 60°$ and $\varphi_0 = 45°$

b.s.c.s. We have not included the distribution of the real and imag-

inary parts of the electric field over the slot for $\varphi_0 = 45°$ and

$\eta = \eta_{01}$ and η_{11} . The objectives of this chapter are in no way

injured by this omission. Inspection of Figure 42 shows that for

$\eta = \eta_{01}$ constraint requirement II of eq. (97) is most likely the

applicable requirement on the slot electric field to maintain the

interior electric field physically a realizable one. Clearly con-

straint requirement I completely fails to apply for this situation.

Studying Figure 43 for the $\eta = \eta_{11}$ resonance frequency we see clearly

that this corresponds to the last constraint requirement of eq. (97).

Constraint I definitely does not apply now. This result can be made

much more plausible by realizing that Figure 43 represents a situa-

tion where the wavelength is shorter for the same size opening than

for the results depicted in Figure 42. In effect a larger opening is

presented to the incident radiation. Roughly speaking then the

scattering situation has moved a bit closer to the limiting situation

described above where constraing requirement IV holds. At the lower

mode i.e. η_{01} we probably are somewhat between the two extreme cases

at which constraints I and IV apply. The $\varphi_0 = 30°$ slotted cylinder

case, we pointed out just above, is behaving pretty much like the

$\varphi_0 = 0°$ case. We expect for $\varphi_0 = 30°$ further departure from this

situation at higher modes which correspond to effectively larger

Figure 42. Real And Imaginary Parts Of The Slot Electric Field; $\eta=2.405$, $\varphi_0=60°$
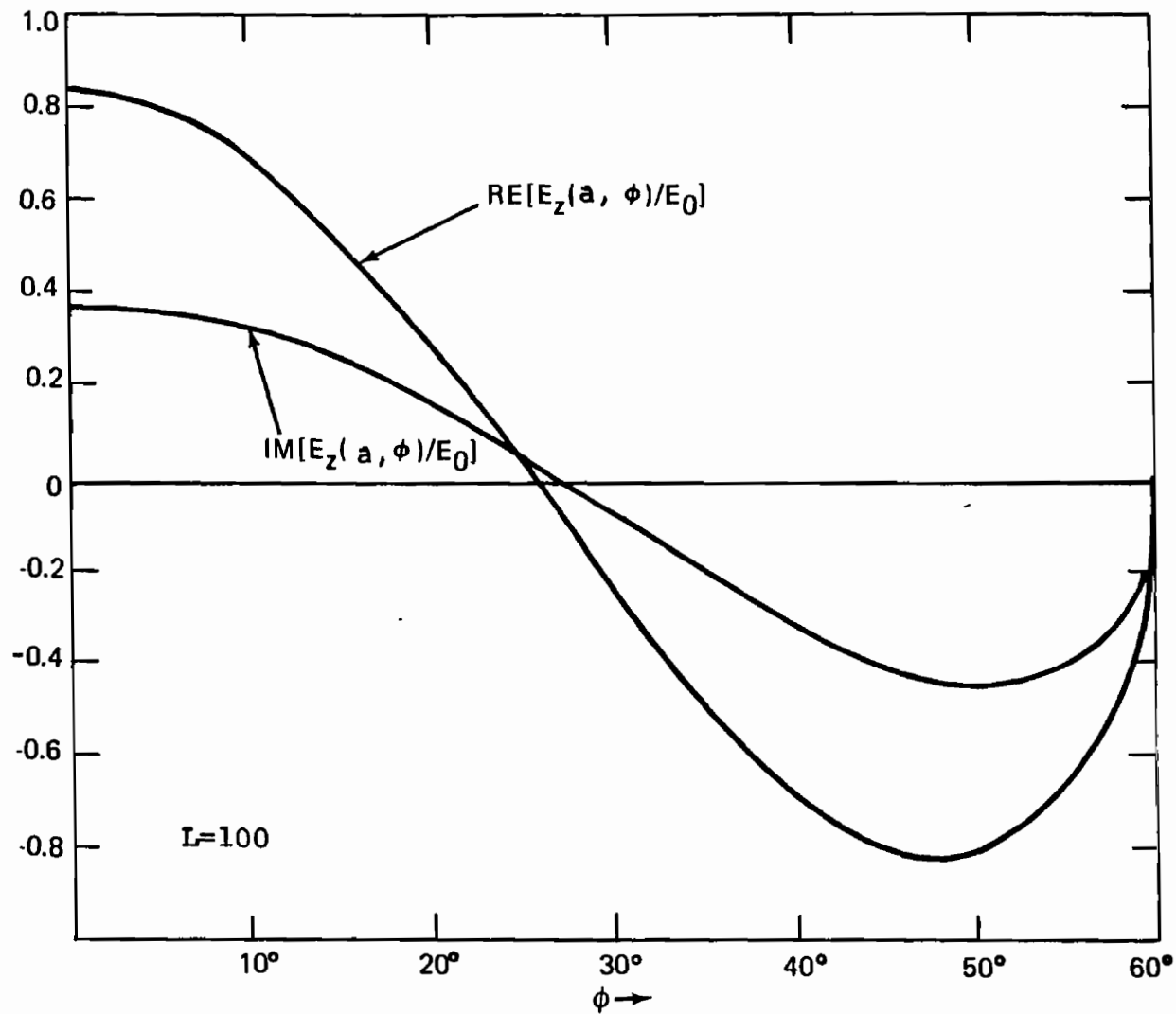
Figure 43. Real And Imaginary Parts Of The Slot Electric Field; $\eta=3.832$, $\varphi_0=60°$

openings in the cylinder as the wavelength decreases.

At the frequencies corresponding to the two lowest TM circular cylindrical waveguide modes we find that constraint requirement IV of eq. (97) holds for the real and imaginary parts of the electric field over the slot when the half slot-angle is $\varphi_0 = 90°$. This is immediately evident for $\eta = \eta_{01}$ as shown in Figure 44. For $\eta = \eta_{11}$ the results as shown in Figure 45 do not at a first cursory glance seem to display this property. In fact it would superficially appear that constraint requirement II just might apply to the aperture electric field distribution. It should be borne in mind though that $\varphi_0 = 90°$ means we are considering a half-cylindrical concave mirror. This is quite far removed from a narrow slot situation. Indeed if the real part of the electric field is weighted by the multiplying factor $\cos\varphi$ we can easily enough observe, using Figure 45, that for the range over which the real part of the aperture field is negative the weighting function $\cos\varphi$ only weakly modifies the amplitude of the field. Meanwhile this weighting function much more markedly damps the amplitude of the field over the range of φ for which the real part of the aperture field is positive. The net result is that the real part times the cosine integrates to zero for $\eta = \eta_{11}$ and $\varphi_0 = 90°$, hence constraint requirement IV is the actual condition that holds. Most probably this continues to hold for the higher modes of the complete circular waveguide. Remember that by satisfying eq. (97) over the aperture results in a finite or well behaved

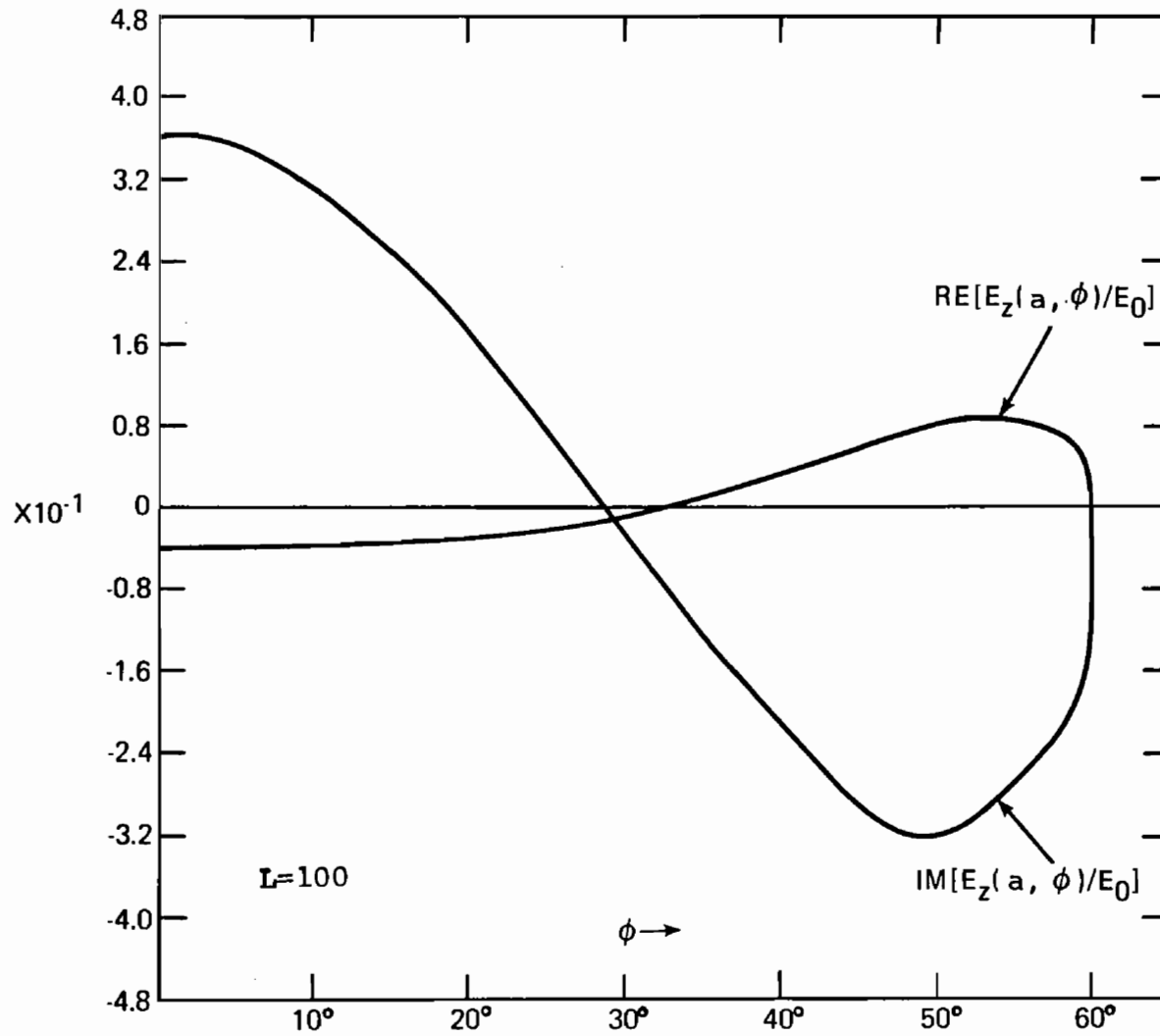Figure 44. Real And Imaginary Parts Of The Slot Electric Field; $\eta=2.405$, $\varphi_0=90°$
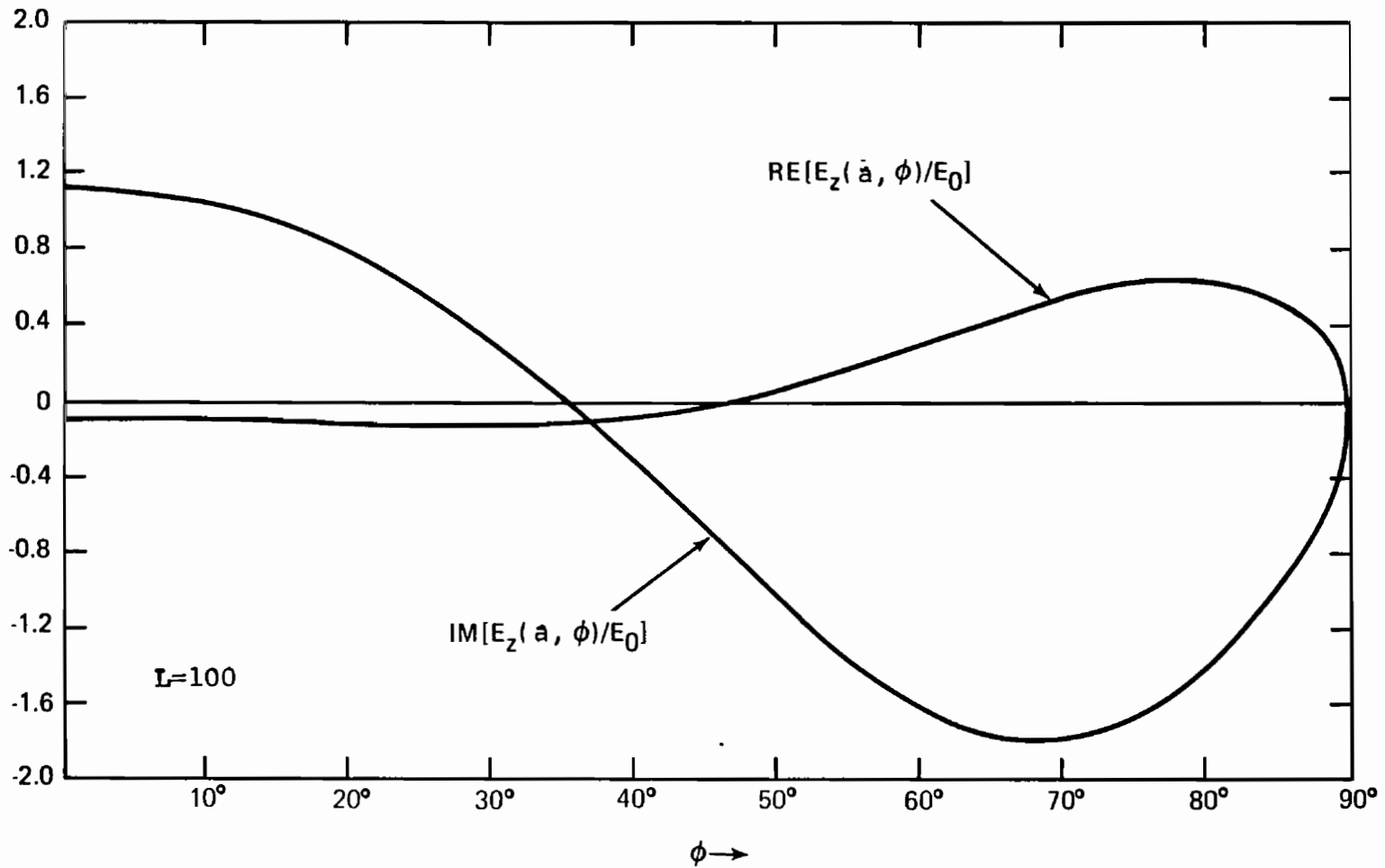
Figure 45. Real And Imaginary Parts Of The Slot Electric Field; $\eta=3.832$, $\varphi_0=90°$

electric field in the interior of the slotted cylinder which is a fundamental physical requirement at the values of η corresponding to the TM eigenmodes of the circular cylindrical waveguide without a slot.

The next case to consider is that for the half slot angle $\varphi_0 = 120°$. We recall that this corresponds to a concave cylindrical strip of central angle $120°$ i.e. one third the original cylinder with $\varphi_0 = 0°$. As expected this in no way is approximated by a narrow slotted cylinder. That this is so is confirmed by inspection of Figure 46 for $\eta = \eta_{01}$ and Figure 47 for $\eta = \eta_{11}$ which clearly indicates that the distributions of the real and of the imaginary parts of the slot electric field do not satisfy constraint requirement I of eq. (97) at the waveguide resonances. Note the case for $\varphi_0 = 120°$ and $\eta = \eta_{01}$ as represented by Figure 46. Once again this presents only a superficial indication that constraint condition III, this time, may hold. However, a more closer scrutiny of the area under the curve of the distribution of the imaginary part of the slot electric field reveals that the proper condition holding in this case is once again constraint requirement IV of eq. (97). Similarly if one undertakes an approximately careful piecewise examination of the effect of the weighting function $\cos\varphi$ for the real and imaginary parts of the slot electric field as shown in Figure 47 for the $\eta = \eta_{11}$ case it results in the conclusion that constraint requirement IV also holds here. This is the case even though it may not be
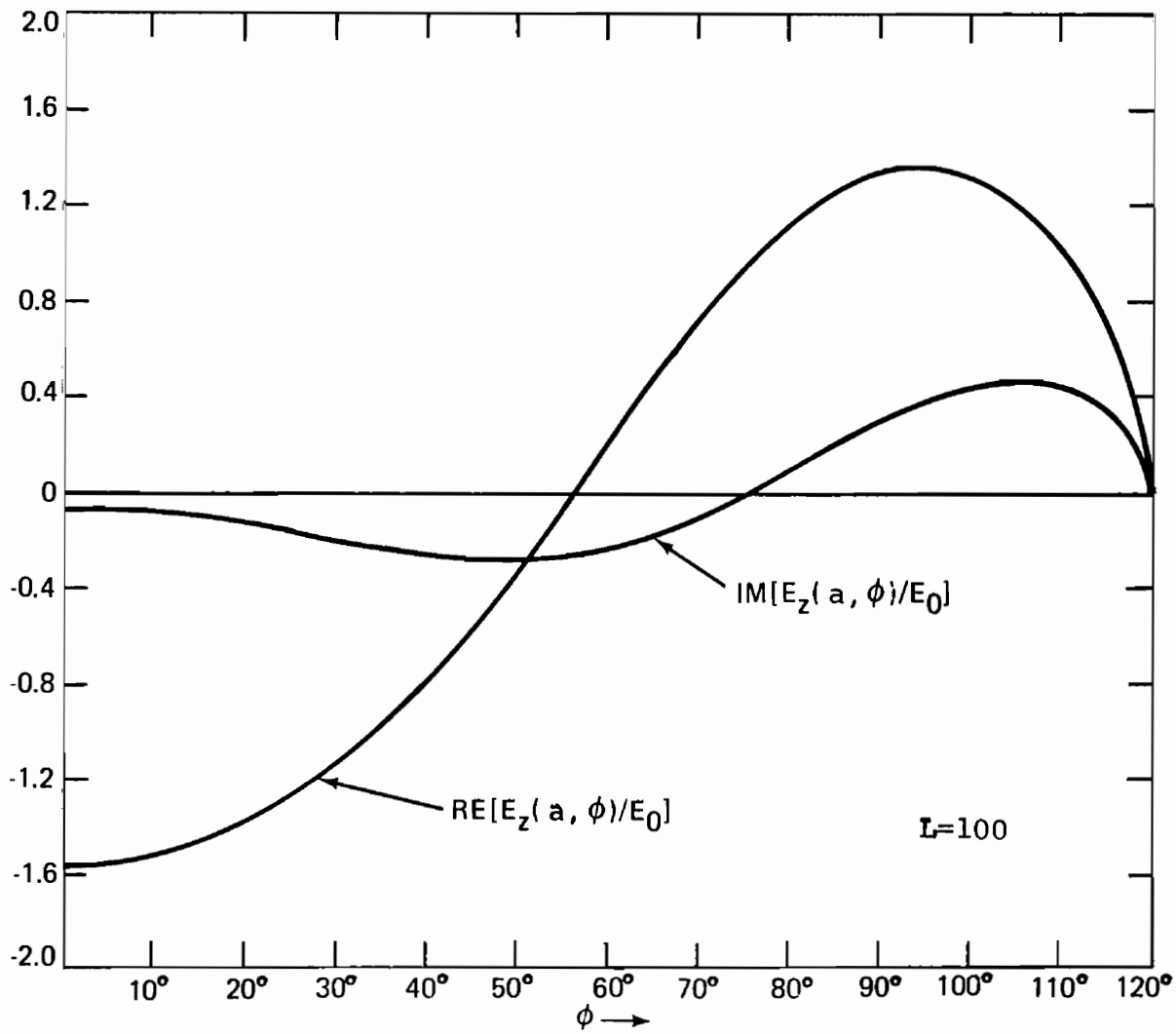
Figure 46. Real And Imaginary Parts Of The Slot Electric Field; $\eta=2.405$, $\varphi_0=120°$
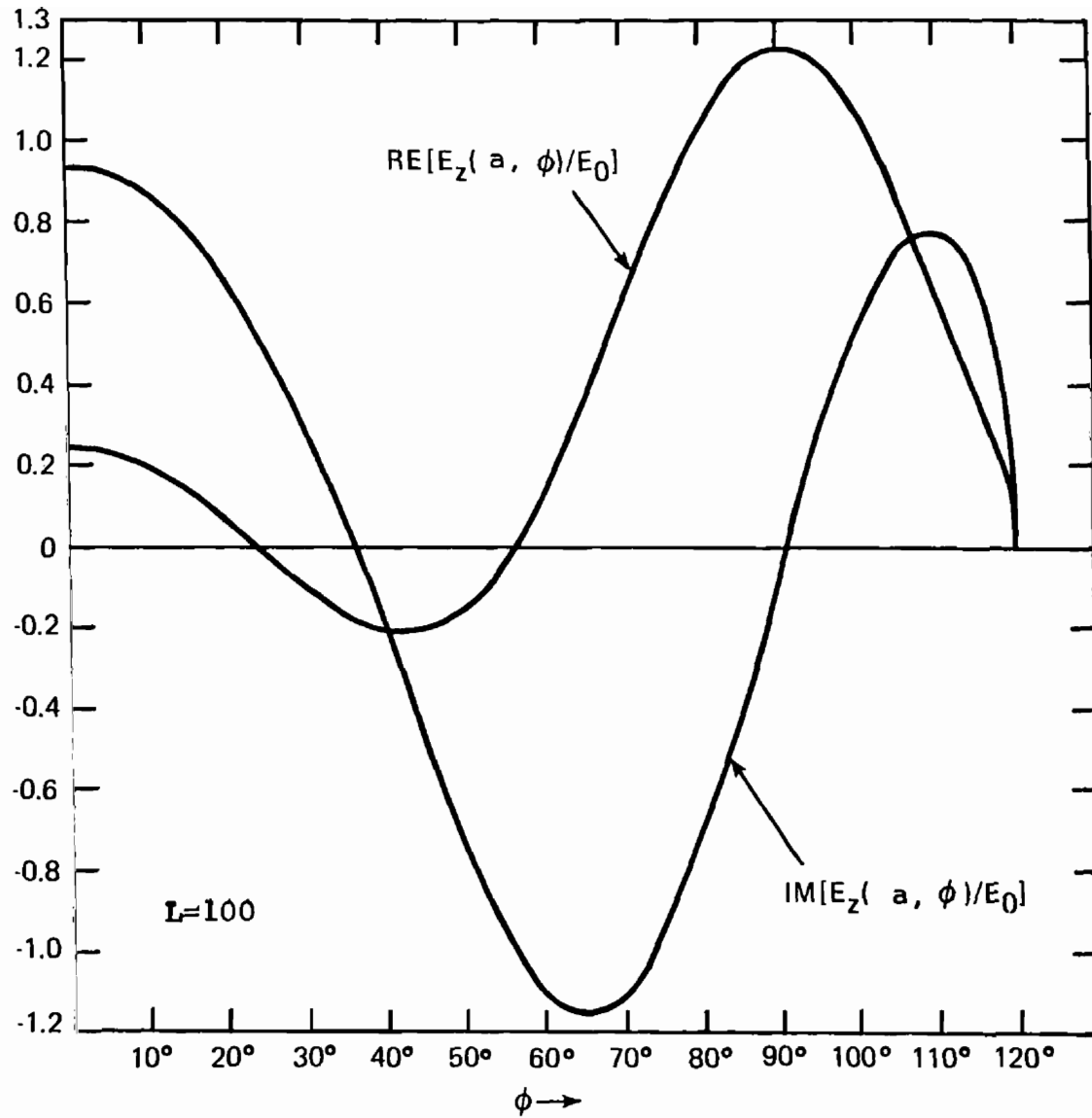
Figure 47. Real And Imaginary Parts Of The Slot Electric Field; η=3.832, φₒ=120°

immediately evident because of the oscillatory behaviour of the real

and imaginary parts of the aperture electric field distribution.

The last case studied and reported on in this paper is the

$\varphi_0 = 150°$ slotted cylinder. This is, of course, the cylindrical

ribbon which subtends an angle of 60° at the cylinder axis. Again it

is crystal clear that constraint requirement I of eq. (97) does not

enter into this situation. Now only a narrow strip consisting of

one-sixth the original cylinder concave towards the radiation is the

target. This is decidely not a case where the narrow slot theory

applies. Figure 48 for the distributions of the real and imaginary

parts of the electric field at the lowest TM eigenmode of the cylin-

drical waveguide shows that constraint requirement IV holds for

$\varphi_0 = 150°$. Obviously we are far along towards the limiting situation

of no cylinder. This limit we recall corresponds to condition IV.

It is also clear from Figure 48 and Figure 38, $\eta = \eta_{01}$ no longer rep-

resents a resonance for $\varphi_0 = 150°$. In spite of the oscillatory

behaviour exhibited in Figure 49 for the distribution of the real and

imaginary parts of the electric field over the aperture in the

$\varphi_0 = 150°$ case it can still easily enough be demonstrated that at

$\eta = \eta_{11}$, upon introducing the weighting function $\cos\varphi$, that con-

straint condition IV applies. This is by now of course not at all

surprising. Again we note clearly by simple inspection of Figures 38

and 49 that $\eta = \eta_{11}$ is no longer a real resonance when the cylinder
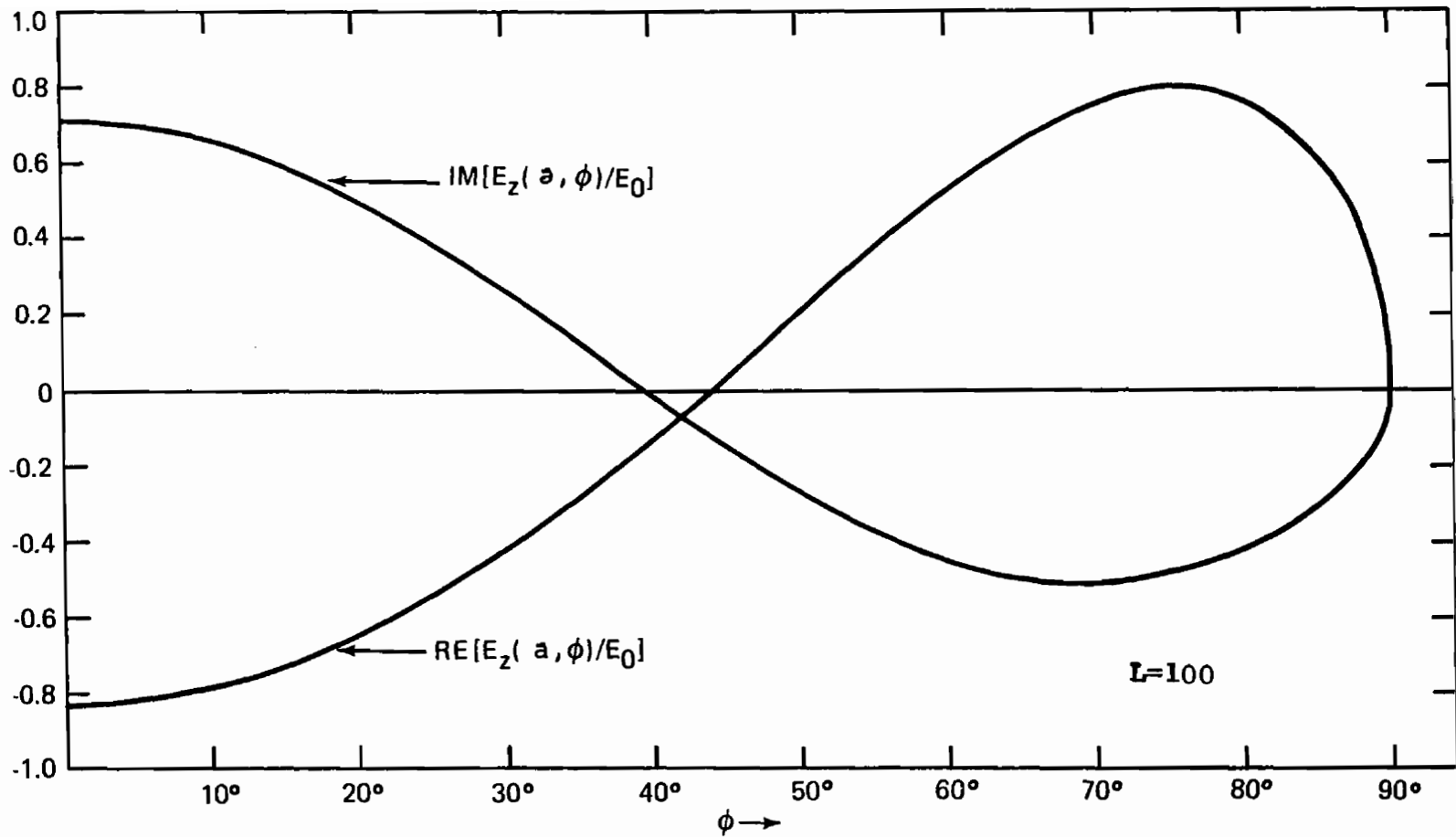
is cut back to a 60° strip.
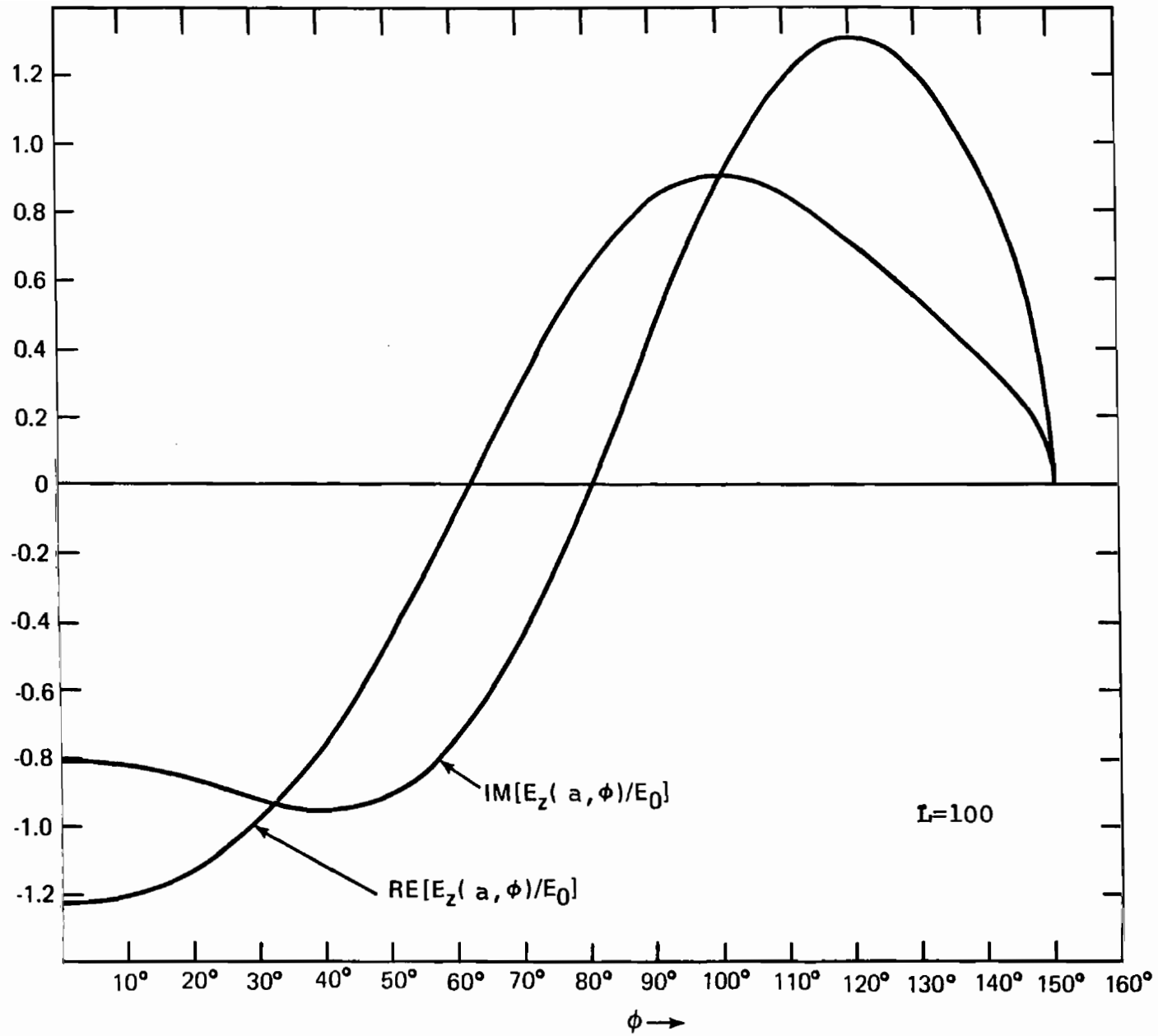
Figure 48.   Real And Imaginary Parts Of The Slot Electric Field; $\eta=2.405$, $\varphi_0=150°$
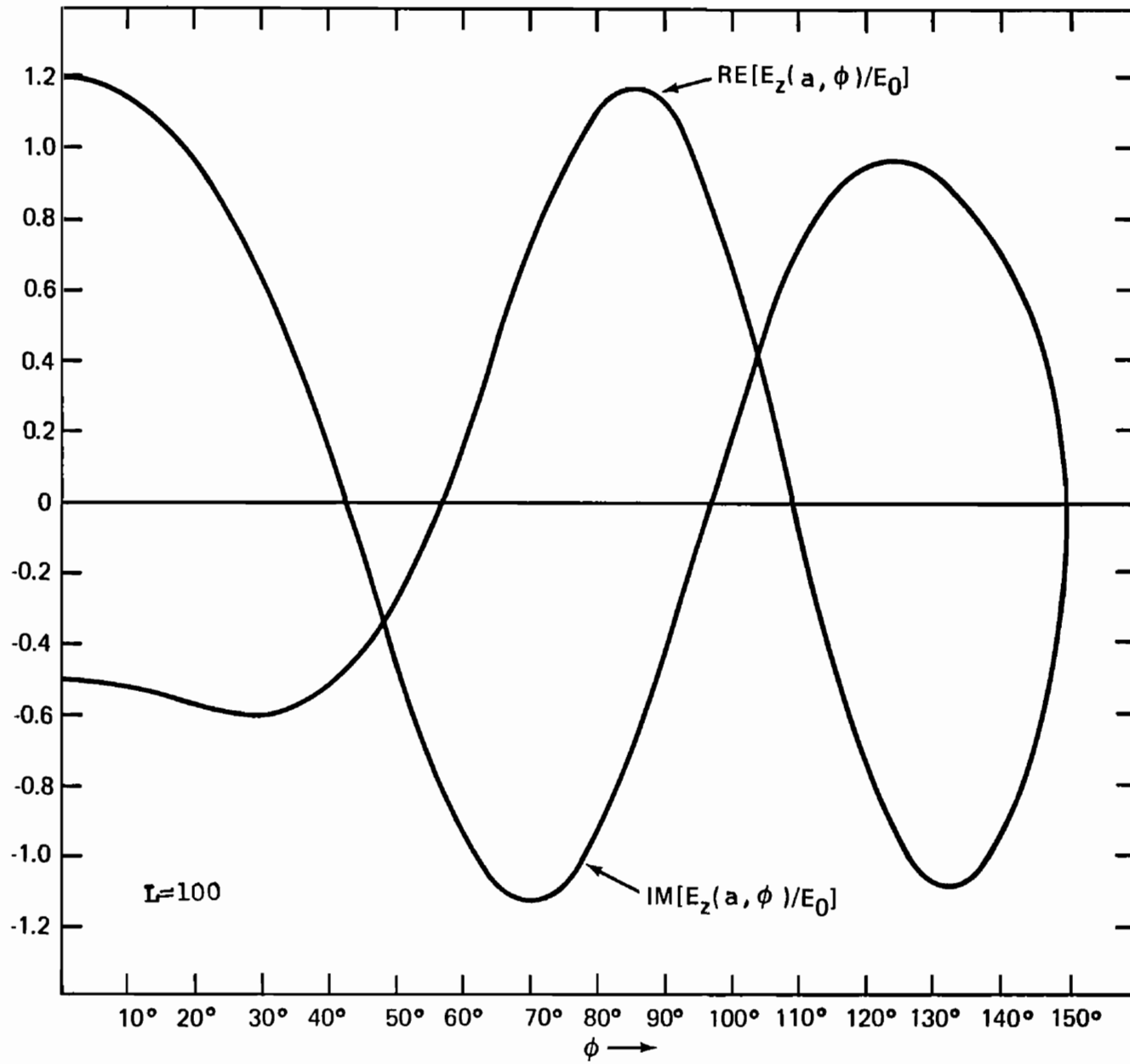
Figure 49. Real And Imaginary Parts Of The Slot Electric Field; $\eta=3.832$, $\varphi_0=150°$

We next briefly summarize the results of this chapter. The requirements that were derived for the electric field in the opening i.e. eq. (97) have been substantiated by numerical results we obtained via the method-of-moments. We have seen that constraint condition I applies for the lower order modes when the half slot angle is $\varphi_0 = 30°$. A case where constraint condition II applies occurred for the cylinder with half-slot angle $\varphi_0 = 60°$. All the remaining cases explicitly considered and included in this report corresponded to constraint requirement IV. It is probably the situation that constraint conditions II and III hold for the cylindrical waveguide resonances when the slot angle falls in the range $30° \leqslant \varphi_0 \leqslant 60°$ for the lower lying modes in the closed cylinder interior spectrum.

X. FURTHER CONSIDERATION OF THE φ_0 = 30° SLOT - COMPARISON OF THREE
    METHODS OF SOLUTION

We begin this section by first developing the Morse and

Feshbach[6] form of solution for the slot electric field distribution.

Morse and Rubenstein[33] solved, exactly, the problem of a plane wave

normally incident on a slotted infinite plane of infinitesimal thick-

ness and of perfect conductivity. When the incident radiation is

polarized parallel to the slot the electric field distribution in the

slot, for wavelengths that are large compared to the slot width, can

be shown to have the form

$$\mathcal{E}(d) \underset{\lambda \to \infty}{\propto} \sqrt{1 - \left(\frac{d}{D}\right)^2}$$

where d is the distance from the symmetry axis of the slot to the

field point in the slot and D is the half width of the slot. This

result can be approximately carried over to a slotted cylinder of

radius a and half slot angle φ_0 by the following substitutions

$$d \cong a\varphi$$

$$D \cong a\varphi_0$$

where φ_0 has been assumed to be very small. Under this transforma-

tion the electric field distribution in the aperture of an axially

6. P. M. Morse and H. Feshbach, "Methods of Theoretical Physics",
    Part II, 1387-1398 McGraw-Hill, New York 1953

33. P. M. Morse and P. J. Rubenstein, "The Diffraction of Waves by
    Ribbons and by Slits", Phys. Rev. 54, 895 (1938)

slotted cylinder for a very narrow slot is given approximately by

$$\mathcal{E}(\varphi) \underset{\lambda \to \infty}{\propto} \sqrt{1 - \left(\frac{\varphi}{\varphi_0}\right)^2}$$

This latter form is the slot electric field distribution assumed by Morse and Feshbach[6]. In Tables 2 and 3 we show respectively the slot field distributions for a slot of $\varphi_0 = 6°$ obtained using the method-of-moments and the results obtained by Morse and Feshbach. These have both been normalized at the slot center. Comparing these two sets of results we note good agreement exists between the two distributions for the wavelengths considered. Two points should be noted, first we are not considering "resonance" situations and second as the slot edges are approached differences between the two distributions appear and increase in magnitude although they are not very large. Note that as the wavelength decreases this deterioration in agreement becomes more pronounced.

Now let us compare the results obtained for the $\varphi_0 = 30°$ slot electric field distribution by the method-of-moments to the corresponding distribution predicted by Morse and Feshbach using the narrow slot approximation. The two distributions are shown in Tables 4 and 5. These slot field distributions have been normalized to the values at the slot center. Observation of these tables shows that the two

---

6. P. M. Morse and H. Feshbach, "Methods of Theoretical Physics", Part II, 1387-1398 McGraw-Hill, New York, 1953

Table 2. Normalized Distributions of the Electric Field in a Slot Where $\varphi_0 = 6°$ from the Method-of-Moments

	$\eta=0.5$	1.0	2.0	3.0	4.0	5.0
$\varphi = 0°$	1.000	1.000	1.000	1.000	1.000	1.000
1°	0.985	0.988	0.987	0.988	0.987	0.987
2°	0.950	0.950	0.949	0.949	0.948	0.947
3°	0.883	0.883	0.882	0.881	0.880	0.878
4°	0.781	0.780	0.780	0.778	0.776	0.773
5°	0.629	0.628	0.627	0.625	0.623	0.619

Table 3. Normalized Distribution of the Electric Field in a Slot Where $\varphi_0 = 6°$ from the Work of Morse and Feshbach

	$\sqrt{1-(\varphi/6°)^2}$
$\varphi = 0°$	1.000
1°	0.986
2°	0.943
3°	0.866
4°	0.745
5°	0.553

Table 4. Normalized Electric Field Distribution In a Slot For
          $\varphi_o = 30°$ By The Method-of-Moments

	$\eta = 0.5$	1.0	2.0	3.0	4.0	5.0
$\varphi = 0°$	1.000	1.000	1.000	1.000	1.000	1.000
5°	0.986	0.985	0.984	1.982	0.980	0.967
10°	0.942	0.940	0.935	0.928	0.921	0.873
15°	0.864	0.861	0.852	0.836	0.822	0.741
20°	0.745	0.740	0.726	0.702	0.680	0.593
25°	0.562	0.556	0.539	0.511	0.485	0.431

Table 5. Normalized Electric Field Distribution In a Slot For
          $\varphi_o = 30°$ from Morse and Feshbach

	$\sqrt{1 - (\varphi/30°)^2}$
$\varphi = 0°$	1.000
5°	0.986
10°	0.943
15°	0.866
20°	0.745
25°	0.553

distributions are nearly identical over the entire slot for $\eta = 0.5$ and $\eta = 1.0$. However as η increases the disagreement between the two distributions steadily increases. This is not unexpected. Thus for $\eta = 4$ say the arclength of the slot is approximately $2\lambda/3$ which is hardly a narrow slot.

In Figure 50 we simultaneously display the slot electric field distributions for $\varphi_0 = 30°$ and $\eta = 10.472$ obtained by Morse and Feshbach, by Barth[10], and by the method-of-moments for $L = 200$. All three are normalized to the value at the center of the slot. The method-of-moments prediction for the distribution of the slot electric field is in very good agreement near the slot edges with the Morse and Feshbach slot field distribution. Over the larger range of the slot these two field distributions differ considerably. On the other hand we observe that the slot field distribution of Barth is in reasonable agreement with the Morse and Feshbach theory over most of the slot. Near the slot edges this agreement seriously deteriorates.

All these discrepancies displayed in Figure 50 can be readily understood if we take into consideration several factors. To begin with the wavelength that corresponds to $\eta = 10.472$ is roughly

$$\lambda \sim \frac{2}{3} a$$

10. M. J. Barth, "Interior Fields of a Slotted Cylinder Irradiated with an Electromagnetic Pulse", Tech. Rep. No. AFSWC-TR-69-9, Air Force Special Weapons Center, Kirtland Air Force Base. New Mexico, August 1969
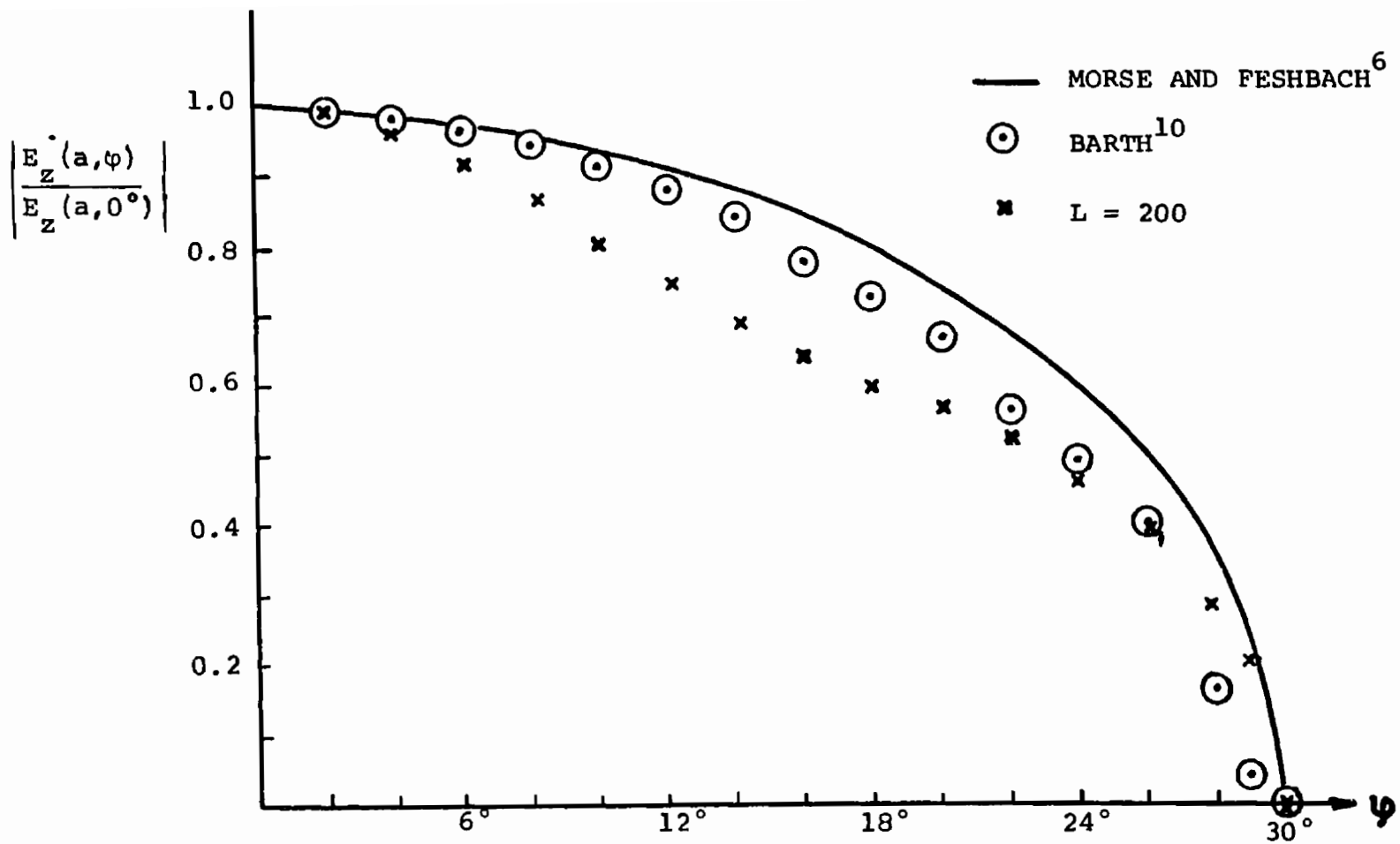
Figure 50. THREE NORMALIZED SLOT ELECTRIC FIELD AMPLITUDES,

$\eta = 10.472, \quad \varphi_0 = 30°$

and the slot width is

$$2a \sin 30° = a$$

so that the wavelength is comparable to the width of the slot. Then the Morse and Feshbach distribution, which is an approximation holding for a wavelength that is large compared to the slot width, should not be capable of reliably describing the electric field over most of the slot region. Agreement at the slot center with the method-of-moments is forced by the assumed normalization to the slot center. The next point to be considered is the behaviour required for the electric field near the slot edges. Near an edge the tangential electric field must go as the square root of the distance from the field point to the slot edge. Close to the edge, then, the slot field distribution at any wavelength behaves as

$$\sqrt{2a \sin\left(\frac{\varphi_o - \varphi}{2}\right)} \underset{\varphi \to \varphi_o}{\propto} \sqrt{1 - \left(\frac{\varphi}{\varphi_o}\right)}$$

Near the slot edge the Morse and Feshbach distribution becomes

$$(109) \qquad \sqrt{1 - \left(\frac{\varphi}{\varphi_o}\right)^2} = \sqrt{1 + \left(\frac{\varphi}{\varphi_o}\right)} \sqrt{1 - \left(\frac{\varphi}{\varphi_o}\right)} \underset{\varphi \to \varphi_o}{\propto} \sqrt{1 - \left(\frac{\varphi}{\varphi_o}\right)}$$

Thus very near the slot edges the Morse and Feshbach field distribution has the correct limiting form for any wavelength. This accounts for the good agreement of the Morse and Feshbach results with the method-of-moments result at $\eta = 10.472$. Barth's results also have been forced into agreement with ours at the slot center by the method

chosen for normalization of the field distribution. Over the remainder of the slot but not close to the edge Barth's results are an improvement over those of Morse and Feshbach since his formulation essentially contains a somewhat larger number of adjustable parameters. However Barth's assumed form for the slot electric field distribution fails utterly to satisfy another basic edge condition. Jones[37] has shown that the normal component of the magnetic field at an edge possesses a singularity the order of which depends on the curvature of the edge. Since this component of the magnetic field is given by the derivative of the tangential electric field we can see from Figure 50 that Barth's assumed slot electric field rather unfortunately and unphysically has a derivative that vanishes at an edge. Since this electric field does not have a vertical slope at the edge the normal component of the magnetic field is not singular at the edge. The Barth formulation is therefore fundamentally wrong.

37. D. S. Jones, "The Theory of Electromagnetism", pp 566-569, Pergamon Press, New York 1964

XI. THE CYLINDRICAL STRIP FOR $\varphi_0 = 174°$

Another special case we investigated is that of the scattering by a cylindrical strip, of radius a, concave toward the normally incident axially polarized radiation. This strip corresponds to $\varphi_0 = 174°$ or equivalently half of the strip subtends an angle of 6° at the cylindrically axis. The method-of-moments applied to the integral equation for the surface current density is ideally suited for the situation of a narrow cylindrical strip. That is, a minimal number of uniform current zones are required to approximate the narrow strip and still achieve a desired degree of accuracy. This is clearly evident upon inspection of Table 6 where the back-scattering cross-section at different wavelengths are given for the narrow strip of $\varphi_0 = 174°$ in two orders of approximation, namely L = 40 and L = 60. Over the range of η from 0.5 to 5.0 the difference in the results between the two orders of approximation ranges from .1% to .2%. This indicates that a relatively small number of uniform current elements would yield quite accurate results for the back-scattering cross-sections.

Plotted in Figure 51 are the values of the b.s.c.s. for L = 60 taken from Table 6. Also in Figure 51 are plotted b.s.c.s. for a flat or planar strip. These latter results were obtained using the Rayleigh approximation for a flat ribbon. The Rayleigh approximation

formula used is[38]

$$(110) \quad k\sigma_B = \pi^2 \left[1 + \left(\frac{k^2 d^2}{4} \right) \right]^2 \bigg/ \left[\frac{\pi^2}{4} + \ln^2 \left(\frac{4.48}{2kd} \right) \right]$$

where 2d is the width of the flat strip. Now the distance between

the edges 2W of the cylindrical ribbon of radius a is

$$(111) \quad 2W = 2a \sin (\pi - \varphi_0) = 2a \sin (\pi/30) \approx 2\pi a/30$$

We can see how good an approximation a flat strip makes to our cylin-

drical strip by substituting for d in eq. (110) the expression for

W given in eq. (111). This gives the following approximate expres-

sion for the back-scattering cross-section

$$(112) \quad k\sigma_B = \pi^2 \left[1 + \frac{1}{4} \left(\frac{\pi\eta}{30} \right)^2 \right]^2 \bigg/ \left\{ \frac{\pi^2}{4} + \ln^2 \left[\frac{2.24}{(\pi\eta/30)} \right] \right\}$$

The resulting close agreement of the cylindrical strip results with

the flat strip results is hardly a surprising outcome. This is a

direct consequence of the fact that the shortest wavelength consid-

ered for the incident radiation namely the $\eta = 5.0$ case is on the

order of ten times greater than the width of the strip. At these

long wavelengths the back-scattering properties should be nearly

indistinguishable between the flat planar strip of width 2d and a

38. G. T. Ruck, ed. "Radar Cross Section Handbook", Vol. 2. p 502, Plenum Press, New York, N. Y. 1970

Table 6. Numerical Values of Back-Scattering Cross-Section, $B = k\sigma_B$, by the Method-of-Moments for $\varphi_0 = 174°$ i.e. The Cylindrical Ribbon

	$B = k\sigma_B$	
η	$L = 40$	$L = 60$
0.5	0.5939	0.5945
1.0	0.8337	0.8346
1.5	1.0433	1.0446
2.0	1.2414	1.2431
2.5	1.4355	1.4376
3.0	1.6297	1.6322
3.5	1.8268	1.8299
4.0	2.0291	2.0328
4.5	2.2384	2.2428
5.0	2.4564	2.4615
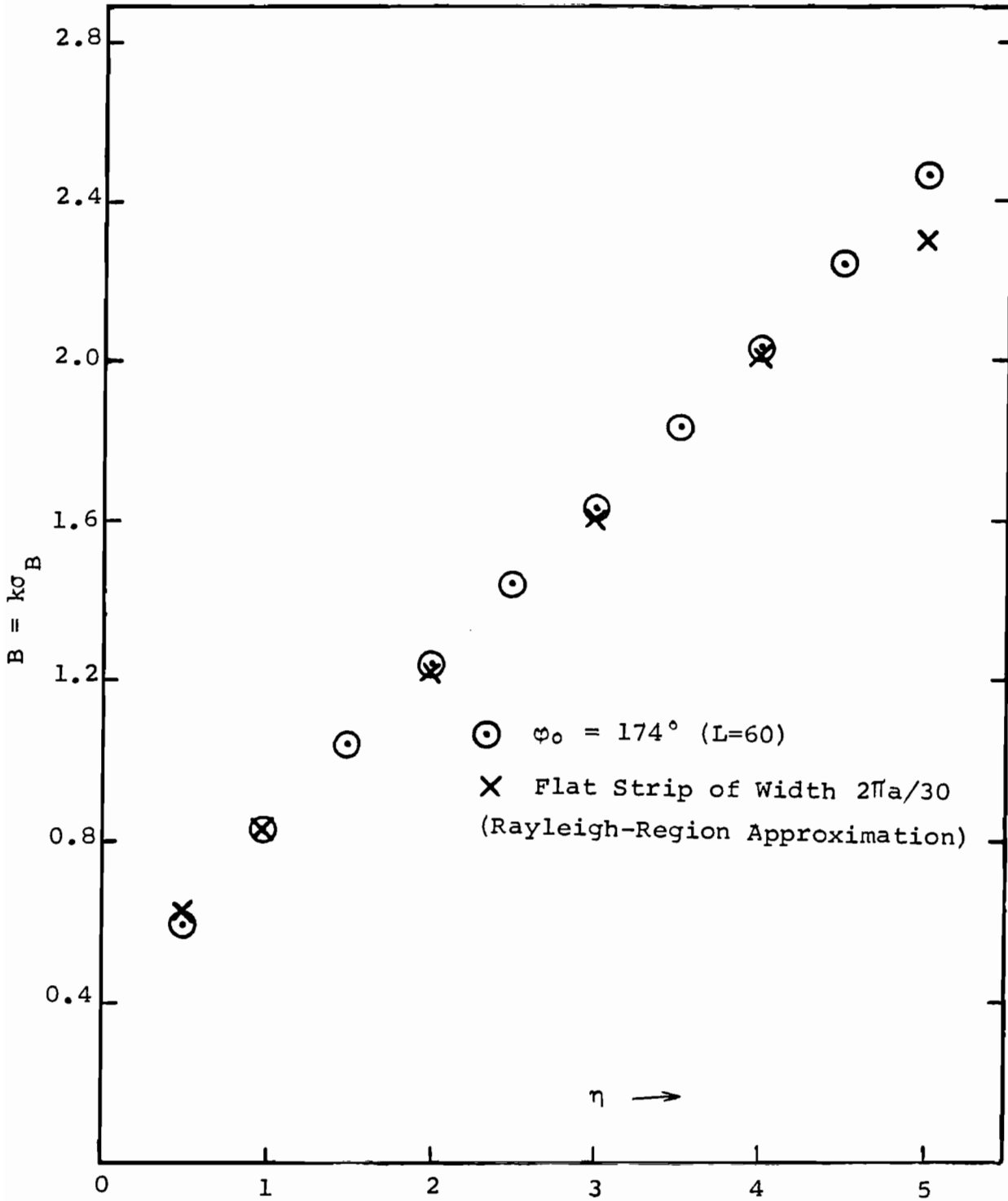
Figure 51. Comparison of The Planar Strip and the Cylindrical Strip Back-Scattering Cross-Section For $\varphi_0 = 174°$ and Planar Strip Width $2\pi a/30$

symmetrically positioned cylindrical strip whose projection on a plane facing the incident radiation has width $2W \simeq 2d$.

Figure 52 exhibits the results obtained for the surface current distribution on the symmetrical positioned strip, concave to the incident axially polarized plane wave electromagnetic radiation. We show for the case $\varphi_0 = 174°$ and $\eta = 0.5$ the results obtained from a Rayleigh approximation as given in an earlier paper[4] as well as those we obtained by our method-of-moments calculation. To facilitate comparison both sets of results have been normalized to the magnitude of the surface current at $\varphi = \pi$ i.e. at the center of the "shadow" region of the strips. The normalizing factors adopted are

$$(113) \qquad \left| K_z \ (\varphi=\pi) \right|_{\eta=0.5} = 10.49 \ H_o$$

for the Rayleigh approximation, and

$$(114) \qquad \left| K_z \ (\varphi=\pi) \right|_{\eta=0.5} = 9.36 \ H_o$$

for our theoretical determinations. As can be quickly and clearly observed in Figure 52 the two distributions of the magnitudes of surface current density over the cylindrical strip are for all practical purposes identical except in the close-in neighborhood of the edges. We demonstrated in a previous paper[4] that the theoretical Rayleigh

---

4.   J. N. Bombardt and L. F. Libelo (NAVSURFWPNCEN) "S.E.R.A.: IV
      Slotted Cylinders and Cylindrical Strips in the Rayleigh Limit",
      HDL-RT-1607, Harry Diamond Lab., Washington, DC, August 1972
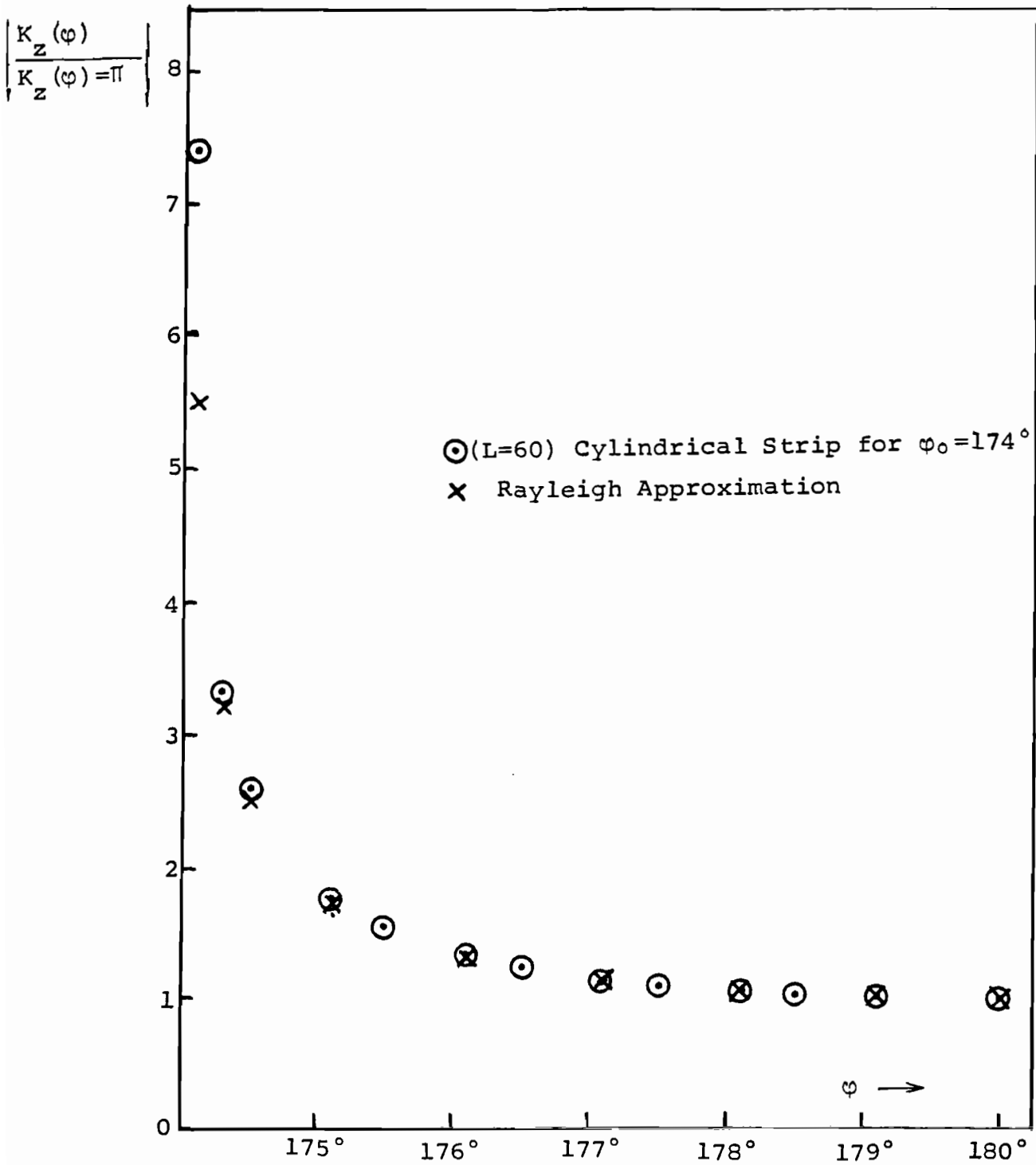
Figure 52. The Surface Current Distribution Over the Cylindrical Strip for $\varphi_0 = 174°$, $\eta \doteq 0.5$ and for the Corresponding Flat Strip.

result for the surface current at the narrow cylindrical strip edges

exhibits the singular behaviour required for agreement with the phys-

ically established edge conditions. The Rayleigh approximation

actually only lags the rate of increase of the actual amplitude near

the edge by an amount less than that shown in Figure 52. Recall that

we have forced the two sets of results into agreement at the strip

center normalizing each set separately. The corresponding normaliza-

tion factors are given in eqs. (113) and (114). By inspecting these

we note that they differ by about 2% with the Rayleigh normalizing

factor being the larger. Consequently the Rayleigh curve will be

pulled down much more drastically as the edge is approached. At the

same time the relative effect away from the edge is hardly signifi-

cant. We thus have determined the surface current density over the

narrow strip and it is in good agreement with the asymptotic predic-

tions of the Rayleigh limit approximation. Although we have not ex-

plicitly included them the corresponding results for the distribution

of amplitude of surface current density at other wavelengths in the

range of $1.0 \leq \eta \leq 5.0$ were found for the same cylindrical ribbon. These

are not significantly different from the results shown for $\eta = 0.5$ in

Figure 52.

XII. COMMENTS ON THE COMPUTER PROGRAM

1. The Main Program

A program which we have dubbed with the title STEPS has been constructed. This program solves the silumtaneous system of algebraic equations collected together in eq. (82). In this set of equations the unknowns quantities to be solved for are the step-function pulse amplitudes of the surface current density distribution on the conduction portion of the cylinder. Once the surface current density is computed the program then computes the electric field at $\rho = a$ over the cylindrical aperture. This is accomplished using eq. (89). Finally in the same program the surface current density results are then utilized to calculate the back-scattering cross-section per unit length via eq. (92).

Complex function subroutines have been written for the known co-efficients in eq. (82), the set of simultaneous equations. These known quantities are required in eq. (89), for calculating the aperture electric field distribution, and in eq. (92) for evaluating the back-scattering cross-section in the form $B = k\sigma_B$. An existing IBM subroutine for solving simultaneous linear equations was modified to solve sets of simultaneous linear equations with complex coefficients. Both an existing IBM subroutine for calculating n-th order Neumann functions with real argument and a subroutine written for n-th order Bessel functions of the first kind with real argument were used in

the complex function subroutines just mentioned. We shall briefly

discuss these subroutines below.

STEPS proceeds generally as follows. The input data is read in.

A "DO" loop is set up for calculating the desired quantities at all

specified values of the circumference-to-wavelength ratio parameter η.

Next additional "DO" loops calculate and load the coefficient matrix

and right-hand side vector into the computer memory. Using appropri-

ate subroutines, the simultaneous system of algebraic equations is

solved and proceeding through another "DO" loop the azimuthal angle

and complex surface current density, amplitude and phase, are printed

out. Next cycling through another "DO" loop the electric field dis-

tribution is calculated at ρ = a over the aperture and the azimuthal

angle and the complex electric field, amplitude and phase, are then

printed out. Lastly the summation which gives $B = k\sigma_B$ is calculated

and the printed output consists of the frequency parameter η, $B=k\sigma_B$

itself and an error code for the IBM subroutine GELG (a Gaussian

elimination method). The program repeats the above procedure for

each value of η until the final value of η (for a given set of input

data) is attained. At this point the program is ready for a new set

of input data.

Our computer program STEPS requires the following data input:

i) PHIO $\equiv \varphi_0$, a positive angle to be given in degrees and

should be a positive integer if the electric field over the aperture

at ρ = a is to be computed,

ii)   L ≡ an even (non-negative) integer which represents the order of approximation of the calculation and is the number of equally spaced points on the perfect conductor at which the surface current density distribution over the cylinder is to be calculated,

iii)   BEGETA ≡ the initial value of the circumference to wavelength ratio, η, at which the surface current density and aperture electric field at $\rho = a$ and at which the back-scattering cross-section $B = k\sigma_B$ are to be computed,

iv)   FINETA ≡ the final value of the frequency parameter η at which the desired quantities are to be calculated,

v)   DETA ≡ the increment for the frequency parameter - a positive non-zero integer NETA is first established such that the relation DETA * NETA = FINETA - BEGETA holds.

The amount of computer time required for a given set of input data depends upon three factors:

i)   the number of simultaneous algebraic equations that are to be solved, namely L/2 for each value of η,

ii)   the value of φ_0, the half-slot angle, and

iii)   the number of desired η values.

To illustrate the estimation of the computer time required consider the choice of L = 100, which corresponds to a system of 50 simultaneous equations, and a half-slot angle $\varphi_0 = 30°$. It takes about 75 seconds on a CDC 6400 computer to obtain the surface current density distribution over the conductor, the electric field

distribution over the cylindrical aperture and the value of the back-scattering cross-section $B = k\sigma_B$ for a single value of η. If instead $L = 80$ is chosen, i.e. a system of 40 simultaneous equations, it takes about 52 seconds per η value to calculate the desired quantities. If we again choose $L = 100$ and the half-slot angle $\varphi_0 = 60°$ is selected it requires approximately 120 seconds for each value of η to calculate the desired back-scattering cross-section, surface current distribution and aperture electric field distribution.

Naturally as the number of simultaneous algebraic equations to be solved is increased the amount of computer memory required also increases. When a system of 40 simultaneous equations are to be solved the number of 60 bit words of computer memory required is 46,700 (octal). For a system of 100 such simultaneous equations to be handled the number of 60 bit words of memory required increases to 65,000 (octal).

An option built into the main program permits the array of co-efficients in the sets of simultaneous equations to be printed out if they are explicitly desired for any reason.

We have decided not to explicitly include the actual computer program in this report for reasons of economy. The program is available upon request from either author.

2. Subroutines and Function Subprograms

A subroutine we entitle DJSER calculates the Bessel functions of

the first kind, of integral order and with real argument from the series expansion

$$J_n(x) = \sum_{m=o}^{\infty} \frac{(-1)^m (x/2)^{2m+n}}{m! \; (m+n)!}$$

The necessary factorials are computed by means of another simple function subprogram we call DFAC. The order n can be zero or a positive integer but the real argument must be greater than zero. An error code is returned in the calculation if n is less than zero and another if the argument x is not greater than zero. Termination of the evaluation of the series occurs when the q-th term computed is less than a prespecified tolerance, D, times the sum of the preceding q-1 terms. Upon termination the sum of the first q-terms is returned as the value of the Bessel function.

Subroutine BESY taken from an IBM manual[39] computes the Bessel functions of the second kind with integral orders and real arguments via the recurrence relation

$$Y_{n+1}(x) = (2n/x) \; Y_n(x) - Y_{n-1}(x)$$

Values of Y_0 and Y_1 are first calculated, for a specific argument, from an appropriate and accurate approximation for large or for

39. "SYSTEM/360 Scientific Subroutine Package" (360A-CM-03X), Version II, Programmers Manual, Publication H20-0205-2, International Business Machines Corp. 1967

small arguments. Cycling through the recurrence relation then yields Y_n. The order is restricted to be zero or a positive integer but the real argument must be greater than zero. Should the order n be less than zero an error code is returned by the program. In the same manner another error code will be returned if x is less than or equal to zero.

Another subroutine from the IBM manual, ARRAY[39], is used to convert the doubly dimensioned array of coefficients into a singly dimensioned vector. This vector is in the same location in memory as the array. The IBM version of ARRAY was modified in order to convert arrays with complex elements.

To solve the systems of simultaneous linear equations we used GELG[39] another subroutine from the IBM manual. Solution is effected by means of Gauss elimination with complete pivoting. We can illustrate the method by considering the following simple system of simultaneous equations:

$$a_{11}x_1 + a_{12}x_2 + a_{13}x_3 = b_1$$
$$a_{21}x_1 + a_{22}x_2 + a_{23}x_3 = b_2$$
$$a_{31}x_1 + a_{32}x_2 + a_{33}x_3 = b_3$$

The method systematically reduces this set of equations to the "triangular" form

---

39. "SYSTEM/360 Scientific Subroutine Package" (360A-CM-03X), Version II, Programmers Manual, Publication H20-0205-2, International Business Machines Corp. 1967

$$x_1 + c_{12}x_2 + c_{13}x_3 = d_1$$

$$x_2 + c_{23}x_3 = d_2$$

$$x_3 = d_3$$

Then starting at the bottom of this triangularized set we can compute all the unknowns x_3, x_2 and x_1 by working upward. Such a triangular form can be generated by selecting the element in the original co-efficient matrix with the largest absolute value. Let us assume a_{kj} is this element. We designate it as the first pivot element. Then compute the following multipliers for each value of the index i:

$$m_{ik} = -a_{ij}/a_{kj}$$

Next multiply each element of the row containing the first pivot element (the k-th row in this case) by the appropriate multiplier. Then add the result to the i-th row for each value of i. This process produces a new matrix in which the j-th column consists of zeros and the pivot element. Reducing the array by eliminating the j-th column and k-th row we generate another matrix whose rank is one less than that of the original. Select the element with the largest absolute value from this new matrix as the second pivot element and repeat the above process reducing the matrix rank by one again. This process is carried out N-1 times in succession if the original matrix is of rank N. The triangularized matrix is generated by collecting the discarded pivot rows. This in essence is the systematic pro-cedure followed in order to solve the original system of simultaneous

equations with complex coefficients. A complex function subprogram called AREA evaluates either eq. (83) or eq. (87) depending on whether or not $\bar{\varphi}_\ell$ lies in the interval of integration. AREA is used both to generate the coefficients in the systems of simultaneous equations and calculate the aperture electric field distribution. Finally another complex function subprogram called WEIGHT calculates the $g_\ell(\eta)$ quantities expressed in eq. (91) which are required to calculate the back-scattering cross-section.

The program including all subroutines and function subprograms is available upon request. All the details just briefly commented upon above are very readily understood by simply studying the program itself.

The program STEPS exists and is known at the Defense Nuclear Agency under the name DASC. This is an acronym for the title "Diffraction by an Axially Slotted Cylinder".

XIII.   FINAL SUMMARY AND CONCLUSIONS

It is rather well-known that the radiation properties of slot antennas on conducting cylinders have been studied extensively. In fact so much work has been accomplished by so many workers investigating the radiating antenna that it would be a severely difficult task to properly credit them all. For this reason the authors wish to extend their apologies to all those we have failed to give the credit due them. We have merely cited several representative references[40-46] and stand prepared to absorb the justly deserved reactions of those we have omitted.

The subject of this investigation has been the study of the scattering and diffraction of a linearly polarized plane electromagnetic wave that is normally and symmetrically incident on an axially

40.   S. Silver and W. K. Saunders, "The Radiation From A Transverse Rectangular Slot In A Circular Cylinder", Jour. of Applied Physics, 21, 745 (1950)

41.   L. L. Bailin, "The Radiation Field Produced By A Slot In A Large Circular Cylinder" IRE Transactions AP-3, 128 (1955)

42.   J. R. Wait, "Radiation Characteristics of Axial Slots On A Conducting Cylinder" Wireless Engineer pp 316-322 December 1955

43.   J. R. Wait, "Electromagnetic Radiation From Cylindrical Structures" pp 88-104, Pergamon Press, New York, N. Y. 1959

44.   C. A. Balanis, "Radiation From Slots On Cylindrical Bodies Using Geometrical Theory of Diffraction and Creeping Wave Theory" Doctoral Dissertation, Ohio State Univ., Columbus, Ohio 1969

45.   J. R. Wait, "Survey of Recent Literature on Slot Radiators", NBS Report #5051, U.S. Dept. of Commerce, Washington, DC March 1957

46.   R. W. P. King "Theory of Linear Antennas" Harvard University Press, Cambridge, Massachusetts 1956

slotted cylinder or a cylindrical ribbon. At the start a straight-
forward separation of variables was carried out and upon application
thereafter of the appropriate boundary conditions we concocted a
formulation which led to the integral equation for the electric field
in the aperture of the cylinder. This formulation was also used to
derive the integral equation for the surface current density over the
conducting portion of the cylinder. The integral equation for the
electric field in the slot was shown to give rise to a statement of
Ohm's Law in matrix form wherein an admittance matrix for the
aperture in the cylinder connected a known current vector to an un-
known voltage vector. Equivalently the integral equation for the
surface current density on the conducting portion of the cylinder
gave rise to a complementary statement of Ohm's Law wherein an imped-
ance matrix for the conductor coupled a known voltage vector to an
unknown current vector.

In an earlier report[4] analytical features of the integral equa-
tion for the electric field distribution over the aperture in the
conducting cylinder were studied by deriving solutions for narrow
slots in small cylinders. Similarly in that report analytical
aspects of the surface current density integral equation on the con-
ductor were analyzed by obtaining solutions for narrow cylindrical

4.   J. N. Bombardt and L. F. Libelo (NAVSURFWPNCEN) "S.E.R.A.:
     IV. Slotted Cylinders and Cylindrical Strips in the Rayleigh
     Limit", HDL-RT-1607, Harry Diamond Laboratories, Washington,
     D. C., August 1972

strips. Simplifications of the kernels of the integral operators were the prime reasons which enabled us to derive these analytical solutions. Unfortunately applications of these analytical methods to the integral equations for wavelengths beyond the Rayleigh limit has proved to be intractable thus far for analyzing the general slotted cylinder or cylindrical ribbon.

The method-of-moments was introduced and the interrelationships between this method and other classical techniques for solving integral equations were considered. We chose the integral equation for the surface current distribution for numerical solution using the method-of-moments technique. This choice was motivated by the fact that the kernel in the integral equation is a closed form, computable function at all wavelengths of interest. With the choice of step-function pulses as the set of expansion functions for the surface current and Dirac delta functions as the set of weighting or testing functions, we applied the method-of-moments to the surface current integral equation. This generated a system of simultaneous algebraic equations with the amplitudes of the step functions as the unknown quantities. Taking advantage of symmetry properties of the system the number of these simultaneous equations were considerably reduced.

The simultaneous algebraic system of equations that results from applying the method-of-moments can be equivalently thought of as a matrix equation with a known coefficient matrix multiplying an un-known vector and resulting in a known vector. The elements of this

known coefficient matrix are integrals of the kernel which were evaluated analytically. A computer program was constructed to solve this matrix equation. This program computes not only the surface current distribution at a given wavelength but it also determines the electric field distribution over the aperture in the cylinder and in addition the back-scattering cross-section per unit length for a given φ_0 or half-slot angle.

The computer program was subjected to a reliable check by comparing its results for back-scattering cross-section of a complete cylinder over a spectrum of wavelengths with the corresponding known exact results. Over that range of wavelengths the numerical results obtained from the computer program were found to be in excellent agreement with the known results. Numerical results were then generated from that computer program for a number of slotted cylinders and we presented some of these in this report along with a discussion of them for the specific cases $\varphi_0 = 30°$, $45°$, $60°$. We did the same for the half-cylindrical mirror, i.e. $\varphi_0 = 90°$ and for the two cylindrical ribbons corresponding to $\varphi_0 = 120°$ and $150°$. These results displayed quite clearly the physical behaviour anticipated. The infinitely sharp interior resonances for the closed circular waveguide exhibit themselves in the back-scattering cross-section in the presence of a relatively narrow slot. As the effective size of the slot increases these resonances tend to correspond to broader and broader lines whose centers shift more and more with ever increasing

φ_0. Equivalently we see in our results the evolution of the scattering system from a circular cylindrical one to that corresponding to a flat planar strip at φ_0 increases from 30° through intermediate values to 150° and beyond. Upon examination of the aperture field distributions and surface current density distributions we observe in our results the stationary state resulting from a symmetrically incident axially polarized electromagnetic wave falling upon a slotted cylinder. This it should be recalled is a fourier component, when properly weighted, of an incident pulse irradiating the same cylinder. The incident plane wave induces a surface current distribution, the result of excited surface waves that propagate around the cylinder undergoing reflection at the now present edges. As a result of these induced surface waves we observe in the near field region a transition of behaviour in the electric field as seen in the aperture. This goes from that almost exactly corresponding to the narrow slot distribution through a very rich and interesting variety of distributions as the slot angle φ_0 increases over the range studied and as η changes over the range investigated. This remarkable behaviour for the near electric field distribution accompanies a most unremarkable variation in the surface current on the conductor of the same large range of slot angle φ_0 and of circumference to wavelength ratio η. This fascinating near-field behaviour of the electric field distribution is almost completely masked in the back-scattering cross-section results, i.e. in the far-field behaviour at $\varphi = 0°$.

The series expansion of the interior electric field i.e. for $\rho<a$ led to a set of constraint requirements on the electric field distribution over the slot in the cylinder at certain frequencies. These frequencies are the eigenfrequencies or characteristic interior resonance frequencies for the circular waveguide. In the problem investigated in this paper they are the TM circular waveguide modes. Four different possible requirements on the aperture electric fields arise in a very straightforward and natural way from the physical requirement that the electric field within the slotted cylinder must remain finite at these TM mode resonance frequencies. For the slotted cylinders, the half-cylindrical mirror and the cylindrical strips considered, numerical results for the aperture electric field were given at each of the two lowest TM mode frequencies for each geometry. Discussion of the results obtained for the distribution of the real and imaginary parts of the electric field over the aperture in the slotted cylinder resulted in clearcut confirmation of the validity of the constraint conditions derived. Furthermore these constraining relations were discussed and shown to hold for the limiting cases of no slot in the conducting cylinder and no conducting cylinder. It is very likely that similar sets of constraining requirements exist for other diffraction problems involving a conducting enclosure with an opening which permits the interior modes for the closed conductor to couple to the exterior region.

The numerical technique discussed in earlier portions of this

report was applied to the special case of a slotted cylinder where $\varphi_0 = 6°$. As was mentioned back in the introduction this narrow slot problem is of significant interest all by itself to require a separate report devoted solely to it. For this reason the corresponding results for this case shall appear in a subsequent paper in this series. We did however include the numerically determined results for the narrow concave cylindrical ribbon which subtends a total angle of $12°$ ($\varphi_0 = 174°$) at the cylinder axis. This particular scattering problem provided an ideal situation for application of the numerical technique. The results obtained for the back-scattering cross-section and the surface current density over the narrow strip at $\eta = 0.5$ were excellent. We have demonstrated that the numerical method was successful in predicting with accuracy the gradual evolution and transformation of the scattering characteristics from those of the conducting cylinder with an axial slot to those of the flat strip.

In conclusion we note that the results presented in this report have filled an important gap. The problem of determining the results characterizing the scattering of a plane symmetrically and normally incident, linearly polarized monochromatic, electromagnetic wave by an axially slotted conducting cylinder or cylindrical strip has been solved, numerically. This solution has been generated in a range of wavelength that prior to this time had proven to be an inaccessible region namely that of the primary resonance region spanning that

portion of the frequencies from the Rayleigh limit to the limit of geometrical optics. Clearly the techniques used in this paper to generate the solution for the geometry chosen for investigation can be quite readily extended to a whole host of other problems involving apertures in otherwise closed conducting shields. Many such problems have indeed been subjected to investigation and the results obtained shall appear in forthcoming papers of the series. A considerable amount of general fundamental physical information has been accumulated and this will become evident in the contents of these papers as they are published and then inspected and studied.

The solution for the infinite cylinder scattering problem without a slot has been utilized rather widely as a practical approximation to similar but finite scattering geometries. In fact the number of such approximate applications are legion. The breadth of the spectrum of application of the conducting infinite cylindrical scatterer includes modelling of real aircraft, approximating ship masts as well as other superstructure elements, construction of sensors, and geophysical problems such as locating ore deposits. In turn the solution of the present problem, that is the scattering by an infinite cylinder with a full length axial slot, has already served as a guide and as an approximation to the solution of problems involving finite cylindrical geometries with apertures. Again a host of real practical problems fall into this category. A number of papers to follow in this series will be examples of this.

REFERENCES

1. L. F. Libelo and J. N. Bombardt (HDL) "Scattering of Electromagnetic Radiation by Apertures: I. Normal Incidence on the Slotted Plane", NOLTR 70-58, Naval Surface Weapons Center, White Oak, Silver Spring, Maryland, April 1970

2. L. F. Libelo and J. N. Bombardt (HDL) "S.E.R.A.: II. Oblique Incidence on the Slotted Plane for Parallel Polarization", NOLTR 72-25, Naval Surface Weapons Center, White Oak, Silver Spring, Maryland, January 1972

3. J. N. Bombardt and L. F. Libelo (NAVSURFWPNCEN) "S.E.R.A.: III. An Alternative Integral Equation With Analytic Kernels for the Slotted Cylinder Problem", HDL-TR-1588, Harry Diamond Laboratories, Washington, D. C., August 1972

4. J. N. Bombardt and L. F. Libelo (NAVSURFWPNCEN) "S.E.R.A.: IV. Slotted Cylinders and Cylindrical Strips in the Rayleigh Limit", HDL-TR-1607, Harry Diamond Laboratories, Washington, D. C., August 1972

5. A. Sommerfeld, "Partial Differential Equation", p 29-31 Academic Press, New York, 1949

6. P. M. Morse and H. Feshbach, "Methods of Theoretical Physics", Part II, 1387-1398 McGraw-Hill, New York, 1953

7. R. Turner, "Scattering of Electromagnetic Radiation by an Infinite Cylindrical Mirror", Tech. Rep. No. 161, Cruft Laboratory, Harvard University, Cambridge, MA, 1953

8. L. Chambers, "Reflection of a Wave by a Cylindrical Mirror", Proc. Edinburgh Math. Soc. (2) 9, 1956

9. R. Barakat and E. Levin, "Diffraction of Plane Electromagnetic Waves by a Perfectly Conducting Cylindrical Lamina", Jour. Opt. Soc. of Amer. 54, 1089-1094, September 1964

10. M. J. Barth, "Interior Fields of a Slotted Cylinder Irradiated with an Electromagnetic Pulse", Tech. Rep. No. AFSWC-TR-69-9, Air Force Special Weapons Center, Kirtland Air Force Base, New Mexico, August 1969

11. V. N. Koshparenok and V. P. Shestopalov, "Diffraction of a Plane Electromagnetic Wave by a Circular Cylinder with a Longitudinal Slot", Zh. Vychisl. i Mat. Fiz., 11, 719-737, 1971

12. Z. S. Agranovich, V. A. Marchenko and V. P. Shestopalov, "Diffraction of Electromagnetic Waves by Plane Metallic Gratings", Zh. tekhn.Fiz., 32, 4, 381, 1962

13. M. S. Macrakis, "Backscattering Cross-Section of Slotted Cylinders", Ph.D. Dissertation, Harvard University, Cambridge, MA, 1958

14. H. J. Schmitt, "Backscattering Measurements with a Space Separation Method", Scientific Report No. 14, Cruft Laboratory, Harvard University, Cambridge, MA, 1957

15. R. V. Row, "Electromagnetic Diffraction in a Parallel Plate Region", Ph.D. Dissertation, Harvard University, Cambridge, MA, 1953

16. C. C. Tang, "Backscattering From Dielectric-Coated Infinite Cylindrical Obstacles", Ph.D. Dissertation, Harvard University, MA, 1956

17. J. J. Bowman, T.B.A. Senior and P.L.E. Uslenghi, eds. "Electromagnetic and Acoustic Scattering by Simple Shapes", p 92-93, North-Holland Publishing Co., Amsterdam, The Netherlands, 1969

18. G. Goubau, "Electromagnetic Waveguides and Cavities", p 185-191, Pergamon Press, New York, 1961

19. A. Erdélyi, Ed., "California Institute of Technology, Bateman Manuscript Project. Higher Transcendental Functions, Vol. II", eqs. 14 and 15, p 87, McGraw-Hill Book Co., Inc., New York, N. Y. 1953

20. J. A. Stratton, "Electromagnetic Theory" eq. (11) p 374, McGraw-Hill Book Co. Inc., New York, N.Y. 1941

21. R. F. Harrington, "Matrix Methods for Solving Field Problems", Technical Report No. RADC-TR-66-351 Rome Air Development Center, Griffiss Air Force Base, New York 1966

22. R. F. Harrington, "Field Computation by Moment Methods", The Macmillan Co., New York, N. Y. 1968

REFERENCES (Contd)

23. R. W. P. King and T. T. Wu, "The Scattering and Diffraction of Waves", eq. 18.1, p 68, Harvard University Press, Cambridge, MA, 1959

24. E. D. Reilly, Jr., "Resonant Scattering From Inhomogeneous Non-spherical Targets", Journal of Computational Physics, Vol. 11, No. 4, p 463-492, April 1973

25. E. M. Kennaugh, "Multipole Field Expansions and Their Use in Approximate Solutions of Electromagnetic Scattering Problems", Ph.D. Dissertation, Dept. of Electrical Engineering, Ohio State University, Columbus, Ohio, 1959

26. L. F. Libelo, Jr., "Scattering by Axisymmetric Particles Whose Size is of the Order of the Wavelength", Ph.D. Dissertation, Dept. of Physics, Rensselaer Polytechnic Institute, Troy, N. Y. 1964

27. C. R. Mullin, R. Sandburg and C. O. Velline, "A Numerical Technique for the Determination of Scattering Cross-Sections of Infinite Cylinders of Arbitrary Geometrical Cross-Section", IEEE. Transactions on Antennas and Propagation, AP 13, 141, 1965

28. L. V. Kantorovich and V. I. Krylov, p. 304, "Approximate Methods of Higher Analysis", Interscience Publishers, Inc., New York 1958

29. Lord Rayleigh "Theory of Sound", sections 88 and 89, Vol. I, Dover Publications, New York 1945

30. W. Ritz, "Über eine neue Methode zur Losung gewisser Variations probleme der mathematischen Physik", Journal fur die Reine und Angewandte Mathematik Vol. CXXXV, p 1-61, 1909

31. K. K. Mei, "On the Integral Equations of Thin Wire Antennas", IEEE Transactions on Antenna and Propagation AP 13, 374, 1965

32. D. P. Margolis, C. L. Andrews, J. Heckl and L. Libelo, "Plane Wave Scattering by An Open-Ended Cylinder With An Axial-Slot, Bull. Am. Phys. Soc. Vol. 20, No. 1, p 101, 1975

33. P. M. Morse, P. J. Rubenstein, "The Diffraction of Waves by Ribbons and by Slits", Phys. Rev. 54, 895, 1938

34. I. S. Gradshteyn, I. W. Ryzhik, "Tables of Integrals, Series and Products", eq. 2, Section 8.531 page 979, Academic Press, New York 1965

35. E. Jahnke, F. Emde, "Tables of Functions", Chapt. VIII, Dover Publications, New York, N. Y. 1945

36. M. Abramowitz, I. A. Stegun, "Handbook of Mathematical Functions" Table 9.5, U. S. Department of Commerce, National Bureau of Standards, Applied Mathematics Series-55, 3rd Printing 1965. U.S. Government Printing Office, Washington, D. C.

37. D. S. Jones, "The Theory of Electromagnetism" pp 566-569, Pergamon Press, New York 1964

38. G. T. Ruck, ed. "Radar Cross Section Handbook", Vol. 2. p 502, Plenum Press, New York, N. Y. 1970

39. "SYSTEM/360 Scientific Subroutine Package" (360A-CM-03X), Version II, Programmers Manual, Publication H20-0205-2, International Business Machines Corp. 1967

40. S. Silver and W. K. Saunders, "The Radiation From a Transverse Rectangular Slot In A Circular Cylinder", Jour. of Applied Physics, 21, 745 (1950)

41. L. L. Bailin, "The Radiation Field Produced by a Slot In A Large Circular Cylinder" IRE Transactions AP-3, 128 (1955)

42. J. R. Wait, "Radiation Characteristics of Axial Slots On A Conducting Cylinder" Wireless Engineer pp 316-322 December 1955

43. J. R. Wait, "Electromagnetic Radiation from Cylindrical Structures" pp 88-104, Pergamon Press, New York, N. Y. 1959

44. C. A. Balanis, "Radiation From Slots On Cylindrical Bodies Using Geometrical Theory of Diffraction and Creeping Wave Theory" Doctoral Dissertation, Ohio State University, Columbus, Ohio 1969

45. J. R. Wait "Survey of Recent Literature on Slot Radiators", NBS Report #5051, U.S. Dept. of Commerce, Washington, D.C. March 1957

46. R. W. P. King "Theory of Linear Antennas" Harvard University Press, Cambridge, Mass. 1956